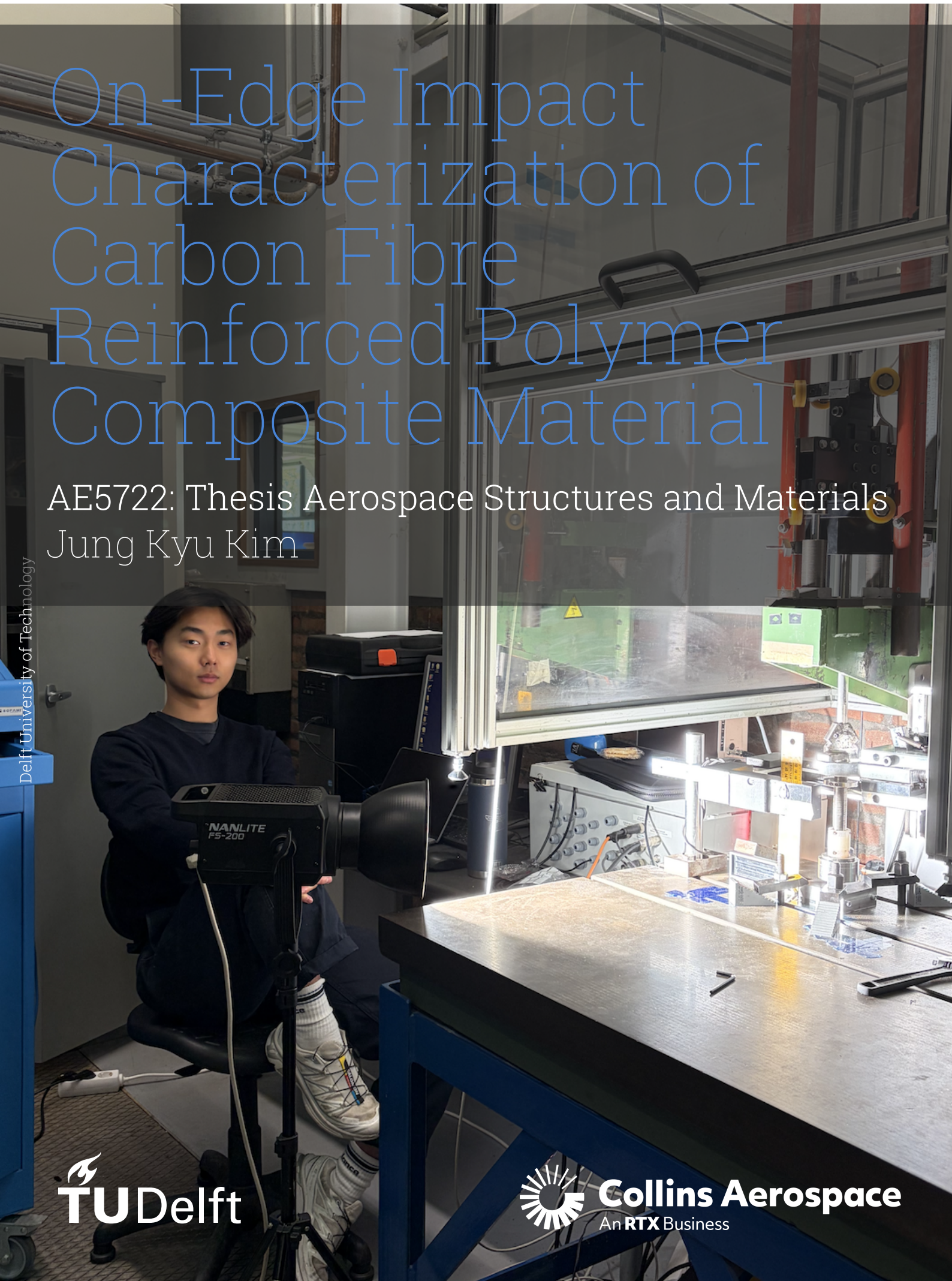
On-Edge Impact Characterization of Carbon Fibre Reinforced Polymer Composite Material

AE5722: Thesis Aerospace Structures and Materials

Jung Kyu Kim

Delft University of Technology



TU Delft

Collins Aerospace
An RTX Business

On-Edge Impact Characterization of Carbon Fibre Reinforced Polymer Composite Material

by

Jung Kyu Kim

University Supervisor:	Dr. -Ing. Saullo G. P. Castro
Company Supervisor:	Dr. Ismet Baran
Thesis Duration:	Nov, 2025 - July, 2026
Faculty:	Faculty of Aerospace Engineering, Delft

Cover: When I was a Masters Student

TU Delft

Collins Aerospace
An RTX Business

Preface

First and foremost, I would like to thank my mother, who has single-handedly supported me and my brother's education until now. Without her support, I would not be here today. I would also like to thank my brother, Dongkyu, who has been helping me out throughout the studies.

Secondly, I would like to thank my supervisor, Dr. -Ing. Saullo G. P. Castro, for his continuous support throughout the thesis and his advices on stepping forward as a young professional. And to my company supervisor, Dr. Ismet Baran, for his feedback throughout the thesis work.

Sharing the gratitude also to my friends, especially Tyco and Jing Jing for being there for me and all the nice chats we had. Rashmi, Alexandre, Eunkyung, Kasper, Max, Chanseo and HP, thank you for all the laughs and beers we had. I will never forget all the lunch boxes we ordered, especially that one day at the Fellowship.

I would also like to share my gratitude with Dr. Calvin Rans, who inspired me to puruse this studies with the focus in Structures and Materials. Without him, I would not be the student I am today, and more importantly, I would not be the person who I am today.

I must also thank Alexander Uithol, who helped me set up all my experiments. Without him, this thesis would not have been delivered on time. Thank you Alex!

Last but not least, I would also like to thank Yoonjae, who has been taking care of my mother and my grandparents while my brother and I are away. I am forever grateful to you.

And to my children, if I ever get to have them, hope you get a chance to read this work and get to see what kind of student dad was.

"I command you: be strong and steadfast! Do not fear nor be dismayed, for the LORD, your God, is with you wherever you go."

- Joshua 1:9

Jung Kyu Kim
Delft, August 2026

Summary

This work presents the analysis of on-edge impact loading of carbon fibre reinforced polymer(CFRP) material. On-egdge impact are rarely researched and they often consume a lot of time and resources to be tested. This work presents a possible easier set-up to analyze the response of the CFRP using a conventional droptower. First, quasi-static tests are performed to gain initial mechanical understandings of the material, including the energy absorbed by the specimen. Then efforts are dedicated to impact load the specimen at same energy using the droptower. Then the impact energies are increased to further investigate the effects of the strain-rate loading for on-edge loading. The damages are compared through the means of microscopy and ultrasonic C-Scan to assess the visible damages and the extent of the damages. While it was possible to perform reliable energy analysis and the damages were compared in a detailed manner per strain-rate used, the force and impulse data of the specimen were not able to evaluated to full extent. The nature of the droptower, measuring the force experienced by the impactor and the vibration caused due to the impact hinders the data significantly. For future, it is recommended to present a set-up which can measure what the specimen experiences directly, rather than relying on the information from the droptower to gain information about the specimen.

Contents

Preface i

1 Introduction 1

2 Problem Statement 2

3 Literature Study 4
3.1 Introduction . . . 4
3.2 Past Works in Impact Analysis of Composite Materials . . . 4
3.2.1 General Work Done on Impact Analysis of Composite Materials . . . 4
3.2.2 Absorption of the Impact and Failures . . . 5
3.2.3 Specific Works on Impact Analysis of CF/PPS . . . 6
3.3 Damage Mechanisms . . . 6
3.4 Relevant On-Edge Loading Example . . . 8
3.5 Set-Up of Impact Testing . . . 9
3.5.1 Different Methods for Impacts . . . 9
3.5.2 Boundary Conditions . . . 10
3.5.3 Impactor Head . . . 12

4 Research Proposal 13
4.1 Introduction . . . 13
4.2 Research Motivation . . . 13
4.3 Steps Towards Research Objectives . . . 14
4.4 Scientific Novelty . . . 14
4.5 Conclusion . . . 15

5 Methodology 16
5.1 Introduction . . . 16
5.2 Required Outcomes . . . 16
5.3 Boundary Condition . . . 17
5.4 Specimen . . . 23
5.5 Impactor . . . 24
5.6 Required Equipments . . . 25
5.6.1 Quasi-Static Tests . . . 25
5.6.2 Impact Test . . . 26
5.7 Test Procedure . . . 29
5.7.1 Quasi-Static Tests . . . 29
5.7.2 Impact Tests . . . 30
5.7.3 Tips and Tricks . . . 31
5.8 Measurement Techniques . . . 32
5.9 Ultrasonic C-Scan . . . 33
5.10 Test Matrix . . . 34
5.11 Conclusion . . . 35

6 Results 36
6.1 Introduction . . . 36
6.2 Quasi-Static Tests . . . 36
6.2.1 Ultrasonic C-Scan of Specimens . . . 43
6.3 Impact Test . . . 45
6.3.1 Force Analysis . . . 50
6.3.2 Energy Analysis . . . 56

6.3.3 Impulse Analysis . . . 57
6.3.4 Ultrasonic C-Scan of Specimens . . . 57
6.4 Comparison Between Quasi-Static Tests and Impact Tests . . . 61
6.5 Conclusion . . . 65

7 Challenges, Recommendations and Evaluation 66
7.1 Introduction . . . 66
7.2 Dropping Heights . . . 66
7.3 Boundary Conditions . . . 66
7.4 Measurements . . . 67
7.5 High-Speed Camera . . . 67
7.6 Abaqus Analysis . . . 68

8 Conclusion 69

References 71

A High-Speed Camera Footage 74
A.1 IM-1 . . . 75
A.1.1 IM-1 Before Impact Energy Calculation . . . 75
A.1.2 IM-1 After Impact Energy Calculation . . . 77
A.2 IM-2 . . . 79
A.2.1 IM-2 Before Impact Energy Calculation . . . 79
A.2.2 IM-2 After Impact Energy Calculation . . . 81
A.3 IM-3 . . . 83
A.3.1 IM-3 Before Impact Energy Calculation . . . 83
A.3.2 IM-3 After Impact Energy Calculation . . . 85
A.4 IM-4 . . . 87
A.4.1 IM-4 Before Impact Energy Calculation . . . 87
A.4.2 IM-4 After Impact Energy Calculation . . . 89
A.5 IM-5 . . . 91
A.5.1 IM-5 Before Impact Energy Calculation . . . 91
A.5.2 IM-5 After Impact Energy Calculation . . . 93
A.6 IM-6 . . . 95
A.6.1 IM-6 Before Impact Energy Calculation . . . 95
A.6.2 IM-6 After Impact Energy Calculation . . . 97
A.7 IM-7 . . . 99
A.7.1 IM-7 Before Impact Energy Calculation . . . 99
A.7.2 IM-7 After Impact Energy Calculation . . . 101
A.8 IM-8 . . . 103
A.8.1 IM-8 Before Impact Energy Calculation . . . 103
A.8.2 IM-8 After Impact Energy Calculation . . . 105
A.9 IM-9 . . . 107
A.9.1 IM-9 Before Impact Energy Calculation . . . 107
A.9.2 IM-9 After Impact Energy Calculation . . . 109

List of Figures

3.1 Schematic of Compression After Edge Impact . . . 5
3.2 Strength vs. strain-rate of CF/PPS [40] . . . 6
3.3 Commonly found damages in CFRP: (a) Elastic microbuckling, (b) Plastic microbuckling, (c) fibre crushing, (d) Splitting of matrix, (e) Delamination [5] . . . 7
3.4 Possible Failure Modes for Composite Cylindrical Tubes [17] . . . 8
3.5 Split Hopkinson Pressure Bar [39] . . . 9
3.6 Schematic of Droptower Impact Machine [43] . . . 9
3.7 Example Set Up of the Fixture [42] . . . 10
3.8 Example Set Up of the Fixture [23] . . . 11
3.9 Impact Result of the Example Set Up [42] . . . 11
3.10 Impact Result of the Example Set Up [23] . . . 11

4.1 Aerospace's building block approach [10] . . . 14

5.1 ASTM D6641 [8] . . . 17
5.2 Design Iterations . . . 17
5.3 Final chosen boundary condition, CAD Model . . . 18
5.4 Block 1 CAD model . . . 18
5.5 Block 2 CAD model . . . 18
5.6 Boundary condition assembly . . . 19
5.7 Free body diagram of the specimen . . . 19
5.8 Force vs. time curve of the preliminary impact tests with unclamped specimen, dropheight $800mm$ . . . 20
5.9 Simplified set-up of the specimen during the loading case . . . 21
5.10 Free body diagram to calculate the clamped force . . . 22
5.11 Schematic of the specimen set-up . . . 24
5.12 Impactor CAD model . . . 24
5.13 Manufactured impactor . . . 25
5.14 Zwick 250kN static test machine . . . 26
5.15 Droptower at TU Delft . . . 27
5.16 Impactor catcher . . . 27
5.17 Impactor catcher mechanism illustration . . . 28
5.18 Impactor dart . . . 28
5.19 Boundary condition set-up . . . 29
5.20 Settlement Run . . . 29
5.21 Simplified Representation of the Quasi-Static Set-Up . . . 30
5.22 Quasi-Static Test Set-Up . . . 30
5.23 Impact test set-up . . . 31
5.24 Impact test set-up . . . 31
5.25 Zwick 250kN static test machine . . . 32
5.26 An example pixel spotting . . . 33
5.27 C-Scan visualization . . . 33
5.28 C-Scan set-up . . . 34
5.29 C-Scan plan . . . 34

6.1 Force and Displacement Curve of the Compliance of the Machine . . . 36
6.2 Force displacement curve of the compression Test . . . 37
6.3 Corrected force displacement curve of the compression Test . . . 37
6.4 Stres-strain curve of the compression test . . . 39

6.5 Microscopy Scan quasi-static QS-1 . . . 40
6.6 Microscopy Scan quasi-static QS-2 . . . 40
6.7 Microscopy Scan quasi-static QS-3 . . . 41
6.8 Microscopy Scan quasi-static QS-4 . . . 41
6.9 Microscopy Scan quasi-static QS-5 . . . 42
6.10 Ultrasonic Scan of QS-1 . . . 43
6.11 Ultrasonic Scan of QS-2 . . . 43
6.12 Ultrasonic Scan of QS-3 . . . 44
6.13 Ultrasonic Scan of QS4 . . . 44
6.14 Ultrasonic Scan of QS-5 . . . 44
6.15 QS-2 damage inspection . . . 45
6.16 Microscopy scan impact IM-1 . . . 46
6.17 Microscopy scan impact IM-2 . . . 46
6.18 Microscopy scan impact IM-3 . . . 47
6.19 Microscopy scan impact IM-4 . . . 47
6.20 Microscopy scan impact IM-5 . . . 48
6.21 Microscopy scan impact IM-6 . . . 48
6.22 Microscopy scan impact IM-7 . . . 49
6.23 Microscopy scan impact IM-8 . . . 49
6.24 Microscopy scan impact IM-9 . . . 50
6.25 Force vs. Time curve, drop height 800mm . . . 51
6.26 Force vs. Time curve, drop height 1000mm . . . 52
6.27 Force vs. Time curve, drop height 1200mm . . . 53
6.28 Impactor's natural frequency calculated by Abaqus . . . 55
6.29 Frequency spotting for natural frequnecy analysis . . . 55
6.30 Comparison of troughs after first peak . . . 56
6.31 Ultrasonic Scan of IM-1 . . . 58
6.32 Ultrasonic Scan of IM-2 . . . 58
6.33 Ultrasonic Scan of IM-3 . . . 58
6.34 Ultrasonic Scan of IM-4 . . . 59
6.35 Ultrasonic Scan of IM-5 . . . 59
6.36 Ultrasonic Scan of IM-6 . . . 59
6.37 Ultrasonic Scan of IM-7 . . . 60
6.38 Ultrasonic Scan of IM-8 . . . 60
6.39 Ultrasonic Scan of IM-9 . . . 61
6.40 Splaying angles comparison . . . 62
6.41 Ultrasonic scan comparison . . . 63
6.42 Splaying degree comparison . . . 64

7.1 ASTM D6641 Gripper Surface [34] . . . 67

A.1 IM-1 Frame 729 . . . 75
A.2 IM-1 Frame 745 . . . 76
A.3 IM-1 Frame 749 . . . 77
A.4 IM-1 Frame 759 . . . 78
A.5 IM-2 Frame 730 . . . 79
A.6 IM-2 Frame 749 . . . 80
A.7 IM-2 Frame 749 . . . 81
A.8 IM-2 Frame 757 . . . 82
A.9 IM-3 Frame 703 . . . 83
A.10 IM-3 Frame 750 . . . 84
A.11 IM-3 Frame 727 . . . 85
A.12 IM-3 Frame 738 . . . 86
A.13 IM-4 Frame 637 . . . 87
A.14 IM-4 Frame 688 . . . 88
A.15 IM-4 Frame 755 . . . 89

A.16 IM-4 Frame 764 90
A.17 IM-5 Frame 722 91
A.18 IM-5 Frame 744 92
A.19 IM-5 Frame 759 93
A.20 IM-5 Frame 765 94
A.21 IM-6 Frame 717 95
A.22 IM-6 Frame 747 96
A.23 IM-6 Frame 749 97
A.24 IM-6 Frame 761 98
A.25 IM-7 Frame 699 99
A.26 IM-7 Frame 734 100
A.27 IM-7 Frame 765 101
A.28 IM-7 Frame 770 102
A.29 IM-8 Frame 709 103
A.30 IM-8 Frame 735 104
A.31 IM-8 Frame 768 105
A.32 IM-8 Frame 773 106
A.33 IM-9 Frame 681 107
A.34 IM-9 Frame 717 108
A.35 IM-9 Frame 744 109
A.36 IM-9 Frame 761 110

List of Tables

3.1 Compressive properties at different strain rates [26] 6

5.1 Material Properties [37] 23
5.2 Quasi-Static Test Matrix 34
5.3 Impact Test Matrix 35

6.1 Slope values for test specimens 38
6.2 Slope values average and standard deviation 38
6.3 Maximum force values for test specimens 38
6.4 Maximum force values average and standard deviation 38
6.5 Energy absorbed per specimen 39
6.6 Slope values for test specimens 39
6.7 Material Properties 54
6.8 Impact test results for clamped samples 56
6.9 Comparison of observed damage characteristics 65

1

Introduction

It is well-known by now that composite material contributes greatly to the aerospace structures. Specifically, carbon fibre reinforced polymer(CFRP) composites have become the star of aerospace industry, due to their high specific strength, high specific stiffness, and excellent resistance to environments, such as corrosion. In recent years, thermoplastic polymer has been getting a lot of attention due to their recyclability, as a contribution to building a more sustainable aviation world. In particular, thermoplastic polymer polyphenylene sulfide, often abbreviated as PPS has been gaining a lot of attention for its cheap price, manufacturability and sustainability. Its ease in manufacturing and sustainable characteristics arises from the composition of the polymer, the non-crosslinked nature and semi-crystalline structure. These characteristics also play a huge role in their response to different loadings, especially for strain-rate loading [32, 9].

Despite the widespread use of CFRP composites, their failure mechanisms remain extremely complex due to interactions of different damage mechanisms, including matrix cracking, fibre fracture, delamation and many more. The development and propagation of these damages, so called the "progressive damage" behaviour of the composite materials are strongly influenced by laminate architecture, material constituents, and loading conditions. While there has been a lot of extensive research on impact and compression response of composite laminates, only very few literatures exists for on-edge loading condition. Understanding the initiation and evolution of the damage mechanisms and strain-rate loading response of the material upon on-edge loading is essential for improving structural reliability and energy absorption capability of composite materials subjected to impacts or crash events. This effort of dynamic characterization will contribute to taking another step towards implementation of the material, for the requirements are for dynamic loading, while oftentimes the materials are assessed based on their static performance.

This thesis investigates the on-edge loading response of woven CF/PPS laminates under both quasi-static and impact loading conditions. Quasi-static testing is used to establish the baseline mechanical behaviour of the specimen, including stiffness, strength and failure characteristics, while the droptower impact test is used to evaluate the dynamic response of the laminate. Highligting the energy absorbed by the specimen, maximum force, and damage evolution, the study aims to provide insight into the role of strain-rate effects and thermoplastic polymer composite materials.

2

Problem Statement

The readiness is all - Hamlet. In the play *Hamlet* by William Shakespeare, Hamlet says this to his friend Horatio, in the face of imminent danger, expressing the idea that prepardness, rather than chance or hesitation, determines the outcome when confronting uncertainty. A comparable principle underlies in modern aviation safety, where passenger survivability during crash events depends on rigorous preparation through certification requirementss, systematic testing and structurally robust design.

Such regulations already exist in place in order to guide the design process. Namely, for this work, the regulations posed by the Federation Aviation Agency, abbreviated as FAA is of interest, for Collins Aerospace is a company based in the United States. These regulations are named Federal Aviation Regulations, which is a part of regulations issued by the United States Federal Agency. Nowadays, the FAR is called 14 Code of Federal Regulations(CFR), as the FAR is a part of the CFR. For simplicity's sake, the regulations will be referred as 14 CFR in this work.

The 14 CFR is structured hierarchically, with regulations organized into Parts. Each Part is subdivided into Subparts, which are further divided into Sections containing the detailed regulatory provisions. For transport category airplanes, occupant safety and seat structure certification requirements are primarily contained within 14 CFR Part 25, Subpart C. Specifically, 14 CFR 25.562 establishes the dynamic testing requirements for aircraft seats by prescribing representative crash pulses that simulate survivable emergency landing conditions. The regulation requires a vertical impact test with a peak floor deceleartion of 14g and a forward impact test with a floor deceleration of 16g. These acceleration pulses generate high loads within the seat structure, requiring the materials to be used in the seat structure to also be tested in a rigorous dynamic manner.

Therefore, this work aims to present a method that could be used to provide aerospace manufacturing companies easier prelimiary assessment of materials that could be used for aircraft interior structures, specifically the seat structures. In the rest of this chapter, the broader research objectives and research questions that can be used to guide the thesis work are defined.

It is essential to define the research objectives to ensure that the thesis work stays on track. Based on discussion between Collins Aerospace and TU Delft, the main research objective is defind as follows.

RO.Main: Investigate the influence of on-edge impact loading on the strain-rate-dependent behavior of composite materials and to develop a cost-effective experimental approach for their evaluation in aerospace applications.

To achieve this objective, several supporting sub-research objectives were defined as mentioned in the following.

RO.1: Characterize failure mechanisms of composite under on-edge loading

This research objective aims to investigate the failure mechanisms of the composite material subjected to on-edge loading in both quasi-static and impact loading conditions. Quasi-static test establishes the baseline mechanical response and identify the dominant failure modes, while dynamic impact tests

capture the damage mechanisms associated with high strain-rate loading representative of aerospace impact events. The experimental observations provide insight into damage initiation and propagation contributing to a better understanding of the strain-rate dependent behaviour of composite materials under on-edge loading.

RO.2: Quantify the energy absorption of composite materials under quasi-static loading to define equivalent impact energy levels for dynamic testing

This research objective aims to establish an experimental methodology that links quasi-static and dynamic on-edge tests through equivalent energy levels. The energy absorbed by the composite specimens during quasi-static loading is quantified and used to determine the corresponding impact energy for the dynamic tests. By maintaining consistent energy input between the two loading conditions, the methodology provides a common basis for investigating the influence of loading rate on the mechanical response of composite materials.

RO.3: Compare failure modes between quasi-static and impact loading for on-edge loading case

This research objective aims to compare the mechanical response and failure behaviour of composite materials subjected to quasi-static and dynamic loading at equivalent energy levels. The comparison evaluates the damages observed in the specimen, clearly establishing how the damages evolve from quasi-static loading and impact loading condition, providing further insights into the strain-rate effects of the composite materials.

RO.4: Investigate how increasing impact energy influences the strain rate-dependent behaviour of composite materials under on-edge loading

This research objective aims to investigate how the response of composite materials evolves as the impact energy is increased beyond the equivalent energy level established in **RO.2**. Dynamic impact tests at greater energy levels are conducted to examine changes in force response, energy absorption, damage evolution, and failure mechanisms. These results provide a broader understanding of the interaction between impact energy and strain-rate effects under on-edge loading conditions.

Achieving these objectives would allow for great reduction of the time and resources, which allows for fast and accurate understanding of the materials prior to conducting the expensive full-scale tests. The proposed approach provides both scientific insight into composite impact mechanics and practical value as a cost-effective and repeatbale tool for early stage design and safety assessment, supporting informed engineering decisions prior to more complex and resource-intensive certification testing.

3

Literature Study

3.1. Introduction

To set a starting point, it is essential to investigate the past works done for similar research motivations. This chapter presents the information needed to perform the work of propsing a new test set-up for characterizing the dynamic impact response of a material which could be used for aircraft interior structure.

3.2. Past Works in Impact Analysis of Composite Materials

This section presents past works which investigate the impact performance of the composite material. Starting from general introduction to the impact analysis of composite materials, how the impact is absorbed, and to finally with works that are directly applicable to this thesis are presented.

3.2.1. General Work Done on Impact Analysis of Composite Materials

With the increase of use in the composite structure, a lot of effort has been devoted into characterizing the composite structure. For aerospace application, the impact loading is one of the bigger interests due to possible crash that could take place during operation. While a lot of work has been devoted to the out-of-plane impact behavior of the structure, the impact applied in the in-plane direction, is not well investigated.

The impact in the in-plane direction can cause barely visible impact damage (BVID) with much lower energy compared to energy required to cause damage through impact in the out-of-plane direction [2]. While not many, there has been research effort made in past to investigate the on-edge low energy impact analysis. Majority of the works investigate the compression strength of the composite laminate after the impact events [42, 27, 36, 12, 23, 24, 41, 35, 2, 28]. All of these works subject their specimens to impact loading cases where the impact load is transmitted in a concentrated manner through the use of hemisphreical or cylindrical impactor heads. Figure 3.1 presents the schematic of how such a test looks like.

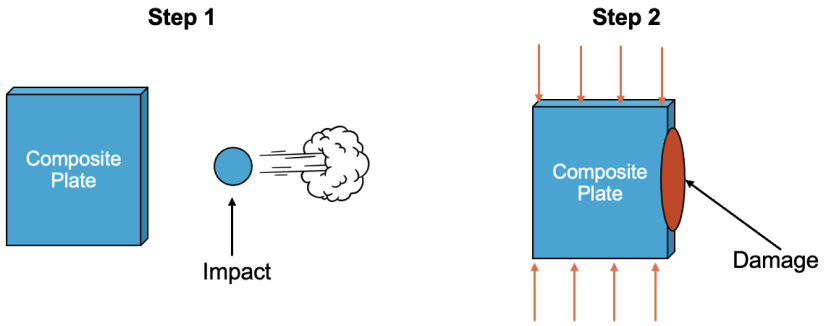


Figure 3.1: Schematic of Compression After Edge Impact

In this work, rather than focusing on the compression strength, the focus is on investigating the on-edge impact response of the material with different types of impact loading.

Impacts are often categorized using the following information: impact velocity, impact energy, impactor mass, non-penetrating or penetrating and damage visibility [36]. For on-edge impact, most of the work is devoted for analyzing the low energy impact that causes BVID as BVID can be caused easily with relatively low energy for on-edge impact compared to on-face impacts.

In addition to categorizing the impact, another point of interest is analyzing how the composite material fails upon the impact loading. Since composite materials consist of different materials and have infinite numbers of combinations for the material and stacking sequence, there is no clear answer for predicting the failure mechanisms of the composite materials subjected to impact loadings. Later in the section, the failure mechanisms of different composite materials are investigated and analyzed to understand how the selected materials for the thesis fail when subjected to the impact loads.

3.2.2. Absorption of the Impact and Failures

Impact loadings have very localized effects on the specimen [36]. Especially the on-edge impacts have effects that are very localized that it can easily be seen with naked eyes even for low energy impacts [36]. In this section, the failures observed and parameters that influence the failures in composite materials subjected to on-edge impact is discussed.

To get started, it is important to understand how the failure takes place and what influences the failures. Generally, the initiation of failures are influenced by the impact energy, peak load and impact duration [36]. The peak load and the impact duration experienced by the specimen increase with the increasing impact energy [36, 16]. After the peak load is reached, the load experienced by the specimen decreases when the damage initiates [36]. In the work by Thorsson et al., they also highlight that the duration between after the damage is initiated and until the impactor bounces back up, stays rather constant for different energy levels even when the impact energy is doubled [36]. Unfortunately, Thorsson et al. does not disclose information on what types of composite materials were used for their work besides the fact that it is a polymer matrix composite material. Therefore, whether this behavior is the case for the material to be used for this thesis is subject to discussion.

The work by Thorsson et al. provides another interesting insight about the damage seen on the specimen and the impact energies. The work presents that damage experienced is significantly different for different impact energies [36]. The indentation depths and the surface delamination lengths increase linearly with the increasing impact energy [36]. This linear behavior is also captured in the work of Malhotra et al., where the glass fibre composite was subjected to on-edge impact tests [16]. Additionally, the linear trend in the size of damage, specifically the crack length is also observed in the work by Xu et al., where they subject carbon fibre reinforced polymer composite material test to impact test [42].

3.2.3. Specific Works on Impact Analysis of CF/PPS

While not many, there exists some relevant researches done in the past, specifically related to this thesis. In these works, the authors subject CF/PPS materials to strain-rate loading. Starting from lower strain-rate of quasi-static rate to dynamic rates, in the range of $400s^{-1}$ $1800s^{-1}$, the authors investigate the response of the CF/PPS subjected to compression loading using SHPB as shown in Figure 3.5 [40, 28, 26].

In the work of Wang et al., the authors subject the specimen to different strain-rate loadings in different temperatures. In this work, the experiments are be performed in room temperature only thus the data points at $23°C$ provides useful insights [40]. Figure 3.2 presents the results of strength of the specimen at different loading speeds.

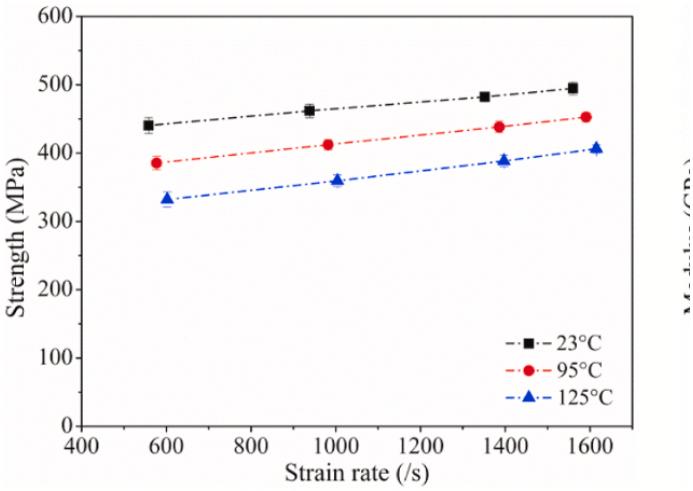


Figure 3.2: Strength vs. strain-rate of CF/PPS [40]

The strength of the specimen does not change drastically per different strain-rates. While there is a slight increasing trend, the increments are very small and can be assumed that the changes are modest. The data from Ramirez also suggests similar trends. As present in Table 3.1, despite the increasing strain-rate, the increase in the peak stresses are almost negligible.

Table 3.1: Compressive properties at different strain rates [26]

Strain Rate (s^{-1})	Peak Stress (MPa)	Strain at Peak Stress (%)	Young's Modulus (GPa)
0.001	521.926	1.203	43.664
0.01	517.869	1.670	42.271
0.1	558.013	0.978	45.643
400.5 DIC	517.342	1.203	59.765
832.3 DIC	552.518	1.487	49.263
Average	533.534	1.323	48.121
Std. Dev.	17.899	0.238	6.279
CV (%)	3.355	17.977	13.048

This behavior is as expected, as the strengths of CFRP are mainly dictated by the strengths of the carbon fibre, which tends to be strain-rate insensitive. Moving forward, this could be used as a validation point to ensure that the tests performed in the thesis align with the physics.

3.3. Damage Mechanisms

Damage mechanisms are different paths which the materials can take to absorb the energies that they are subjected to. In this thesis, the damages which the specimens experience are investigated, therefore it is much of importance to understand how the composite materials' damages are formed and propagated.

The damage mechanisms of the composite materials can be complicated, due to its multi-material nature. This section explores the relevant damages of composite materials relevant to this thesis, specifically the compression and the progressive nature of damage development of composite materials.

During compression loading of CFRPs, there are handful of commonly observed failures [5].

1. Elastic microbuckling (Figure 3.3 (a)): instability where fibres deflect laterally while the matrix deforms elastically.
2. Plastic microbuckling (Figure 3.3 (b)): failure initiated by fibre misalignment and plastic shear deformation of the matrix. Causes localized fibre rotation and kinking.
3. Fibre crushing (Figure 3.3 (c)): failure of fibres due to excessice compressive loading.
4. Splitting (Figure 3.3 (d)): cracks developing along fibre directions.
5. Delamination (Figure 3.3 (e)): ply separation initiated by crack development.

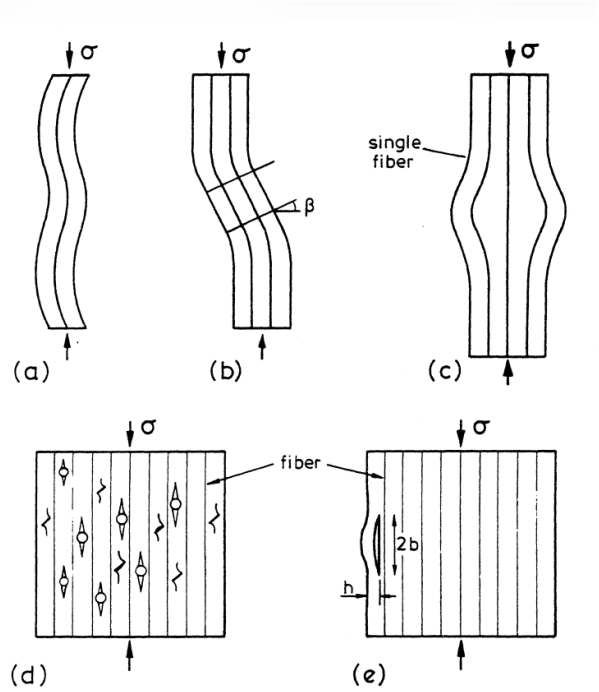


Figure 3.3: Commonly found damages in CFRP: (a) Elastic microbuckling, (b) Plastic microbuckling, (c) fibre crushing, (d) Splitting of matrix, (e) Delamination [5]

In practice, these damages do not occur independently. Instead, damages often develop progressively, where one mechanism triggers another. This is called the progressive failure behviour of the composite materials. For example, when matrix cracking is initiated, delamination may be promoted [38, 19, 30]. Overall failure behavior of composite lamniates is often governed by the interaction and evolution of multiple damage mechanisms rather than a single failure mode [38, 19, 30].

The damage mechanisms too are strain-rate sensitive, just like the material properties [14]. The polymer is very strain-rate sensitive, therefore the fibre-matrix interface behavior changes per strain-rate [14]. The matrix behavior and the interaction between the fibre and matrix has a significant influence on the damage mechanisms thus if they change per strain-rate, the damage mechanism also changes. The polymer becomes more glassy and increases in stiffness when subjected to strain-rate loading. Therefore, the failure observed in the dynamic testing may be significantly different than of observed in quasi-static test [1]. An example by Ali, presents how delamination is more promoted for higher strain-rate loading for CF/PPS [1]. This suggests that more matrix cracks were found with greater strain-rate, which is consistent with the tendency of thermoplastic polymer becoming more glassy with increasing strain-rate.

These damage mechanisms also depend on the layup composition of the CFRP. For this thesis, the woven fabric laminates are be used. Woven laminates are structured in such a way that it has interlaced warp and weft fibre tows. This has a significant effect on the performance of the CFRP [13]. This structure of woven plies prevents crack propagation, increasing the energy required for damage growth [13]. The woven fabrics also have higher fracture toughness than the conventional UD plies [6]. Compared to the UD plies, in woven plies, cracks cannot be initiated easily. This improves their damage tolerance, specifically, for their resistance to impact [13]. In conclusion, the damage mechanisms of the composite materials are very complicated, due to their multi-material nature, lay-up, and different properties observed per strain-rate.

3.4. Relevant On-Edge Loading Example

As mentioned, past works which involve on-edge impact loadings are oftentimes for CAEI. Unfortunately, these works do not investigate the damage of the composite materials to depth. A similar and relevant example for this thesis work is the thin-walled composite cylinders subjected to loading in the directino of the tube.

The ply orientation and stacking sequence play a significant role in how much load each ply carries [19]. This different forces experienced throughout the composite introduces the progressive failure for the composite material, where different parts of the composite fails gradually with different failure mechanisms such as fibre failure, fibre-matrix cracking and more [19].

In the cases of thin-walled cylinders made with composite materials, there are four majors types of failures observed, namely the fragmentation mode, splaying mode, folding mode, and brittle mode as they are damages observed in the wall, not the entire tube structure [17, 19, 31]. Figure 3.4 presents the visual representation of the four failure modes.

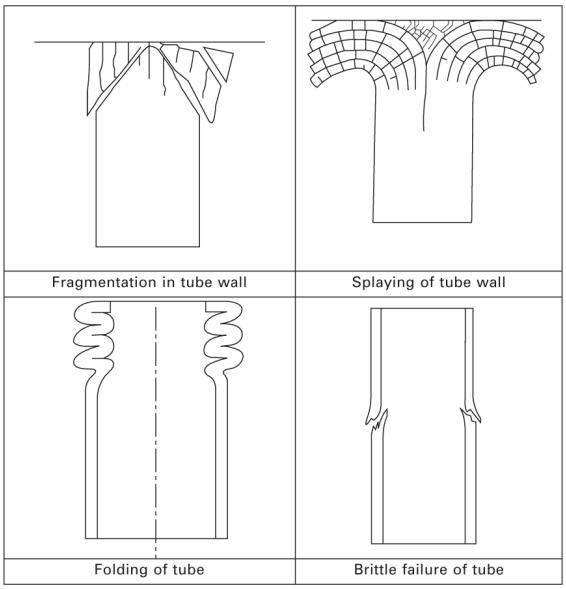


Figure 3.4: Possible Failure Modes for Composite Cylindrical Tubes [17]

As the specimens to be tested in this thesis work is a flat composite subjected to the investigation of on-edge response of the material rather than a tubelike structure, it is assumed that only the first two failure modes, namely the fragmentation and splaying of the tube wall, are relevant. Along with its geometric nature, the specimens are also not exposed enough from the boundary condition to experience the other two failures either.

Fragmentation mode consists of short interlaminar and longitudinal cracks. Usually the lengths of the cracks are less than the thickness of the laminate [20, 17]. The splaying mode consists of interlaminar and intralaminar cracks and fibre bundles bending and splaying [20, 17].

Other work, presented by Tan which investigate the compression of corrugated panel made out of carbon fibre reinforeced thermoplastic composite material to crushing also present splaying and fragmentation as major failure modes [31, 32]. In this work however though, the specimen is chamfered by 45° on the edge, which introduces controlled stress concentrations. The author highlights that once the chamfered region is consumed, the delamination was initiated with the splaying mode. After the delamination started, outer plies started to bend further and the inner plies went under crushing. The role of the chamfered region is to introduce the stress in a gradual manner. Therefore, without the chamfered region, many plies of the specimen are be stressed critically simultaneously rather than gradually, leading to more abrupt delamination than the examples given by Tan. The author also highlights an interesting trend in force. As the delamination and splaying mode are introduced to the specimen the force drops significantly as their stiffness decreases.

3.5. Set-Up of Impact Testing

This section presents the relevant information for experiment planning. Starting from equipments, bondary conditions, impactor used for impact tests used in other works are presented, to build the methodology for this work.

3.5.1. Different Methods for Impacts

Subjecting a specimen to an impact means to subject the specimen to a sudden, high-intensity force over a very short duration [11]. Mainly, there are two ways to induce impact: the Split Hopkinson Pressure Bar, abbreviated as SHPB, and the droptower test as shown in Figure 3.5 and Figure 3.6, respectively.

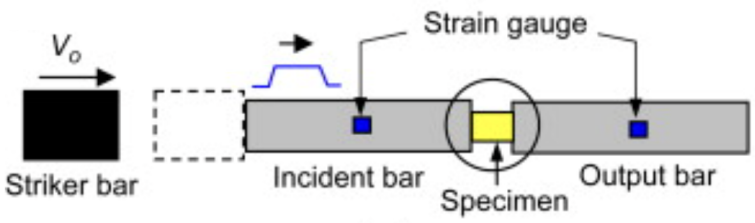


Figure 3.5: Split Hopkinson Pressure Bar [39]

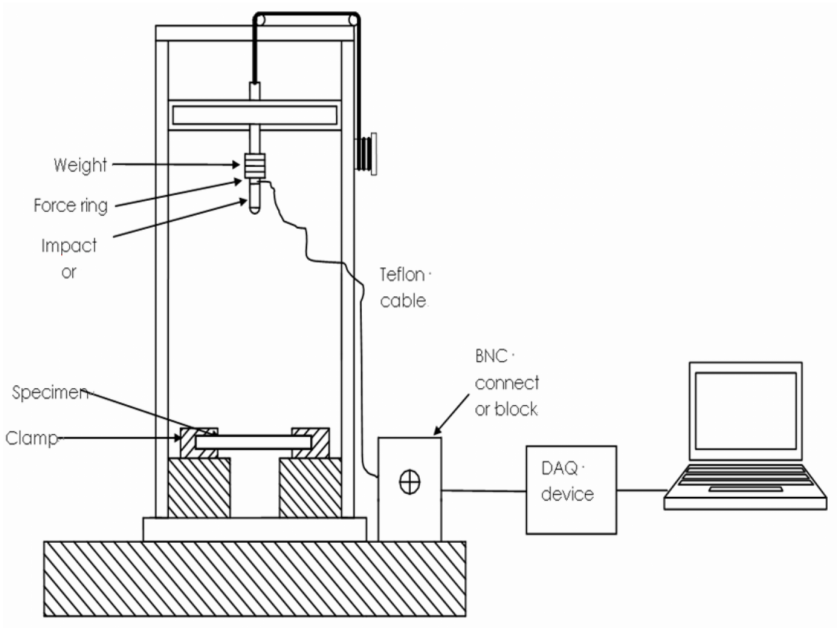


Figure 3.6: Schematic of Droptower Impact Machine [43]

The main difference in the two impact tests is that in SHPB, the load is transferred to the specimen through the incident bar which the striker hits and the droptower impact test induces contacts between the specimen and the impactor head directly.

Another difference lies in the measurement capabilites of each methods. For the case of SHPB, the waves are measured by strain gauges mounted on both the incident and the output bar, also known as the transmitted bar. Through the strain gauges, they track the waves that pass through the different bars [7, 44]. On the other hand, the droptower measures the force at the impactor, with strain gauges usually mounted with the impactor.

It is an understatement to say that SHPB is much more capable to capture the strain-rate effect of the specimen. The SHPB is specifically designed to measure the stress and strains which the specimen experiences during the impact loading. This allows for more specific and precise investigation of the specimen at a defined strain-rate. On the other hand, the droptower only provides an indirect measurement of what specimen experiences, as oftentimes, the only measurement that can be obtained from droptower is the force which the impactor experiences. Along with the differences in the measurement, controlling the strain-rate which the specimens are be subjected to is also significantly different. The SHPB controls the strain-rate directly through controling the loading pulse, which is governed by the striker conditions such as the speed and geometry. On the other hand, the droptower measures the strain rate through the impact velocity and the specimen geometry. In this work, the droptower was used as it was available at the university lab. More information on the droptower impact machine at the universtiy is be elaborated on in chapter 5.

3.5.2. Boundary Conditions

Another important aspect of the impact test is the boudnary condition of the composite materials. The aim of this thesis is to investigate the failure behavior of the composite material when subjected to impact condition. Therefore, a set-up that can ensure that these behaviors can be accurately observed is of importance for this work. In this section, different examples of the set-up for the on-edge testing from the literature are be presented.

One of the most commonly observed phenomenon when working with impact is the buckling of the structure. Buckling is defined as a structural phenomenon where a thin-walled structural member experiences structural instability through a shape change, deforming in the out-of-plane direction when subjected to a load that is below its material strength limits [33]. For a droptower impact testing, the specimens are usually prone to buckling if the specimen is a thin-walled structure, which is the case for this thesis, as the specimens have very small thickness. Additionally, as the buckling is also a form of absorbing energy, if the specimen buckles, the material failure behavior may not be captured fully. Therefore, it is necessary to utilize the fixture in order to prevent buckling of the specimen.

All the works that are referred to in this work have a fixture to prevent buckling [24, 36, 23, 42, 35, 2, 15, 21, 27, 16, 22]. Figure 3.7 is an example fixture from the work of W. Xu et al. [42].

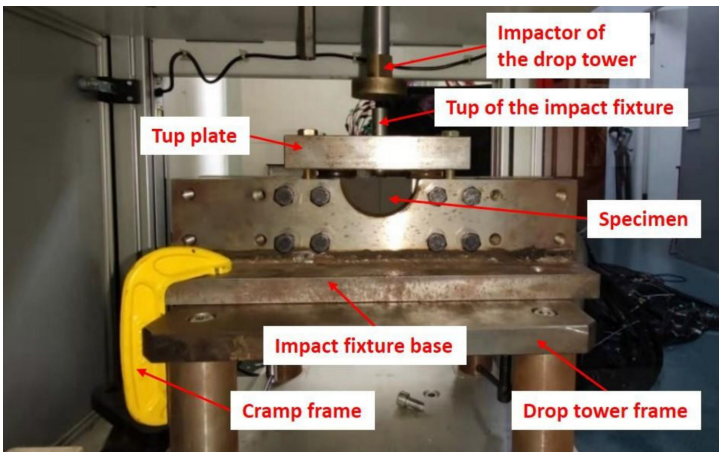


Figure 3.7: Example Set Up of the Fixture [42]

The main goal of the fixtures is to ensure that the plate does not buckle, thus they constrain the plates in such a way that the plate does not buckle and the specimen absorb impact completely. In the case of Figure 3.7, all six degrees of freedom are constrained through the means of bolts. Another example that is also used often is presented in Figure 3.8.

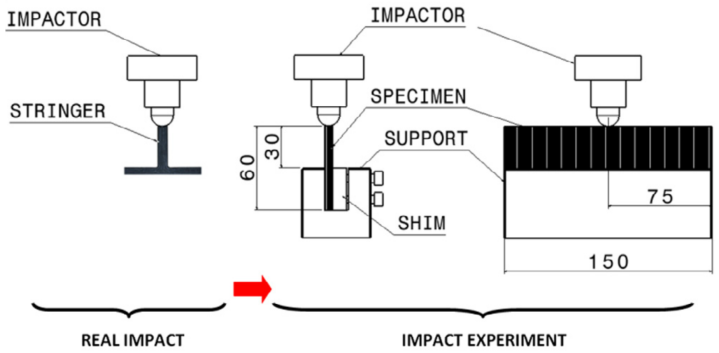


Figure 3.8: Example Set Up of the Fixture [23]

The example in Figure 3.8 is testing for the on-edge impact of a stiffener. On-edge impacts are oftentimes discussed when analyzing the impact response of the structural element within the aircraft that could be damaged during maintenance for example [23]. Regardless, this set-up also aims to isolate the structural behavior and capture the material response of the specimen only. In this set-up, the entire bottom half is clamped to prevent it from buckling.

It is also of importance to ensure that the fixture does not hinder the material's repsonse to the impact. To make sure that the fixture does not hinder the response to impact, it must be verified that loading causes a localized failure on the specimen. The impact has very localized effects on the specimen with minimal global elastic deformation [36]. If the specimen is subjected to impact in the right manner, the energy must be absorbed through the local failure mechanism [36]. Indeed in the past works referred for this thesis work, the results portray localized respones to impacts and minimal global elastic response. Figure 3.9 and Figure 3.10 present the impact result of the set-up presented in Figure 3.7 and Figure 3.8, respectively.

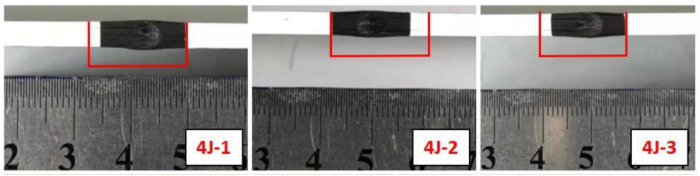


Figure 3.9: Impact Result of the Example Set Up [42]



Figure 3.10: Impact Result of the Example Set Up [23]

Therefore, keeping this in mind, the fixture to be set-up for this thesis should ensure that the damage is induced correctly.

3.5.3. Impactor Head

Impactor head is one of the factor that are used to categorize the responses. As mentioned, oftentimes the work for impact tests are generally done for CAEI, and for this purpose, it is of extreme importance to concentrate the impact to a point, leading the preferred impactor to be a hemispherical impactor.

Majority of the works mentioned in this chapter uses hemispherical impactor, to induce impact in a very localized manner. It must also be highlighted that the hemispherical impactors are also much easily accesible at the lab. However, as it has a specific point which the load will be concentrated aiming the specimen in the correct manner might be challenging. Unfortunately, none of the work browsed made use of a flat impact, besides the SHPB. Thus this work will be able to bridge the gap between the conventional droptower impact testing and SHPB, by using flat impactor on a droptower.

4

Research Proposal

4.1. Introduction

Characterizing impact loading response of composite materials have been investigated thoroughly in the past. Unfortunately, previous efforts have only been in investigating the impact in the out-of-plane direction of the composite plate as mentioned during the literature review. On-edge loading on the other hand, which is the impact loading in the in-plane direction has hardly been investigated. This section presents the research motivation, research objectives and scientific novelties of this work, contributing to bringing the gap of understanding on-edge impact closer.

4.2. Research Motivation

Currently the aerospace industry performs a lot of on-face impact testing using hemispherical impactors to characterize composite material's response to impacts. In the event of a 16g dynamic crash scenario, the structures are not only subject to on-face impact but also on-edge impact. This thesis is dedicated to bridge the scentific gap in characterization of composite material subjected to on-edge impact.

The main motivation behind a lot of the impact tests of composite material is to capture the strain-rate behavior. Characterizing the strain-rate effects of composite materials however, typically requires expensive, high-end equipment like Split-Hopkinson Pressure Bar(SHPB) as highlighted in the previous chapter. However, for low velocity impacts, a SHPB may be an overkill. Therefore, presenting a method to easily capture the strain-rate behavior would add significant values.

Another important player in the impact testing is the impactor's shape, which is often a hemisphere. Using a hemispherical impactor for the impact testing introduces complex geometric challenges, as the impactor sinks into the material, the contact area changes constantly. This makes it difficult to isolate the intrinsic material response from the extrinsic contact mechanics. It is also extremely difficult to ensure that the impactor head hits the desired position, as the impactor's position may deviate during the freefall and the impact. Thus, in this work, an impactor which could induce impacts in a manner such that the material's intrinsic strain-rate response is captured accurately.

Looking further, this work contributes to another step closer towards implementation of the thermoplastic composite materials to different structures in the aircraft. Working with coupon-level testings and gaining preliminary understanding of the material's behavior is a key baseground to move on to different stages in the design phase, as depicted Figure 4.1.

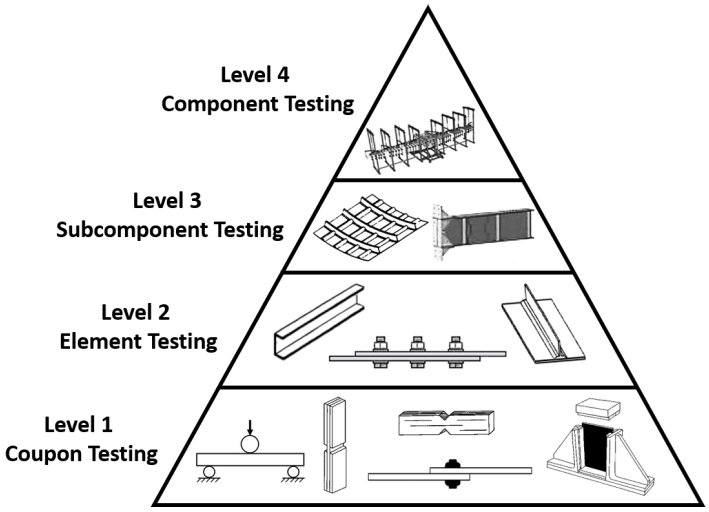


Figure 4.1: Aerospace's building block approach [10]

In conclusion, the scientific gaps to be investigated in this work is clear. **First, there needs more investigation of how the on-edge impact influences the strain-rate effects of composite materials. Second, an affordable, fast, easier test set-up is necessary in order to speed up the implementation of composite materials in aircraft structures.** In the next sections, the plans and logistics of how these gaps can be brought closer is discussed.

4.3. Steps Towards Research Objectives

This section introduces the three major steps to be taken to meet the research objectives established previously. For more details on the methodologies, refer to chapter 5.

Step 1: Static Compression Loading

The static compression test is performed in order to establish a preliminary mechanical understanding of the coupons and to make a comparison between the material's performance when it is subjected to quasi-static loading and dynamic loading. The tests are done using the Zwick UTM located at the Vliegtuighal and the force-displacement curve is obtained.

Step 2: Drop Tower Impact Loading

After successful quasi-static tests, the droptower is used to induce impact loading to the specimen. Different impacts are induced with the droptower at different heights, inducing different impact energies and impact velocities. High-speed camera are used to reocrd the impact event, which is used to analyze the response of the specimen and the impactor during post-processing.

Step 3: Post-Processing and Analysis

After obtaining the necessary data from the experiments, post-processing and analysis take place to draw conclusions. During the post-processing, different variables such as, force, displacement, time, stress, strain, energies, and impulse are obtained to assess if the set-up is suitable to achieve the research objectives defined earlier. For more details on the post-processing and analysis, refer to chapter 5 and chapter 6.

4.4. Scientific Novelty

This work aims to investigate the strain-rate effects of the CF/PPS subjected to on-edge impact. There exists a lot of literature about out-of-plane impacts. In-plane impacts are also significantly important to fully characterize and understand the mechanical behavior of a material. Therefore, this work contains scientific novelties, to contribute to further understanding of impact loading, specifically, on-edge impact. To explicitly highglight, this thesis work aims to present the following three scientific novelty.

1. **Investigation of the on-edge impact of composite materials**
2. **Investigation of the effects of flat impactor on on-edge impact of composite materials**
3. **Investigation of impact induced strain-rate effects on composite materials**

4.5. Conclusion

In conclusion, the gaps are clear and straightforward: there needs more data on on-edge impact starting, which requires understanding of strain-rate behavior of composite materials and there needs cheaper and faster method to characterize the on-edge response. Following sections define the specifics of the experiment methodologies and analysis of the results.

5

Methodology

5.1. Introduction

This section presents the methodology used in this thesis work. Establishing and assessing a new methodology to assess the on-edge impact behavior of the specimen is a major part of this thesis work. Starting from defining the required outcomes from experiments, the boundary condition which allows for those required outcomes to be obtained are presented. Major efforts are dedicated to preliminarily assessing and justifying the choices made for the boundary condition. Then the details of the specimen and impactor used for the thesis work, from its basic material properties to the sizes are defined. Finally, the test procedures, including the equipments used for the tests and test matrix are presented.

5.2. Required Outcomes

The main objective of this thesis is to present a method and to investigate the on-edge impact loading of CFRP. To investigate the impact behavior is to understand, how different loading speeds affect the response of the material. The question to be answered is: what variables could be used to compare the material's response?

To answer this question, it is important to go back to the pyramid approach mentioned in chapter 4. The role of this work in the pyramid approach is to provide a preliminary understanding of the material through an affordable method. Through the understanding of the material, further works can be developed to ensure that the material can be a part of the aircraft structures. First step towards this would be get an understanding of how much force and energy the material can take for both quasi-static tests and impact tests to ensure its performance during possible crash events.

From the standard quasi-static tests, the Force vs. Displacement curves are obtained. Using this data, the energy which the specimen absorb during the loading can be calculated simply by identifying the area under the curves. Further processing this curve, the Stress-Strain curves can be obtained, allowing for the calculation of the Young's modulus of the specimen, which could be used to verify the proposed boundary condition can capture the material behavior correctly. The stiffness information of the specimen would also be relevant for analysis during the impact, to assess the wave propagation through the specimen.

Moving further, a handful of information can be obtained from the impact tests as well. Firstly, the energy absorbed by the specimen can be calculated. The lab at TU Delft unfortunately, do not have any resources available to track the energy of the impactor before and after the impact nor the energy absorbed by the specimen during the impact. Therefore the energy analysis must be performed using a high-speed camera and tracking the frames, calculating the velocity of the impactor before and after the impact. Next the Force vs. Time curve of the impactor per different heights can also be obtained from the droptower. This information would be essential to understand the strain-rate behavior of the specimen in terms of force.

With these information, the thesis work evaluate the set-up proposed to assess its performance in

investigating the on-edge impact behavior of a composite material. The following sections detail how these specific outcomes are obtained as well as the procedure for setting up the experiment.

5.3. Boundary Condition

In this work, the specimen are subjected to compression on the edge. Therefore, the typical compression test from ASTM standard, the ASTM D6641 is not a suitable method for this work, since the edge is not exposed to be loaded. Figure 5.1 presents the ASTDM6641 for reference.



Figure 5.1: ASTM D6641 [8]

With the boundary condition like Figure 5.1, it is challenging to subject the specimen's edge to high strain-rate loading. In this work, the boundary condition which allows the edge to be impacted is required. Figure 5.2 presents the potential designs considered prior to starting the experiment campaign.

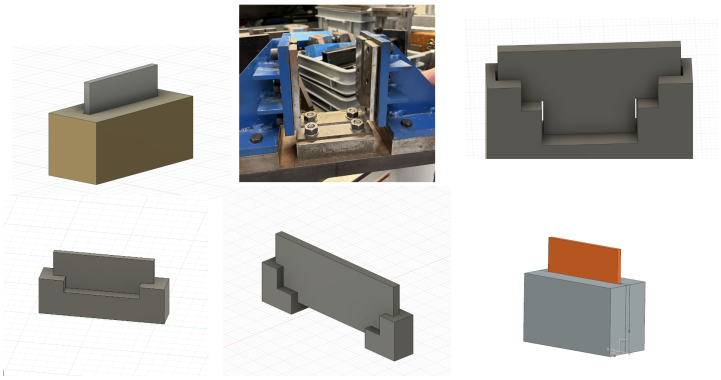


Figure 5.2: Design Iterations

The main requirement for the boundary condition is that the boundary condition should expose the specimen for loading and to hold the specimen vertically in a stable manner during the loading. It should also be wide enough that it does not tip over upon the loading. The final design shown in Figure 5.3 is decided as the final design. This design allows the user to clamp the specimen for different thicknesses and hold the specimen in a stable manner.

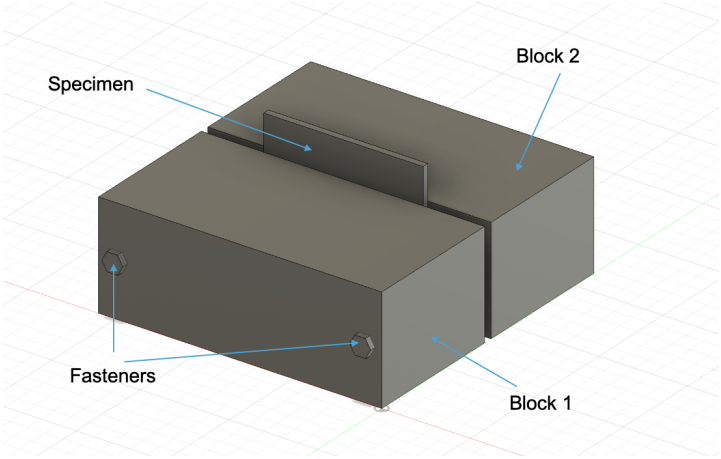
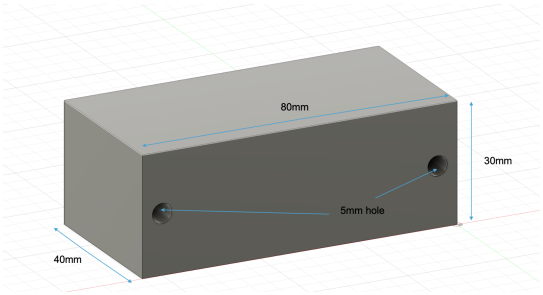
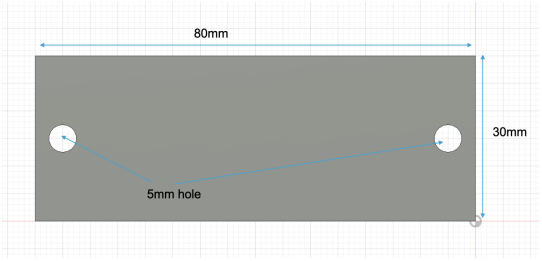


Figure 5.3: Final chosen boundary condition, CAD Model

The presented boundary condition consists of two blocks and two fasteners. The first block has two holes going through the entire block. Note that the holes through the block are smooth, to ease the inserting of the fasteners through the block.



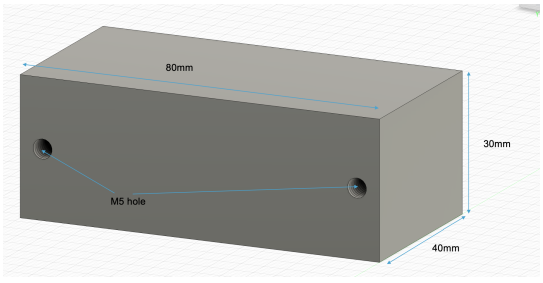
(a) Block 1



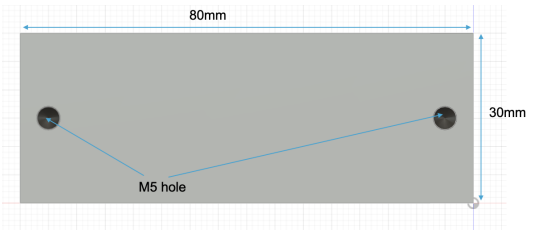
(b) Block 1 cross-section view

Figure 5.4: Block 1 CAD model

The second block has a hole that has been threaded for the fasteners so the block can be tightened together. In order to ensure the uniform gaps between the blocks for all tests, washers of thickness $2mm$ were inserted through the fasteners between the blocks. This entails that for future studies with different specimen of different thickness can also be tested with this boundary condition, just with different washers to match the thickness.



(a) Block 2



(b) Block 2 cross-section view

Figure 5.5: Block 2 CAD model

Figure 5.6 presents the exploded view of the assembly of the boundary condition.

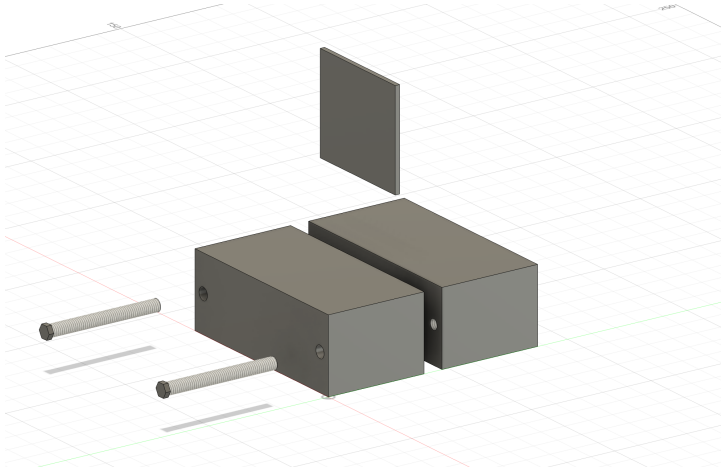


Figure 5.6: Boundary condition assembly

Figure 5.7 presents the free body diagram of the specimen during the loading case.

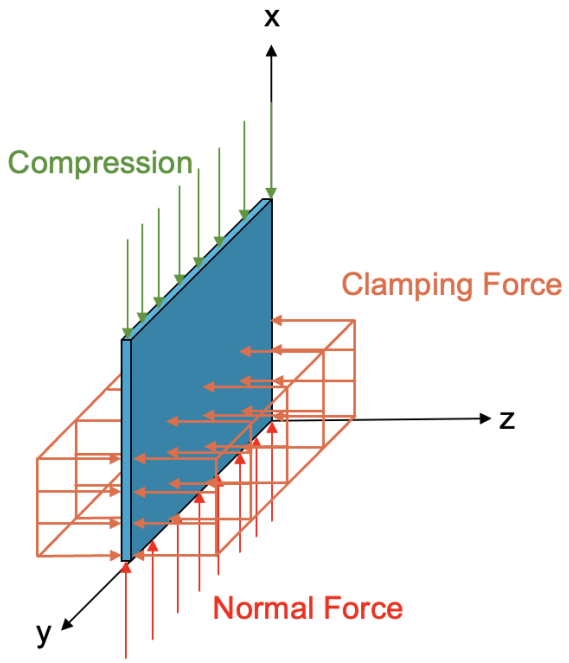


Figure 5.7: Free body diagram of the specimen

Diving into more details of the boundary condition, the clamping force is also be determined. In the earlier stage of the work, it was considered to not fully clamp the specimen, to allow the specimen to be supported by the blocks and stands, but no sufficient friction acts on the specimen to dissipate energy during the impact loading. Upon running some preliminary tests, the Force vs. Time curve obtained from the droptower provide no physical significance which could be used for analysis. Figure 5.8 presents the Force vs. Time curve from the droptower.

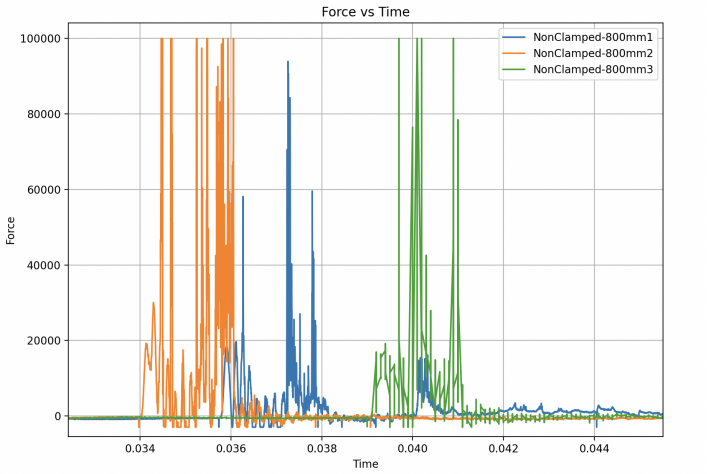


Figure 5.8: Force vs. time curve of the preliminary impact tests with unclamped specimen, dropheight $800mm$

As clearly seen, there exists no similarities between the three test runs despite the same testing conditions. The force is also measured to reach $100kN$, in fact, possibly even more since $100kN$ was the upper limit of the machine. A $100kN$ force for a specimen with the area of $1.85mm * 45mm$ is equivalent to a stress of $1.20GPa$. This is an unreasonable amount, as the peak stress during tension is found to be $578.26MPa$. This could be due to the vibration caused during the impact loading. Therefore, despite the fact that friction energy takes a small part of the calculated energy consumed by the specimen, it is decided to clamp the specimen in the end.

In the end, it was decided to fully clamp the specimens. The clamping force must be sufficient to hold the specimen tightly during the loading case, in case the specimen moves during the impact loading. If the specimen moves or deforms slightly, friction may dissipate some energy, and it is important to be aware of the possible effects of friction. The possible energy dissipation and the clamping force are closely related, as the energy dissipated is dependent on the clamping force. Thus, along with the clamping force calculation, possible energy dissipation due to the friction which the clamping force would induce, are calculated.

To simplify the calculations, equivalent static model is used. This approach neglects transient phenomena such as inertial effects, stress-wave propagation and structural vibrations, for a preliminary understanding the approach is reasonable. Note that the peak loads from the preliminary tests yielded that both the quasi-static and impact tests had an average maximum force of $23kN$. This similarity indicates that the specimen experiences comparable peak loading under both conditions, providing further justification for using the equivalent static model as preliminary step.

The set-up of the static model is simplified as present in Figure 5.9. The friction force which acts on the specimen is assumed to be a distributed load along the specimen.

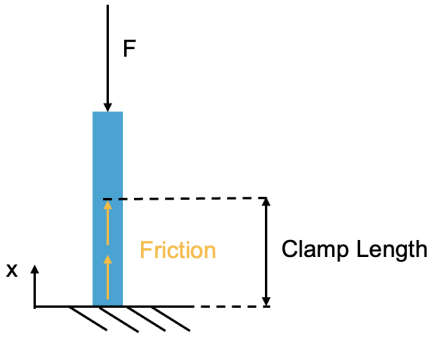


Figure 5.9: Simplified set-up of the specimen during the loading case

The deformation of the specimen can be calculated using Equation 5.1, where $P(x)$ is the normal force experienced by the specimen, E is the elastic modulus of the specimen, A is the cross-sectional area of the specimen, F is the load applied, and q is the the friction distributed load in unit of force per length.

$$u(x) = \int_0^x \frac{P(x)}{EA} dx \tag{5.1}$$

$$u(x) = \frac{1}{EA} \int_0^x (F - qL_{clamped} + qx) dx \tag{5.2}$$

Performing the integration, the following expression is obtained.

$$u(x) = \frac{1}{EA} \left[(F - qL_{clamped})x + \frac{qx^2}{2} \right] \tag{5.3}$$

Then the work done by the friction force can be calculated by integration.

$$W_{friction} = \int_0^{L_{clamp}} qu(x) dx = \frac{F_{friction} L_{clamp}}{EA} \left(\frac{F}{2} \frac{F_{friction}}{3} \right) \tag{5.4}$$

$$W_{friction} = q \int_0^{L_{clamp}} \left[\frac{1}{EA} \left((F - qL_{clamp})x + \frac{qx^2}{2} \right) \right] dx \tag{5.5}$$

In order to quantify the friction, it is first needed to identify the normal force exerted by the clamps. The normal force is calculated by simply performing force equilibrium of Figure 5.10.

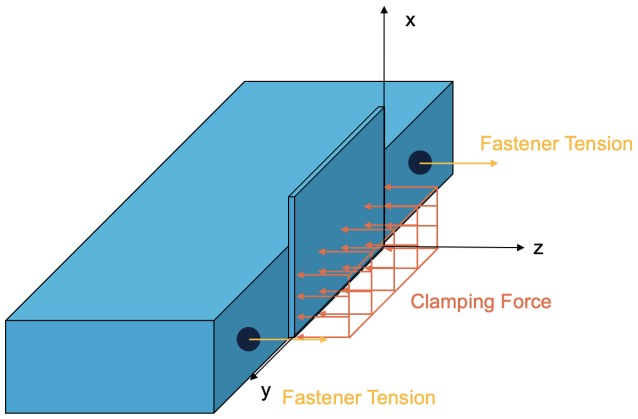


Figure 5.10: Free body diagram to calculate the clamped force

Then it yields the Equation 5.6, where $F_{fastener}$ is the tension of the fastener and the N is the clamping forces.

$$\Sigma F \rightarrow + : 0 = 2 * F_{fastener} - N \tag{5.6}$$

Fastener tensions are calculated using the Equation 5.7, which is a commonly used equation to calculate the tension force of a fastener for a torque applied to the fastener [3]. T is the torque applied to the fastener, which is measured by the torque wrench, K is the torque coefficeint of value 0.2 [3], and d is the diameter of the fastener. The torque value was measured using the torque wrench Garant 656050, with a possible measuring error of ±4% [25].

$$F_{fastener} = \frac{T}{Kd} = \frac{3Nm}{0.2 * 5 * 10^{-3}m} = 3000N \tag{5.7}$$

Torque value of $3Nm$ is also often used for similar fasteners in ASTM standards and was the maximum torque which could be applied with bare hands. Then the clamping force is calculated to be $6000N$ using Equation 5.6. The friction force is calculated using Equation 5.8, where μ_k is a dynamic coefficient of friction. Note that the friction force is mulitplied by 2 as there are two surfaces which the friction acts on. Coefficient of friction is found to be 0.28 [4].

$$F_{friction} = \mu_k * N * 2 = 0.28 * 6000 * 2 = 3360N \tag{5.8}$$

$$\begin{aligned} W_{\text{friction}} &= \frac{F_{\text{friction}} L_{\text{clamp}}}{EA} \left(\frac{F}{2} - \frac{F_{\text{friction}}}{3} \right) \\ &= \frac{3360\,\text{N} \cdot 30 * 10^{-3}\,\text{m}}{25.5 * 10^{9}\,\text{Pa} \cdot 1.85 * 10^{-3}m \cdot 45 * 10^{-3}\,\text{m}} \left(\frac{23 * 10^{3}\,\text{N}}{2} - \frac{3360\,\text{N}}{3} \right) = 0.49J \end{aligned} \tag{5.9}$$

The energy dissipated through the means of friction is $0.49J$. This preliminary calculation provides a first-order estimate of the work dissipated through friction. As the peak load governs this value and the peak loads are similar for both quasi-static and impact tests, it is expected that the work done by friction during impact test would be in similar order of magnitude.

At this stage for the given set-up, effects of friction is inevitable and one should be aware that friction plays a small role in the energy measured. Unfortunately, the current set-up does not allow for easy quanitifcation of possible energy dissipated by the friction.

5.4. Specimen

The specimens are obtained from one of the manufacturing site of Collins Aerospace here in the Netherlands. These are scrap materials therefore the information on manufacturing process such as the pressure, or the temperature at which the specimens were manufactured is not available. The material of the specimen is a Carbon fibre Reinfoced Thermoplastic, Toray Cetex TC 1100 Polyphenylene Sulfide. The laminate has a six layer of 5HS-woven fabric, with (0/90) and (±45) taking 66.7% and 33.3% of the total layup respectively. Specific layup information is not discussed as requested by Collins Aerospace. Total thickness of the specimen is 1.85mm.

From a previous student's work, basic parameters of the materials are already identified. Table 5.1 presents the summary of relevant information.

Table 5.1: Material Properties [37]

Property	**Value**
Young's Modulus	25.5 GPa
Peak Stress	578.26 MPa
Weight per Ply	496 g/m^2
Resin Content (by Weight)	43%
Consolidated Ply Thickness	0.31 mm
Density	1.55 g/cm^3

The specimen were in random shapes, thus, using CompCut ACS-600, the specimen are cut into deisred shapes. Details of the specimen sizes are discussed later in this section. The CompCut ACS-600 employs a thin diamond-coated circular saw blade with cooling water to minimize heat generation, residual stresses and other defects that could be introduced during cutting.

Commenting on the desired shape of the specimen, this is one of the major part of the design process of this thesis work. There are some physical design constraints due to the droptower set-up. The Zwick 250kN does not impose any physical requirements on the test set-up, but the droptower tests impose two major constraints. Firstly, the impactor which can be mounted to the droptower could have a maximum diameter of 60mm. Considering this constraint and taking into account that the impactor's final position might deviate, the specimen width is decided to be 45mm.

Secondly, the specimen must be shorter than 80mm due to the small gap between the table and the impactor. Therefore, a short but sufficiently tall specimen should be used for testing. To meet this requirement and also to prevent buckling, the total height of the specimen is decided to be 40mm with 10mm exposed above the clamp blocks. 10mm would also be a sufficient distance to capture the localized impact behavior of the specimen, based on the literature, as the damage depth is less than 5mm for an impact using almost triple the energy which the specimen will be subjected to [23].

In addition to the literature study, some preliminary calculations are performed to justify the length. By simplifying the plate as a column, the Euler buckling equation is used to estimate the critical buckling load. For this work, the boundary condition clamps the specimen on one end and other end is loaded. As the loaded edge will not be able to translate, the Pinned-Fixed case would be the best representative of experiment set-up for this work. Therefore the following equation is used. The equation is retrieved from the textbook Aircraft Structures by T.H.G Megson [18].

$$P_{cr} = \frac{\pi^2 E I_{xx}}{(0.69992 * L)^2} \tag{5.10}$$

Substituting the values, the following calculation is obtained.

$$P_{cr} = \frac{\pi^2 E I_{xx}}{(KL)^2} = \frac{\pi^2 E * \frac{1}{12} b h^3}{(0.69992 * L)^2} = \frac{\pi^2 * 25 * 10^9 * \frac{1}{12} * (45 * 10^{-3}) * (1.85 * 10^{-3})^3}{(0.69992 * 10 * 10^{-3})^2} = 119588.5N \tag{5.11}$$

As the calculation for the buckling is much greater than the maximum force in the tension loading case, the length choice is deemed to be safe from buckling.

Note that the characteristic length used in the calculation is the height of the specimen exposed above the boundary condition as shown in Figure 5.11, expressed by L. The final dimensions of the specimens are presented in Figure 5.11.

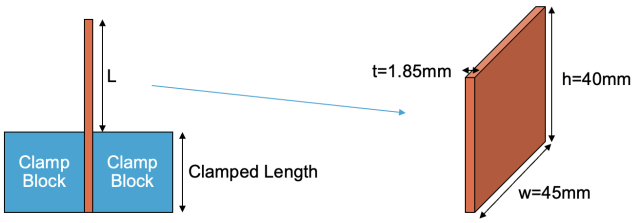


Figure 5.11: Schematic of the specimen set-up

5.5. Impactor

In order to subject the specimen to on-edge compression for the entire specimen, a flat impactor is needed. Unfortunately, none is available at the TU Delft, thus a new impactor is manufactured for this thesis. The size of the impactor also influences the size of the specimen as the specimen should be smaller than the impactor in order to induce full on-edge compression.

The impactor diameter is chosen to be $60mm$, which is the maximum diameter allowed for the droptower. Next, the height of the impactor is decided. This too, is constrained by the droptower. The common height used for the droptower at the lab is $30mm$ and this is used for the impactor height. Next, the diameter for the threads is also decided. Again, this is governed by the droptower's specification, which is M10. Finally, the depth of the thread, is also governed by the droptower, which was about $15mm$. In order to ensure that it fits, the depth of $20mm$ is chosen. Figure 5.12 presents the CAD model of the impactor and the Figure 5.13 presents the manufactured impactor.

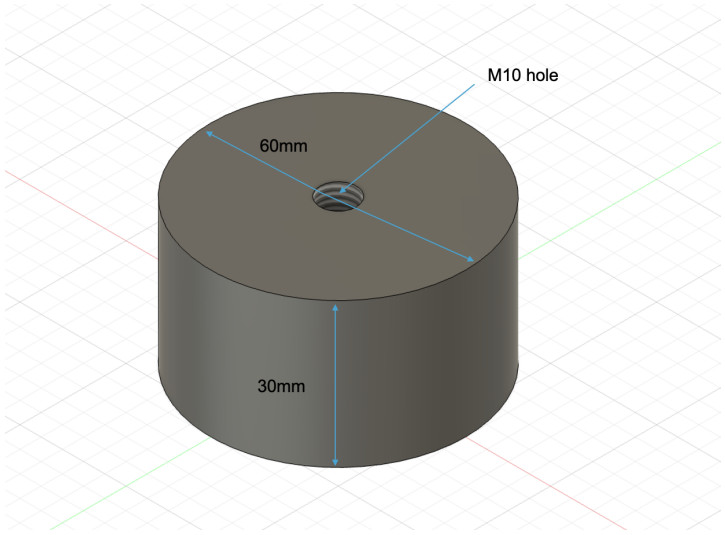


Figure 5.12: Impactor CAD model

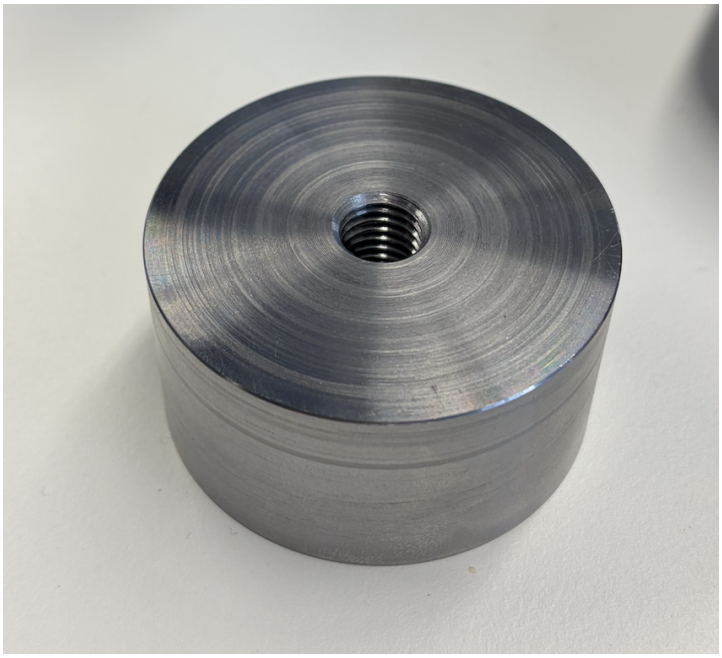


Figure 5.13: Manufactured impactor

Along with dimension, the most important part of the impactor is the material which the impactor is made out of. As the impactor is designed to be striking the specimen in the on-edge direction, which is the direction which the material has the greatest stiffness, the impactor must be much stiffer than the specimen to prevent any possible deformations. Based on previous student's work, the specimen provided for this thesis work has a Young's modulus of $25GPa$. The aim is to use the material that is much greater in stiffness for the impactor. The off-the-shelf material at the TU Delft manufacturing site is used, which is the Uddenholm Impax Supreme, with the Young's modulus of $205GPa$, with density of $7800kg/m^3$.

5.6. Required Equipments

For the equipments required to carry out the experimental work, the section is divided into two sections: quasi-static and impact tests. This section details the equipments needed for each tests.

5.6.1. Quasi-Static Tests

For the quasi-static test, the Zwick 250kN at the faculty is used. Figure 5.14 is a picture of the machine. Loading speed of $2mm/min$ is used. Displacement controlled experiment is a better fitted method for this test set-up, as it allows for stable data collection up until failure.



Figure 5.14: Zwick 250kN static test machine

Regarding the different quasi-static test runs and test procedure, refer to section 5.7.

5.6.2. Impact Test

For the impact test, the TU Delft's in-house built droptower as shown in Figure 5.15 is used. Like any other droptower for impact testing, the droptower drops the impactor from a chosen height.



Figure 5.15: Droptower at TU Delft

The droptower has a catching mechanism in order to prevent the impactor from hitting the specimen multiple times. Figure 5.16 highlights the catcher and Figure 5.17 presents the steps of this mechanism. In Step 1, the catcher is not yet released and the impactor drops down to hit the specimen. Then in Step 2, the impactor hits the specimen. As the impactor bounces up and goes through the sensor for the second time in Step 3, the sensor releases the catcher and catches the impactor as it drops back in Step 4.

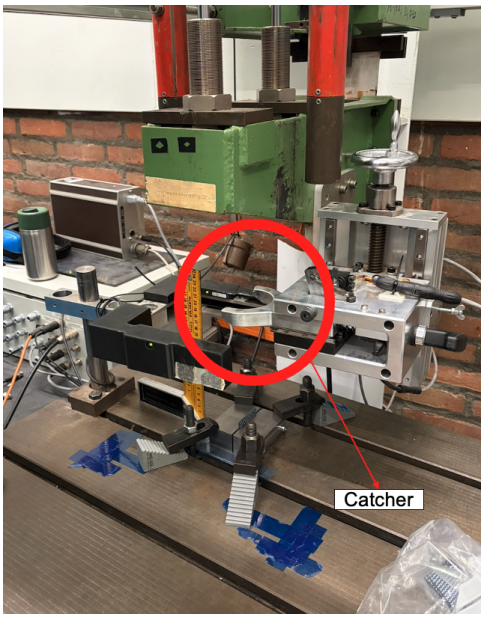


Figure 5.16: Impactor catcher

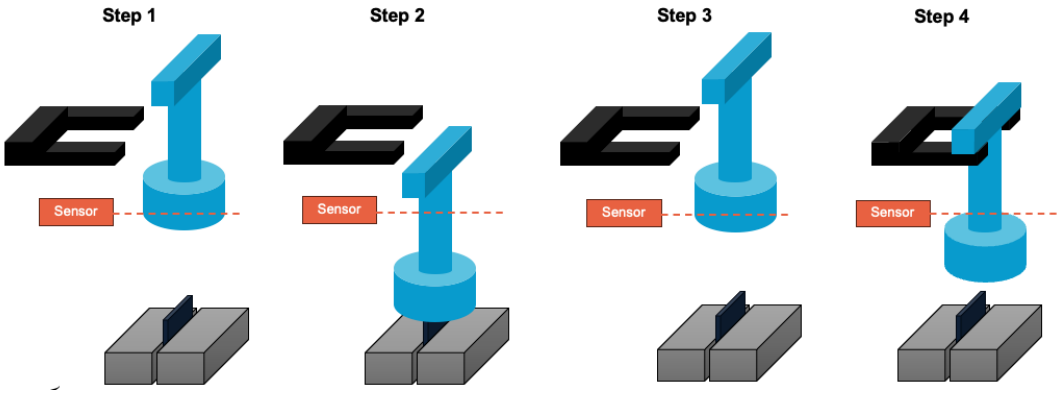


Figure 5.17: Impactor catcher mechanism illustration

The droptower drops the so-called impactor dart to the specimen. The dart consists of three parts, namely the rod, load cell, and the bottom threads, where the impactor is screwed onto. Figure 5.18 presents the picture of this dart.

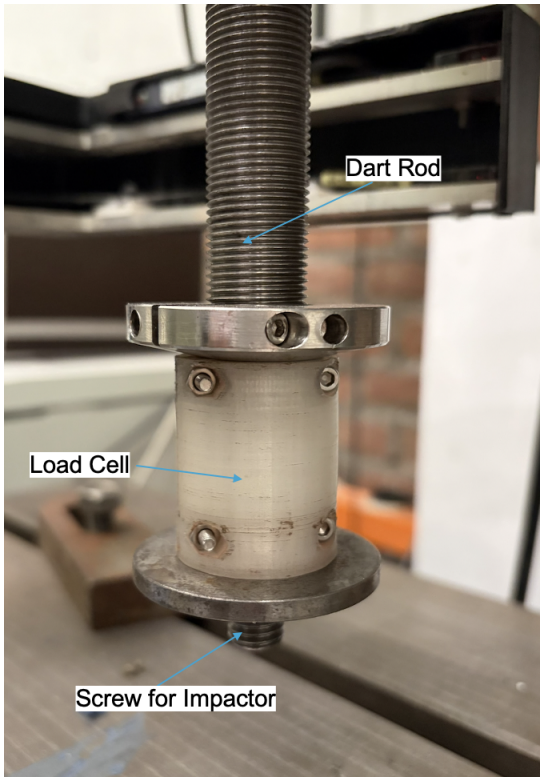


Figure 5.18: Impactor dart

The total mass of the dart is measured to be 2.3kg, including the mass of the impactor of 652.4g of impactor.

Below the droptower is a table, where the specimens are placed. In order to ensure that the boundary conditions is correctly mounted on the table, the clamps were used, restraining all six degrees of freedom. Refer to Figure 5.19 to see how the boundary condition is mounted on the table.

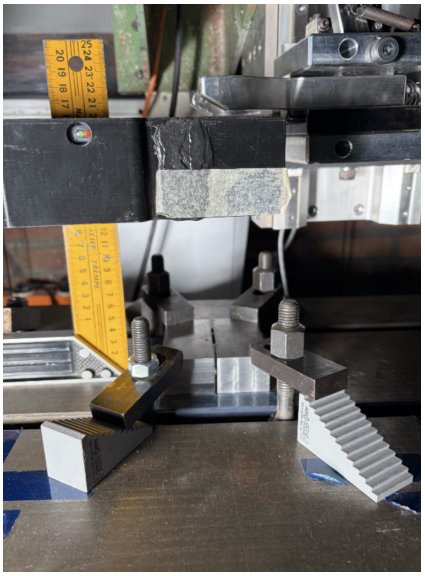


Figure 5.19: Boundary condition set-up

Next section is dedicated to elaborate on how these equipments are used to achieve the research goals of this thesis work.

5.7. Test Procedure

With the test equipments and the specimen specifications defined, the test procedures can be detailed. This section presents the steps to be taken for the experiment campaign, for both quasi-static and impact tests.

5.7.1. Quasi-Static Tests

For the quasi-static test, the Zwick 250kN is used. To eliminate any discrepancies of the machine, first, the machine compressed the compression head and the bottom floor without the specimen as depicted in Figure 5.20. The run was conducted until $100kN$, which is far beyond what the coupon could take.

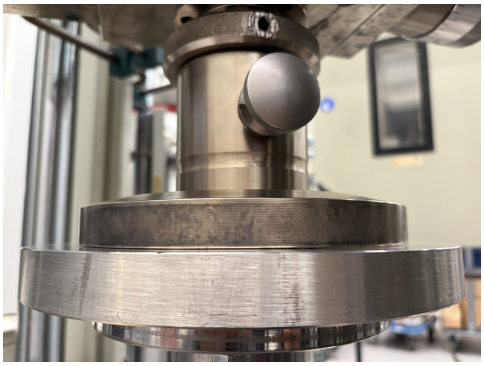


Figure 5.20: Settlement Run

After the first run, which should have closed the gaps and other discrepanices in the machine, the machine is once again run without the specimen up until $50kN$, to measure the compliance machine.

Essentially, the experiment set-up can be assumed to be two springs in series as shown in Figure 5.21. The measured displacement and force from the machine is of both machine and coupon, therefore the machine's contribution must be subtracted from the measured quantities. Therefore this compliance runs helps meausre the stiffness of the machine, which is later be used to obtain the coupon-only data.

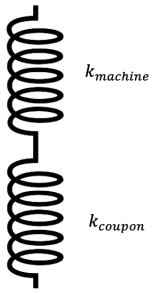


Figure 5.21: Simplified Representation of the Quasi-Static Set-Up

After the compliance run, the specimen is placed under the compression head as present in Figure 5.22. It is important to ensure that the specimen is located in the same orientation at all times, to ensure the repeatability of the results. The standard quasi-static test speed, $2mm/min$ is used to carry out the tests.

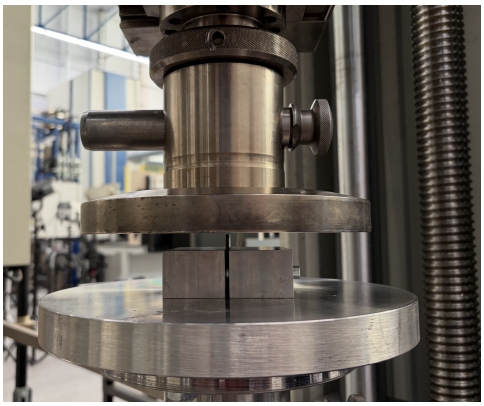


Figure 5.22: Quasi-Static Test Set-Up

This concludes the test procedure for the quasi-static tests. Throughout the tests, one must pay attention on the failure modes and the position of the set-up to establish repeatbaility of the tests.

5.7.2. Impact Tests

The main aim of the impact test is to subject the specimen to strain-rate loading. Therefore, choosing which height the impactor should be dropped from is a key to this test. In order to have a preliminary understanding of the height which it should be dropped from, the energy conservation method is used.

$$E_{initial} = E_{final} \tag{5.12}$$

$$\frac{1}{2} m_{impactor} v_{before}^2 = E_{specimen} + \frac{1}{2} m_{impactor} v_{after}^2 \tag{5.13}$$

$E_{initial}$ is the energy of the system before the impact event, and the E_{final} represents the energy of the system after the impact. $m_{impactor}$ is the mass of the impactor, v_{before} is the velocity of the impactor before the impact, $E_{specimen}$ is the energy specimen absorbed during the impact, and v_{after} is the velocity of the impactor after the impact.

$E_{specimen}$ is determined during the quasi-static testing by identifying how much energy is absorbed by the specimen until the failure point.

$$E_{specimen} = \frac{1}{2} m_{impactor} v_{after}^2 - \frac{1}{2} m_{impactor} v_{before}^2 \tag{5.14}$$

To contribute to research objective of comparing the quasi-static and impact loading, subjecting the specimen to same energies in both cases is essential. Unfortunately, after many attempts and also referring to momentum approach, it was not possible to analytically identify the height at which the impactor should be dropped from, as both v_{after} and $E_{specimen}$ are to be obtained through measurement after the impacts. Therefore, trial-and-error is the only way to identify the correct height to drop the impactor from. A lot of specimens are sacrificed for this purpose.

Moving on to the final set-up, the specimen is inserted between the clamp blocks as shown in Figure 5.23.

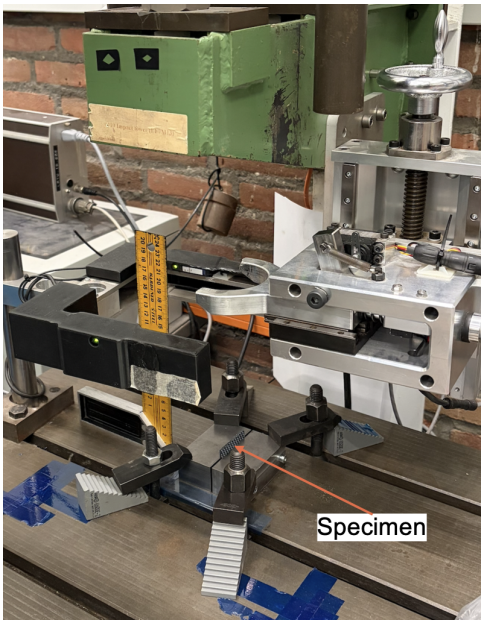


Figure 5.23: Impact test set-up

In order to capture the better resolution pictures with the highspeed camera, the set-up is also illuminated.

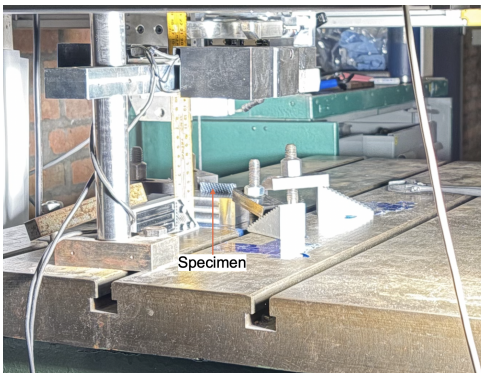


Figure 5.24: Impact test set-up

5.7.3. Tips and Tricks

It is extremely important that the loading condition stays the same for all the specimen. Especially in this test set-up, where the alignment of the compression head and the specimen will differ if the specimen is placed differently per trial, it could have a significant influence on the failure modes and

the Force vs. Displacement curves. Therefore, it is highly recommended to draw lines or use tapes to mark the specific position to show how the specimen is positioned.

5.8. Measurement Techniques

Both quasi-static and the impact tests measure various variables from the experiments. In this section, the measurement methods for both quasi-static tests and impact tests are detailed.

The quasi-static tests provides a Force vs. Displacement curve which is used to calculate the energy absorbed by the specimen. In displacement controlled test, the crosshead is driven at a prescribed displacement rate, while measuring the force constantly throughout the loading. Refer to Figure 5.25 for reference.



Figure 5.25: Zwick 250kN static test machine

Moving on to the impact test, to capture the energy before and after the impact, the high-speed camera is placed directly in front of the impact set-up. The high-speed camera has a frame rate of 6400fps and captures a black and white picture of the impact test set-up. With the framerate and tracking a point of the impactor, the speed of the impactor before and after can be calculated. For reference, to identify the size of a pixel, a ruler is also placed next to the set-up. Figure 5.26 is an example frame showing how the the pixel is spotted per frame. This is done multiple times and using simple mathematics, the velocities are calculated, which is used to calculate the kinetic energies.

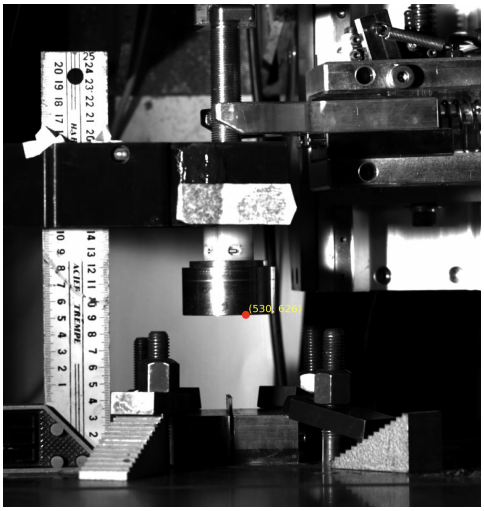


Figure 5.26: An example pixel spotting

While the high-speed camera is indeed useful and essential for the energy analysis, one of the purpose of placing the high-speed camera is to capture the behavior of the specimen when subjected to the impact.

Along with the energy analysis and assessing the specimen behavior, another measurement to be obtained from this set-up is the Force vs. Time curve from the droptower. The droptower has a strain-gauge at the impactor dart, which collects force information over time during the impact. The load-cell collects data at a rate of $500kHz$. However, note that this is the rate where the load which the impactor experiences is collected. It was considered to build a load measurement system directly from the specimen in the earlier stage of the thesis work, however due to time constraints and the resources available, it was not pursued. For future, it would be extremely useful to build a system where the load from the specimen can be collected directly.

5.9. Ultrasonic C-Scan

As mentioned previously, composite materials go through complicated damage processess. Damages such as delamination, matrix cracking and ply separation can propagate through the specimen, with no clear visible signs. Therefore, the ultrasonic C-scan is used after the experiment campaign to assess the possible internal damages.

The C-Scan system consists of both transmitter and receiver, which are separated by $10cm$. Specimen which is scanned is placed at the mid-point as presented in Figure 5.27. The trasmitter sends signals with $5MHz$ of frequency and the receiver measures how much frequency is received. Final result of the scan shows a decibel level, which presents how much signals were lost. Decibel values closer to zero represents lower signals lost, as the decibel values are determined from logarithmic ratio between the signal amplitudes before and after the ultrasonic wave travels through the specimen.

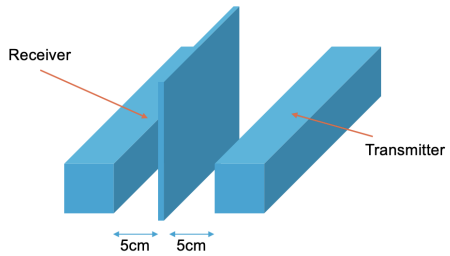


Figure 5.27: C-Scan visualization

As depicted in Figure 5.28, the specimen must be clamped on the edges of one edge of the specimen. This leads to some parts of the top or bottom edges not being exposed for the scans. Therefore, two scans are performed per specimen, to capture both edges correctly.

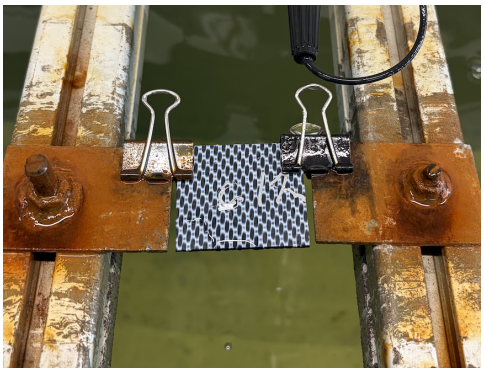


Figure 5.28: C-Scan set-up

Figure 5.29 presents the diagram which shows how the specimen are positioned for the two scannings.

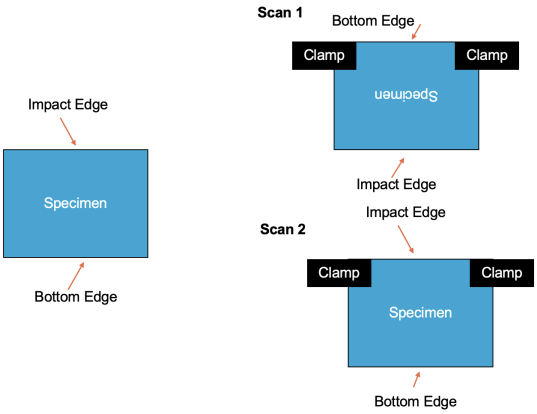


Figure 5.29: C-Scan plan

5.10. Test Matrix

Following the methodologies defined for the thesis work, this section presents the test matrix to be followed during the thesis work. Note that all the tests use the same specimen. Table 5.2 presents the quasi-static test matrix.

Table 5.2: Quasi-Static Test Matrix

Test ID	Test Type	Loading Rate	Temperature
QS-1	Quasi-Static	2 mm/min	Room Temp.
QS-2	Quasi-Static	2 mm/min	Room Temp.
QS-3	Quasi-Static	2 mm/min	Room Temp.
QS-4	Quasi-Static	2 mm/min	Room Temp.
QS-5	Quasi-Static	2 mm/min	Room Temp.

Table 5.3 presents the impact test test matrix. Some initial practice runs are performed to determine the heights at which the impactor should be dropped from. $800mm$ is the best option in order to exert similar energy obtained from the quasi-static test as lower heights such as $700mm$ and lower introduced

a lot of variability. This could be due to discrepancies of the droptower, as small discrepancies could have more influence on the energy of the impactor before the impact event for lower initial energy.

Table 5.3: Impact Test Matrix

Test ID	Test Type	Loading Height
IM-Test-1	Impact	1300 mm
IM-Test-2	Impact	1000 mm
IM-Test-3	Impact	900 mm
IM-Test-4	Impact	700 mm
IM-1	Impact	800 mm
IM-2	Impact	800 mm
IM-3	Impact	800 mm
IM-4	Impact	1000 mm
IM-5	Impact	1000 mm
IM-6	Impact	1000 mm
IM-7	Impact	1200 mm
IM-8	Impact	1200 mm
IM-9	Impact	1200 mm

5.11. Conclusion

To conclude, this section defined all the parameters, materials, equipments, and procedures to be followed for the thesis work. Following sections will be dedicated on the result, analysis and possible recommendations on the thesis work, as well as recommendations on the procedures defined in this chapter.

6

Results

6.1. Introduction

With the methodologies established in the previous chapter, the experiment work is carried out. This chapter presents the results and analysis of the experiment work which builds the conclusions of this thesis work.

6.2. Quasi-Static Tests

In this section, the result obtained from the Quasi-Static tests are discussed. Due to the compression nature of the quasi-static test, the test set-up is far more difficult to calibrate than the tensile test. Including the challenges encountered due to this nature, results, and analysis on the results are presented.

As mentioned previously in the chapter 5, during the compression tests, not only do the specimen get compressed but the machine itself also gets compressed. The effects of the machine compliance must be subtracted from the measured force-displacement curve in order to obtain the response of the specimen only.

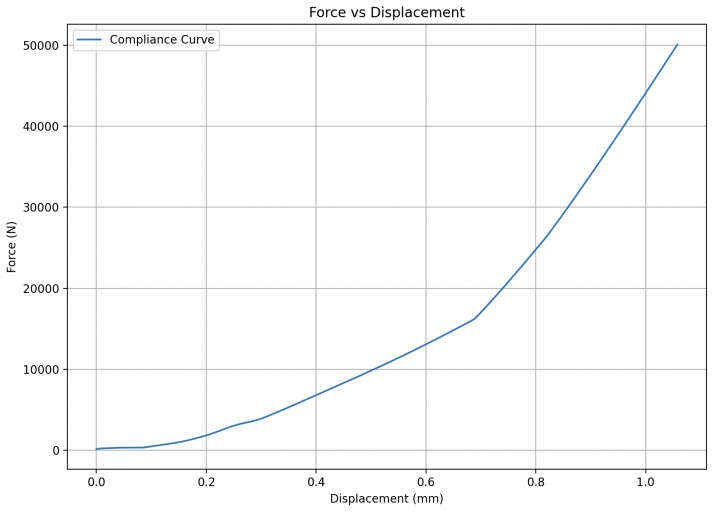


Figure 6.1: Force and Displacement Curve of the Compliance of the Machine

The compliance curve, as shown in the Figure 6.1 only settles and has a constant stiffness after it reaches $16000N$ of load. Therefore, this region is used trying to understand the behavior of the machine. The approach to getting the specimen data only, is to use the idea of two springs in series. In such a case, the

force the specimen and the machine experience are the same and only the displacements differ. Therefore, Equation 6.1 is used to get the coupon-only displacement, where $x_{specimen}$ is the displacement of the specimen, $x_{measured}$ and $F_{measured}$ is the displacement and force measured by the machine respectively, and the $k_{machine}$ is the stiffness of the machine, which is found to be $103930.906146 N/mm$ using the linear fit in the Figure 6.1.

$$x_{specimen} = x_{measured} - \frac{F_{measured}}{k_{machine}} \tag{6.1}$$

Figure 6.2 presents the Force vs. Displacement curve from the experiment. Note that in this figure, the influence of the machine is not subtracted.

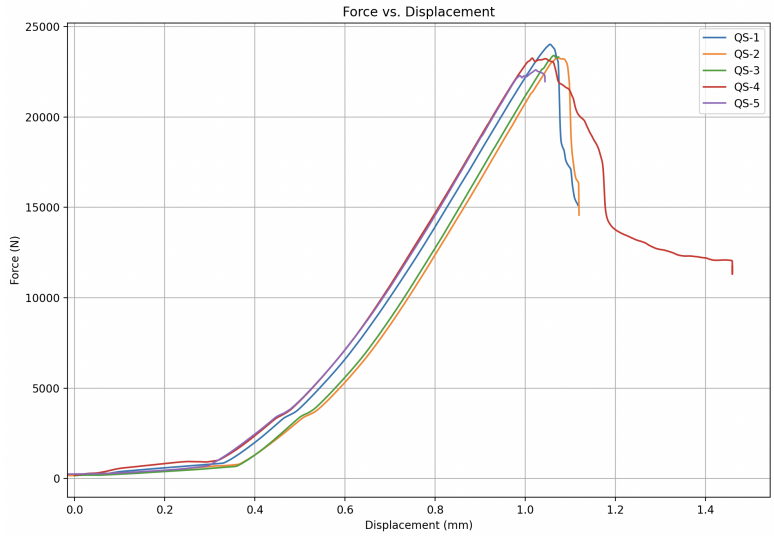


Figure 6.2: Force displacement curve of the compression Test

And Figure 6.3 presents the Force vs. Displacement curve with the influence of the machine subtracted. Note that the only the displacement is adjusted, as both the specimen and the machine experience same force.

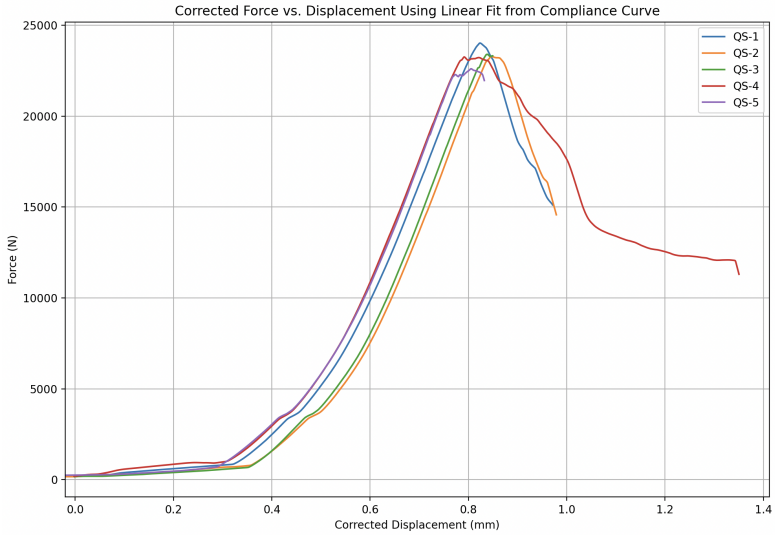


Figure 6.3: Corrected force displacement curve of the compression Test

All five specimens present very similar behavior. The stiffness of the specimen are in average of 65474.56N/mm and the maximum force experienced by the specimen is 23245.13N in average. Exact data points are presented in Table 6.1 and Table 6.3 for stiffness and the maximum force values respecitvely.

Table 6.1: Slope values for test specimens

Specimen	Slope (N/mm)
QS-1	66206.0
QS-2	64410.6
QS-3	65595.1
QS-4	65859.4
QS-5	65301.7

The measured values are 65474.56 ± 681.82N/mm. Table below presents the average and the standard deviation.

Table 6.2: Slope values average and standard deviation

Variable	Value
Average	65474.6
SD	681.8

Table 6.3: Maximum force values for test specimens

Specimen	Max Force (N)
QS-1	24016.1
QS-2	23272.8
QS-3	23399.1
QS-4	23253.1
QS-5	22284.6

The measured values are 23245.14 ± 620.78N/mm. Table below presents the average and the standard deviation.

Table 6.4: Maximum force values average and standard deviation

Variable	Value
Average	23245.1
SD	620.8

One interesting trend to notice from the Force-Displaceent Curve is the non-linearity of the curves. As the specimens are loaded, they all reach a specific load about 800N, where the trend changes. It is anticipated that until this point, the specimens are not fully loaded. This could be a machine non-linearity, as it is also present in the compliance curve.

The energies which the specimens absorbed are also calculated using the calibrated Force vs. Displacement curve in Figure 6.3. Since the trends of the Force vs. Displacement curves are similar, the energy absorbed by each specimens are also similar. In order to calculate the energy, the areas underneath the Force vs. Displacement curves are calculated. The average energy absorbed with standard deviation is 4852.0 + 289.92J

Table 6.5: Energy absorbed per specimen

Specimen	Energy (Nmm)
QS-1	5232.3
QS-2	4860.4
QS-3	4817.6
QS-4	4931.5
QS-5	4423.0

Table 6.6: Slope values for test specimens

Variable	Value
Average	4853.0
SD	289.9

Further post-processing the result, the stress-strain curves are obtained as presented in Figure 6.4. For the calculation of the stress and strain, engineering stress and strain are used to simplify the set-up, and the nature of small displacement justifies the choice of choosing this method.

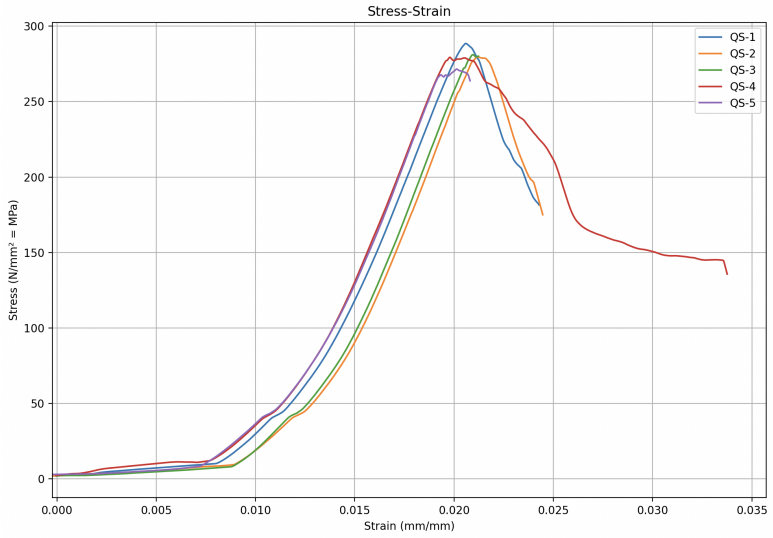
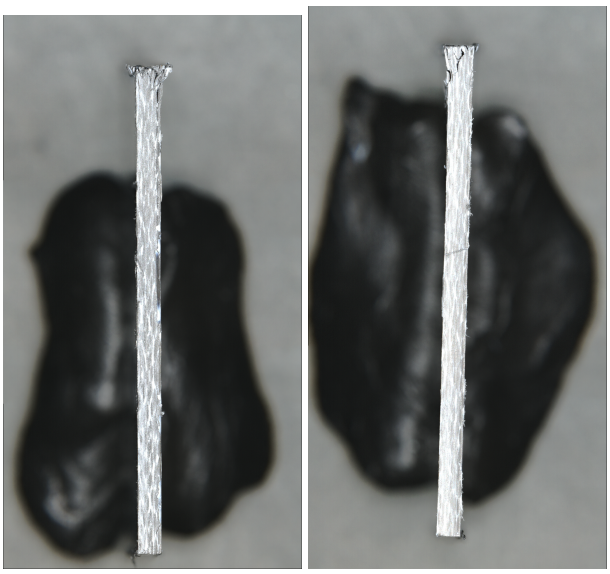


Figure 6.4: Stres-strain curve of the compression test

With the present stress-strain curve, the average Young's modulus of the specimen is calculated to be 26090MPa, which is similar to the Young's modulus calculated from tensile test of with the ASTM D3099, of 25500MPa.

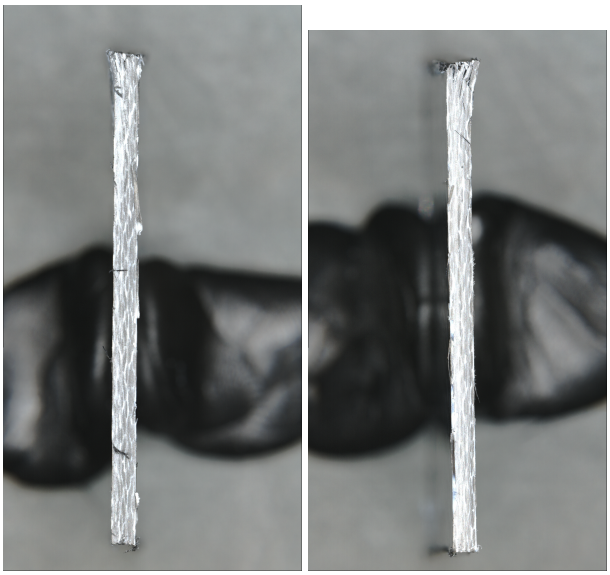
The failure modes observed in the specimen are also investigated as a part of the post-processing. As mentioned many times in this section, all five specimens show very similar behavior, and this behavior is also apparent in the failure mode of the specimen.

Figure 6.5, Figure 6.6, Figure 6.7, Figure 6.8, and Figure 6.9 present the cross-section of the specimen for QS-1, QS-2, QS-3, QS-4 and QS-5 respectively, captured by the microscope.



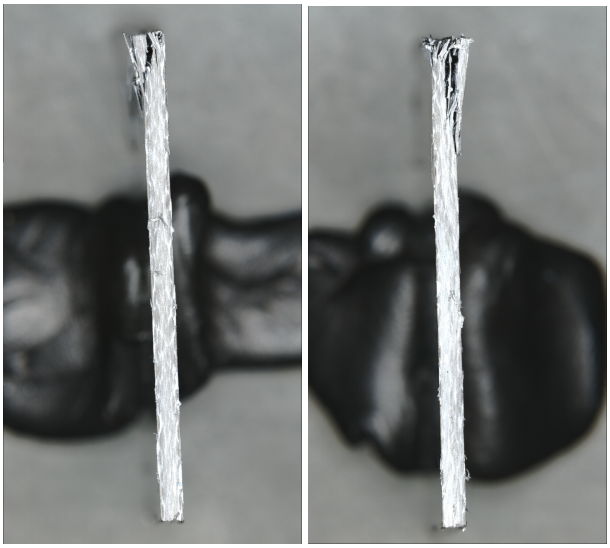
(a) Front side **(b)** Back side

Figure 6.5: Microscopy Scan quasi-static QS-1



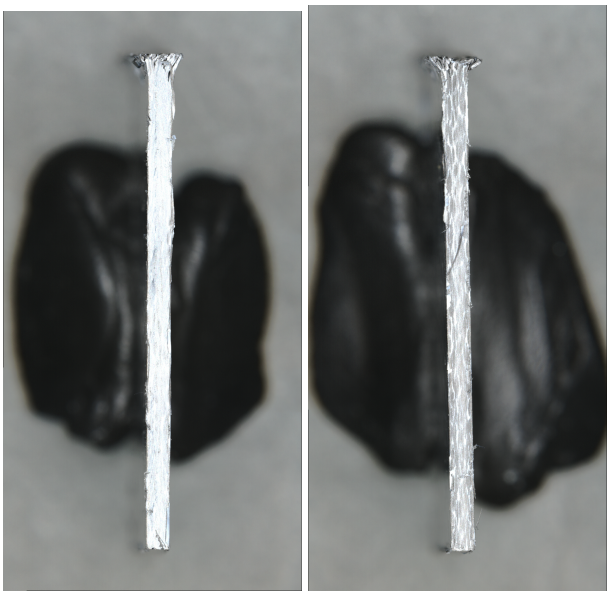
(a) Front side **(b)** Back side

Figure 6.6: Microscopy Scan quasi-static QS-2



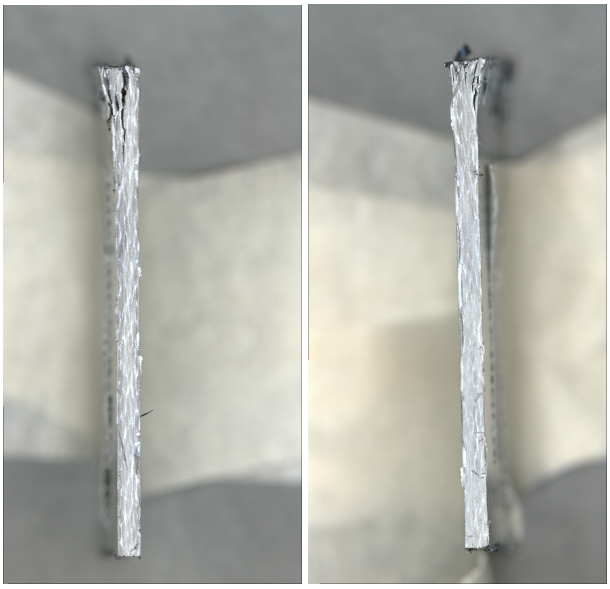
(a) Front side **(b)** Back side

Figure 6.7: Microscopy Scan quasi-static QS-3



(a) Front side **(b)** Back side

Figure 6.8: Microscopy Scan quasi-static QS-4



(a) Front side **(b)** Back side

Figure 6.9: Microscopy Scan quasi-static QS-5

In all samples, the major failure observed is the delamination with a slight crushing. Particularly QS-3 and QS-5 present large delaminations that are visible from the side. The greater delamination is, the greater the loss in specimen's stiffness. This is also apparent in their curves in Figure 6.3, at the maximum displacement, where the force curve stops, as the machine stops recording due to significant loss of the specimen's stiffness. Other samples, namely QS-1, QS-2 and QS-4 have relatively smaller delamination and slowly loses its strength as present in the Figure 6.3.

Besides delamination, some splayings are also observed. They are observed lightly in all the samples, but specifically for QS-4, a heavy splaying is observed as presented in Figure 6.8 with small delamination zone compared to other samples. This suggests that a larger portion of the deformation energy was dissipated through ply separation and splaying rather than extensive interlaminar crack propagation. One possible explanation is that the loading could have been more localized in QS-4, promoting outward ply bending and separation near the loaded edge.

The different damage mechanism also influences the Force vs. Displacement and stress-strain curves of the specimen. Compared to other samples, the rate of decrease in force is much slower for QS-4. As mentioned, with delamination being introduced, the structural integrity decreases suddenly, but as the failure in QS-4 is rather localized, the force decreases slowly as the compression head crushes the top rather than the delamination propagating to greater area.

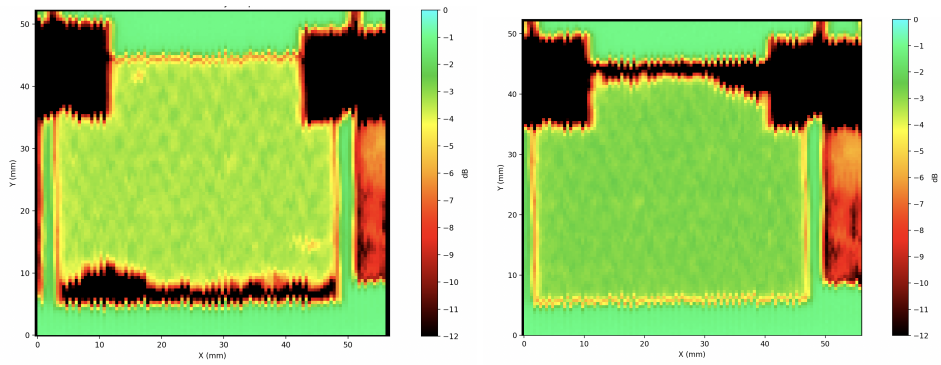
The slight deviations in damage sizes and the damage mode between the specimen suggest that the boundary condition could have been more calibrated through the means of flatting out the compression head per test since the the compression head could have misaligned after each tests.

The fact that the material used for this experiment is gathered from a box of scrap material also must have played a role here, with the possibility that the specimen used may not be from the same batch or from same production condition. It was ensured by the materials provider that the specimen had identical stacking sequences, as they were collected from one specific box, which only had scraps of one specific type of plates with one specific stacking sequence. However, there is still possibility that the scraps were from different manufacturing sequences with possible deviation in manufacturing temperature and pressures. In order to minimize such deviations as much as possible, bigger scrap materials are collected and cut into small pieces, however there still exits a possibility of manufacturing difference between the specimens.

6.2.1. Ultrasonic C-Scan of Specimens

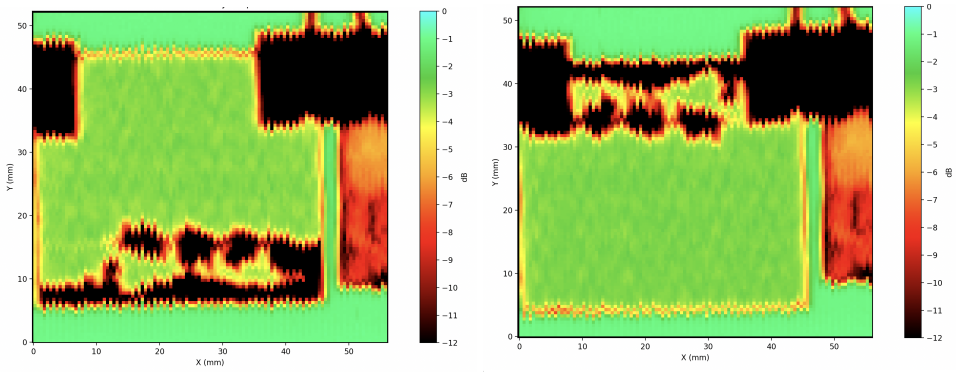
Following the quasi-static tests, ultrasonic C-scans are performed to evaluate the extent and distribution of internal damage within the specimens. While visual inspection and microscopy provide valuable information regarding surface damage and localized failure mechanisms, they cannot fully capture subsurface damages such as delamination and internal cracking.

As mentioned in the chapter 5, the C-scan consists of two parts, the transmitter and receiver. Therefore the higher decibel which are closer to 0dB signifies that the more signals are received by the receiver from the emitter and negative decibels represents that majority of the signals are lost. Figure 6.10, Figure 6.11, Figure 6.12, Figure 6.13 and Figure 6.14 presents the ultrasonic scan of QS-1, QS-2, QS-3, QS-4 and QS-5 respectively.



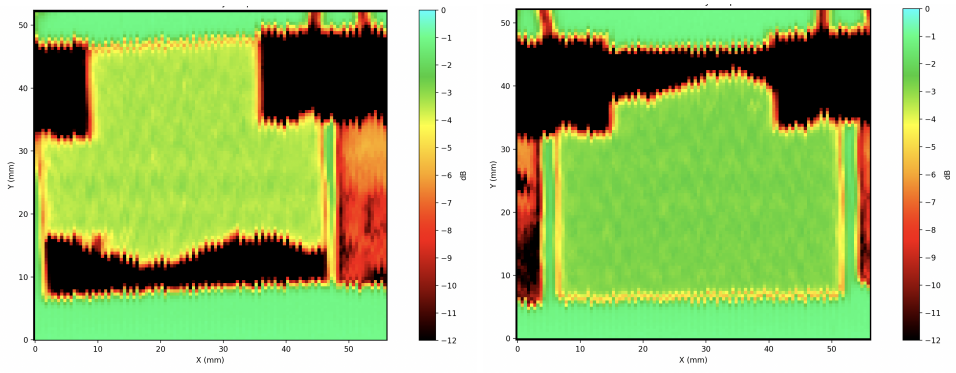
(a) Ultrasonic Scan of QS-1 Scan 1 **(b)** Ultrasonic Scan of QS-1 Scan 2

Figure 6.10: Ultrasonic Scan of QS-1



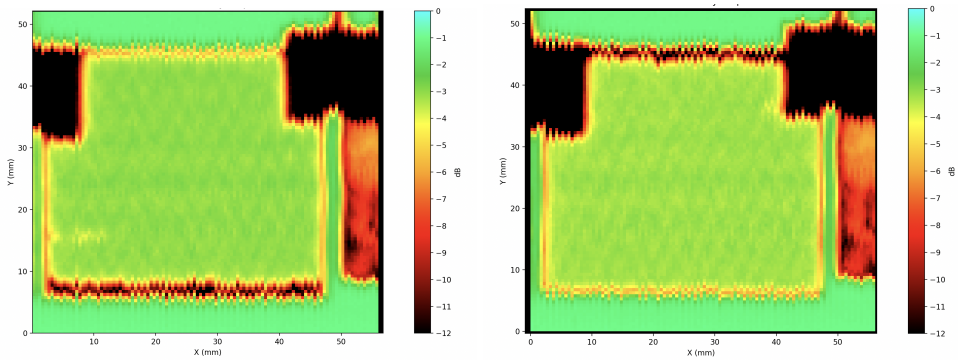
(a) Ultrasonic Scan of QS-2 Scan 1 **(b)** Ultrasonic Scan of QS-2 Scan 2

Figure 6.11: Ultrasonic Scan of QS-2



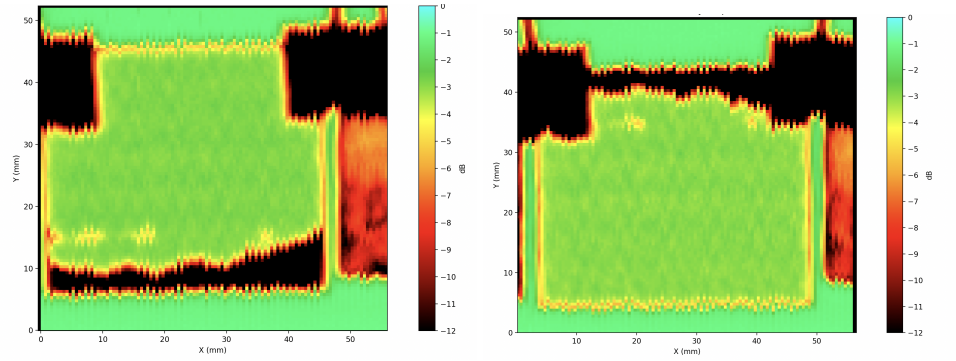
(a) Ultrasonic Scan of QS-3 Scan 1 **(b)** Ultrasonic Scan of QS-3 Scan 2

Figure 6.12: Ultrasonic Scan of QS-3



(a) Ultrasonic Scan of QS-4 Scan 1 **(b)** Ultrasonic Scan of QS-4 Scan 2

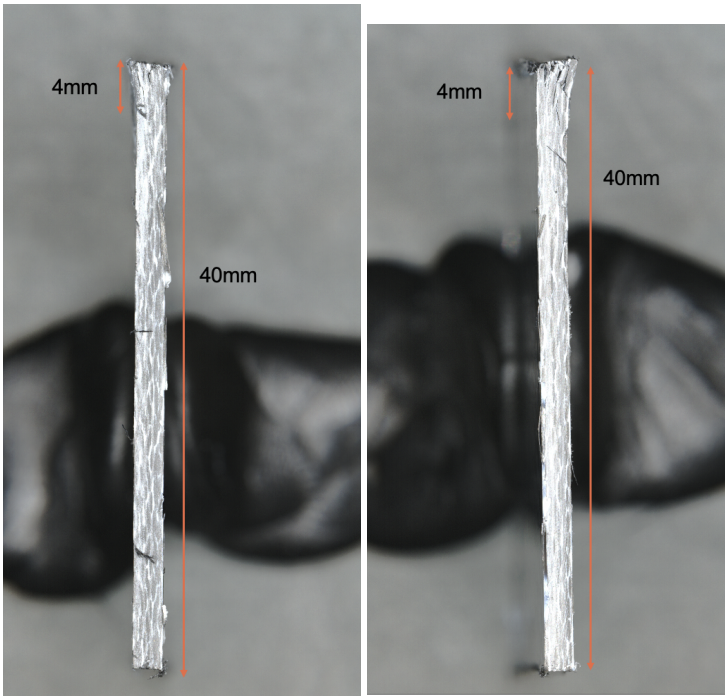
Figure 6.13: Ultrasonic Scan of QS4



(a) Ultrasonic Scan of QS-5 Scan 1 **(b)** Ultrasonic Scan of QS-5 Scan 2

Figure 6.14: Ultrasonic Scan of QS-5

All specimens except QS-4 present extended black area in the specimen. This could due to the fact that QS-4 goes under locally crushing failure. The damages observed from the C-scan seem much greater than of observed from the microscopy. For example, specimen QS-2 presents about $4mm$ of damage depth from the microscopy as measured in Figure 6.15. However the C-Scan pictures present about $15mm$ depth of damages as presented in Figure 6.11. Similar trends of greater damages observed through the C-Scan are apparent in all specimen.



(a) QS-2 damage inspection front side **(b)** QS-2 damage inspection back side

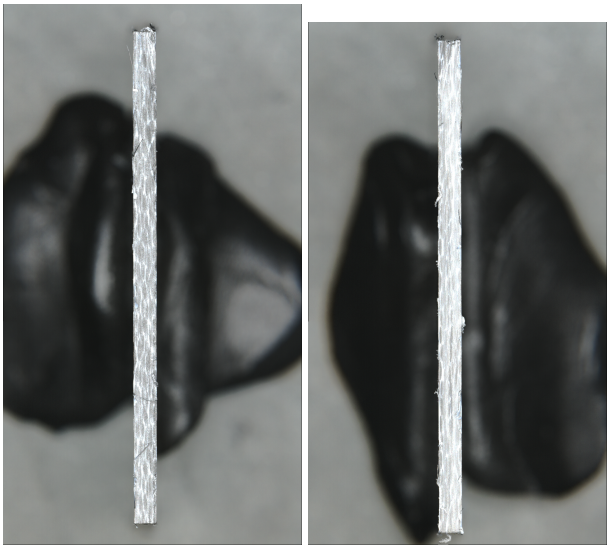
Figure 6.15: QS-2 damage inspection

The dark area with lower decibel from the C-Scan suggest that major delamination and internal cracking occured, hindering the signals to be captured by the probe. The extent of the damage suggests that the damages experienced by the specimen during the quasi-static loading promoted progressive failure of the laminate. As the load gradually increases, different damage mechanisms such as matrix cracking and delamination had sufficient time to initiate and propagate, producing a considerably large damaged region.

6.3. Impact Test

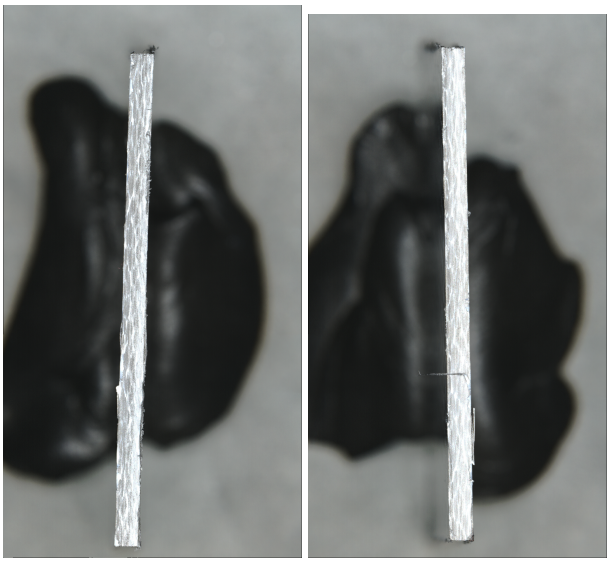
After completing the quasi-static test, the impact test are performed. Choosing the control variable to keep identical between the quasi-static and impact test is not difficult, but to actually keep them the same during the experiment is extremely challenging. Initially, the impact tests specimens were to be subjected to same energy which the specimens absorbed during the quasi-static tests, to assess if the same failure mode are be observed during the impact test. The challenge is knowing how much energy the specimen absorbs when using the drop-tower set-up, as the impactor bounces after hitting the specimen. Therefore, as mentioned in the previous chapter, some initial tests were performed in order to determine the optimal height which the impactor should be dropped from.

Figure 6.16, Figure 6.17, Figure 6.18 present the cross-section of IM-1, IM-2 and IM-3, which used the drop height of $800mm$.



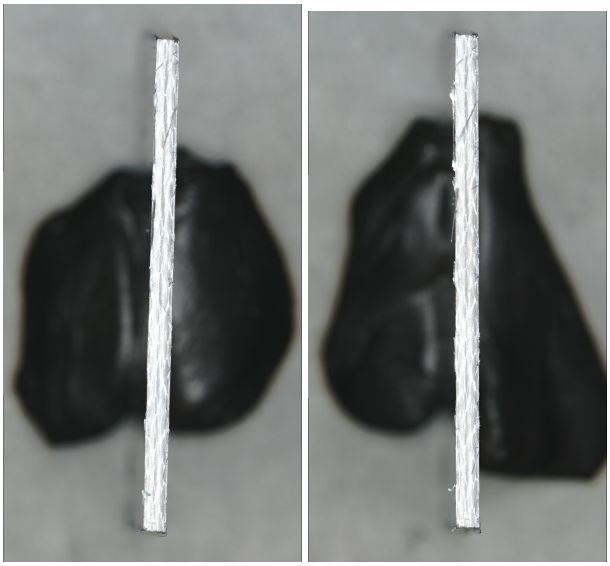
(a) Front side **(b)** Back side

Figure 6.16: Microscopy scan impact IM-1



(a) Front side **(b)** Back side

Figure 6.17: Microscopy scan impact IM-2

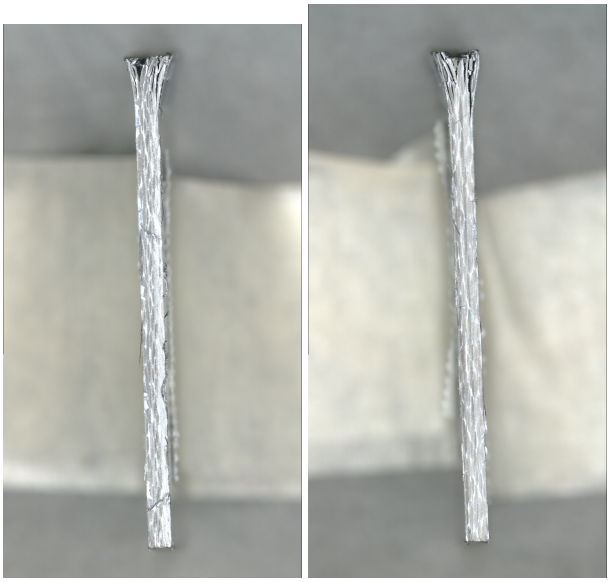


(a) Front side **(b)** Back side

Figure 6.18: Microscopy scan impact IM-3

As clearly seen, no visible damages are observed. It is expected that these specimens remaind completely elastic during the impact.

Figure 6.19, Figure 6.20, Figure 6.21 present the cross-section of IM-4, IM-5, and IM-6, which used the drop height of $1000mm$.



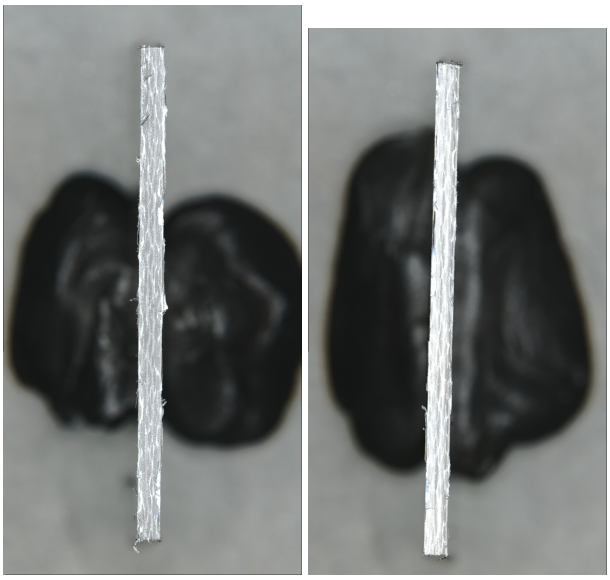
(a) Block 1 cross-section view **(b)** Block 1

Figure 6.19: Microscopy scan impact IM-4



(a) Front side **(b)** Back side

Figure 6.20: Microscopy scan impact IM-5

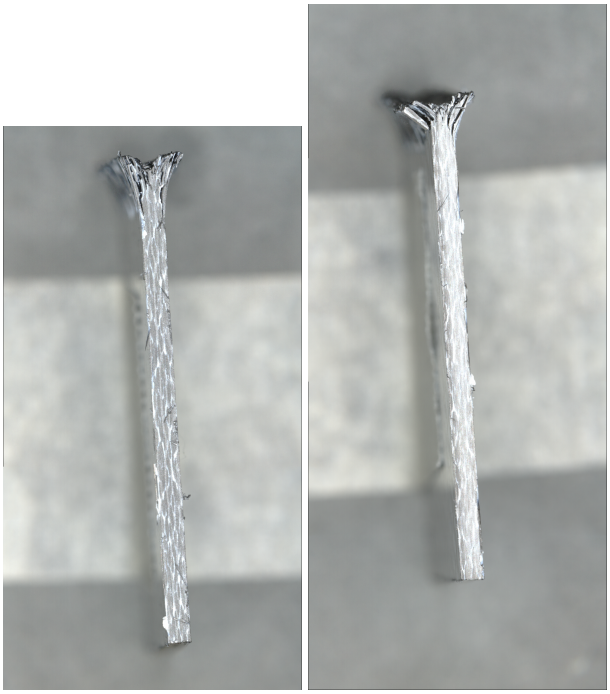


(a) Front side **(b)** Back side

Figure 6.21: Microscopy scan impact IM-6

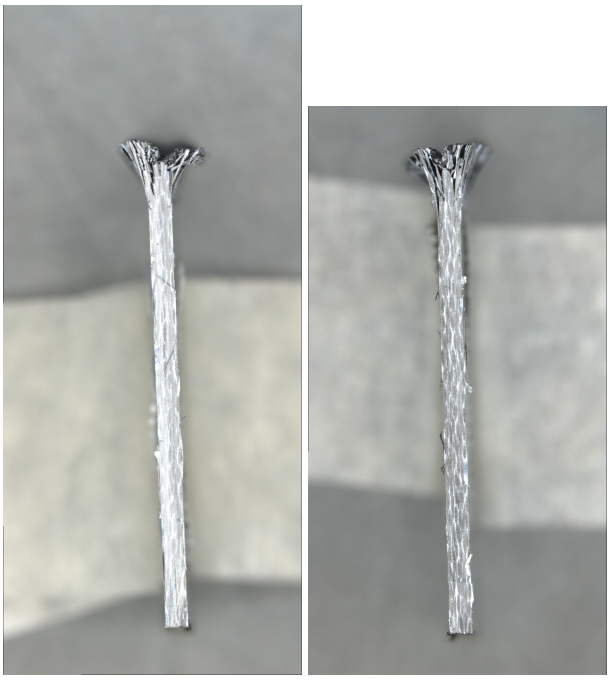
Crushings and splayings are observed from IM-4 and IM-5. Some delaminations are initiated at the top edges, but they do not travel far through the specimen. IM-6 seems to have remained elastic during the impact.

Figure 6.22, Figure 6.23, Figure 6.24 present the cross-section of IM-7, IM-8, and IM-9, which used the drop height of 1200mm.



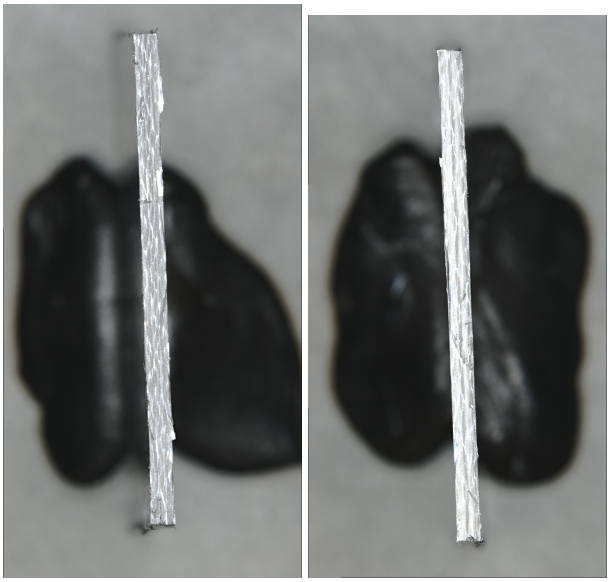
(a) Front side **(b)** Back side

Figure 6.22: Microscopy scan impact IM-7



(a) Front side **(b)** Back side

Figure 6.23: Microscopy scan impact IM-8



(a) Front side **(b)** Back side

Figure 6.24: Microscopy scan impact IM-9

Similar to the previous set, IM-7 and IM-8 have crushing and splaying on the top, which seem to be greater than of observed in IM-4 and IM-5. Here too, there exists IM-9, where no damages are observed.

The specimens which have visible damages, such as IM-4, IM-5, IM-7, and IM-8 present high degrees of delamination and splaying as observed in Figure 6.19, Figure 6.20, Figure 6.22 and Figure 6.23. As the impactor comes in contact with the specimen, a high level of localized compressive stress is generated at the contact region. These stresses likely initiated matrix cracking and fibre matrix interface damages within the laminate. This could have led to delamination of the plies and as the delamination occurs and plies separate, the splayings are triggered.

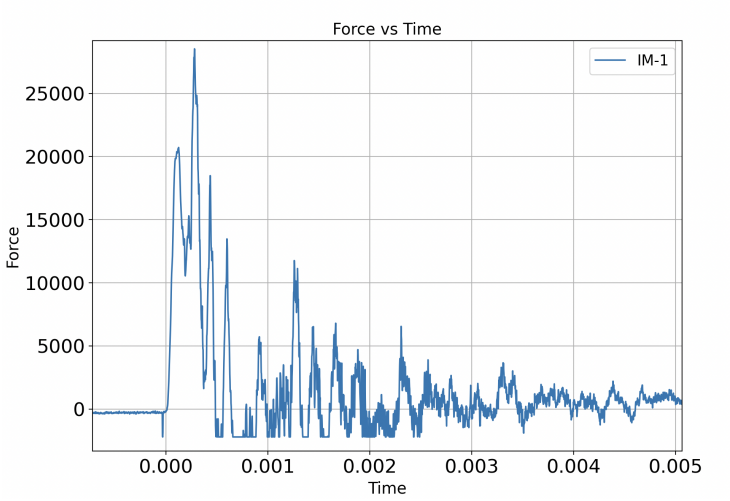
Regarding the influences of the heights, as the drop height and the energy exerted on the specimen increase, the damages also grow. Namely, the damages observed in Figure 6.22 and Figure 6.23 are much greater than Figure 6.19, Figure 6.20. Specifically, the degree of splaying and delamination sizes show clear growth as the drop height increases. Another interesting point is how localized these damages are. Matching with the literature's findings, the damages are much more localized than the quasi-static tests as the loadings are appled in a much more rapid manner. More comparisons with the quasi-static test in terms of force and energy are presented in section 6.4.

As mentioned, the droptower used for the thesis work is not the most fine-tuned machine for drop tower testing. The test heights could not be prescribed and deviated every run and the rail which the impactor dart goes through during the drop induce friction. Therefore some tests, namely IM-6 and IM-9 showed different behaviors than others. These data have no physically meaning as they were not loaded fully. The Force vs. Time curve reaches beyond $100kN$, which is the machine's maximum measurable threshold for force. Reason behind reaching this high of a force is unknown.

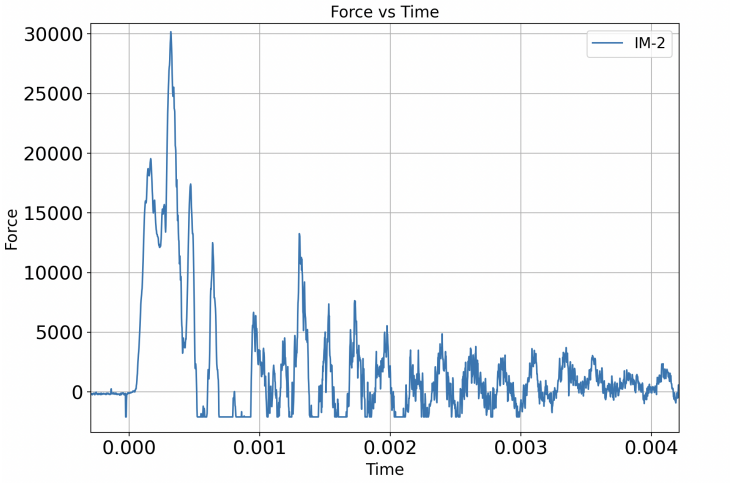
6.3.1. Force Analysis

This subsection analyzes the force measured from the impact tests. The Force vs. Time curve is directly obtained from the droptower, measuring the force experienced by the impactor. Keeping in mind that the force measured is what the impactor experiences, the insights that the data could provide and the limitations are discussed.

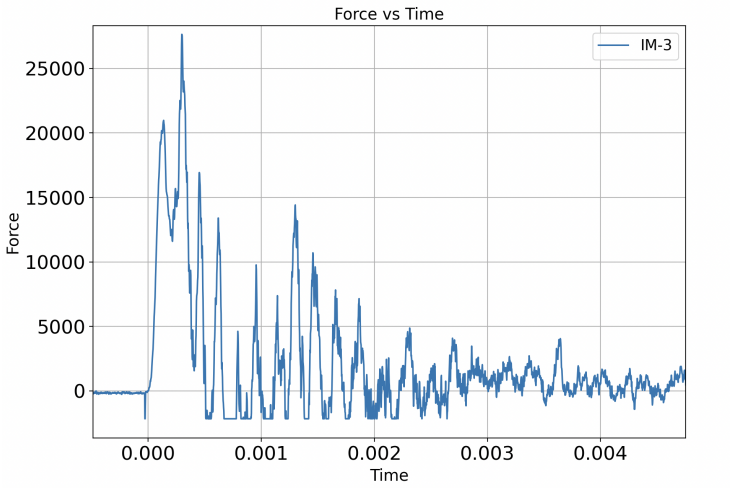
Figure 6.25 presents the Force vs. Time curve of the impact test IM-1, IM-2 and IM-3 respectively. The force data spikes up rapidly after the impactor comes into contact with the specimen. After reaching their first peaks, the curve drops and strikes back up to the maximum values. Same trends are observed across all three specimens.



(a) IM-1



(b) IM-2

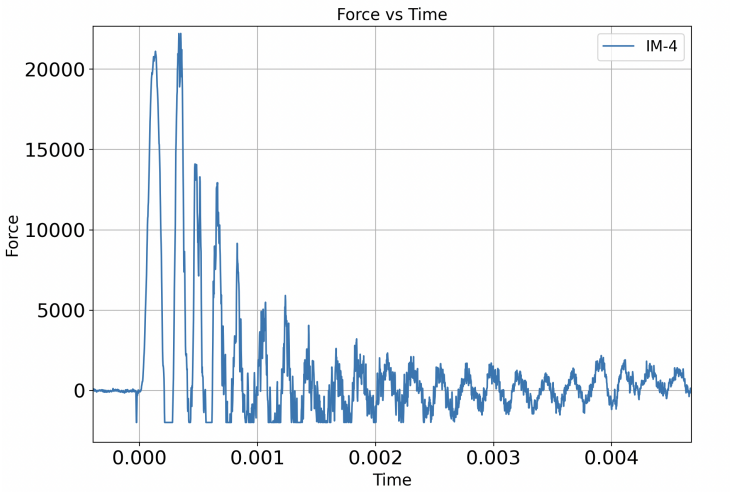


(c) IM-3

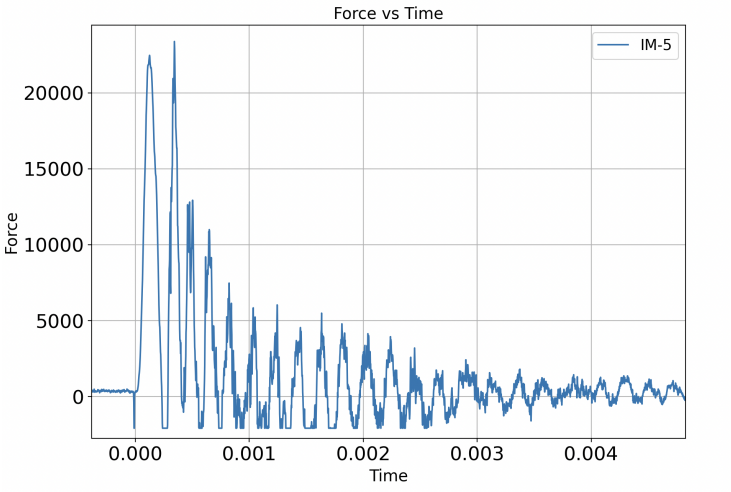
Figure 6.25: Force vs. Time curve, drop height 800mm

Figure 6.26 presents the Force vs. Time curves of IM-4, IM-5 and IM-6 respectively. Unlike the trends observed in the previous three tests, the Force curves drops to the minimum values after reaching the

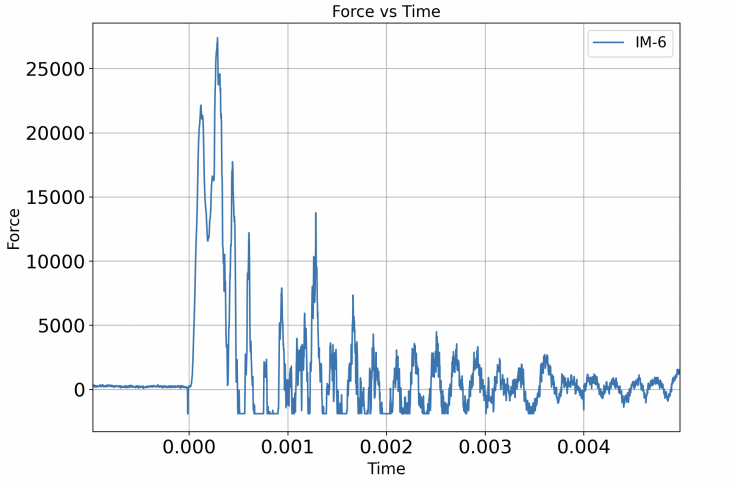
first peak, except for IM-6. The trends of the curves of IM-4 and IM-5 show a smoothly decaying curves, unlike the curves observed in IM-1, IM-2 and IM-3.



(a) IM-4



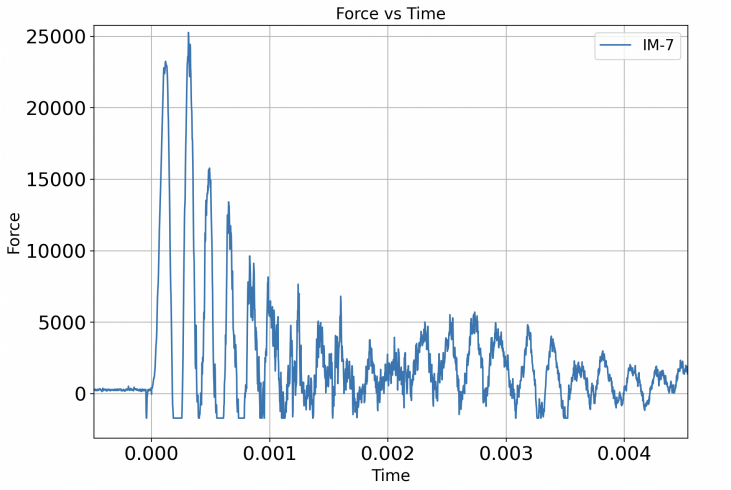
(b) IM-5



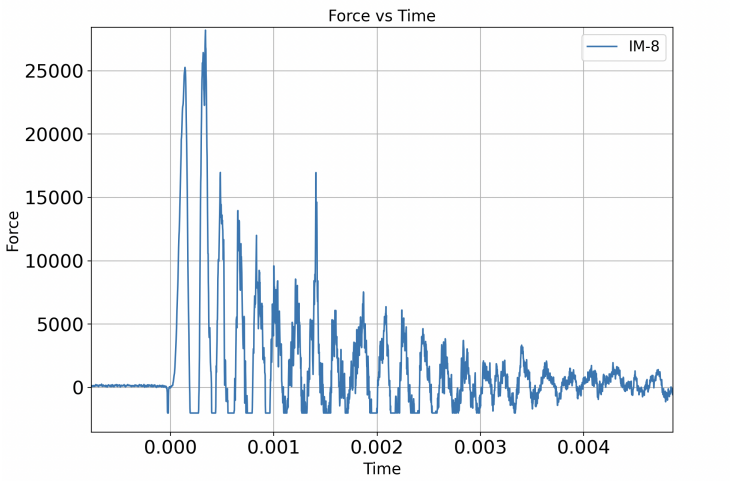
(c) IM-6

Figure 6.26: Force vs. Time curve, drop height $1000mm$

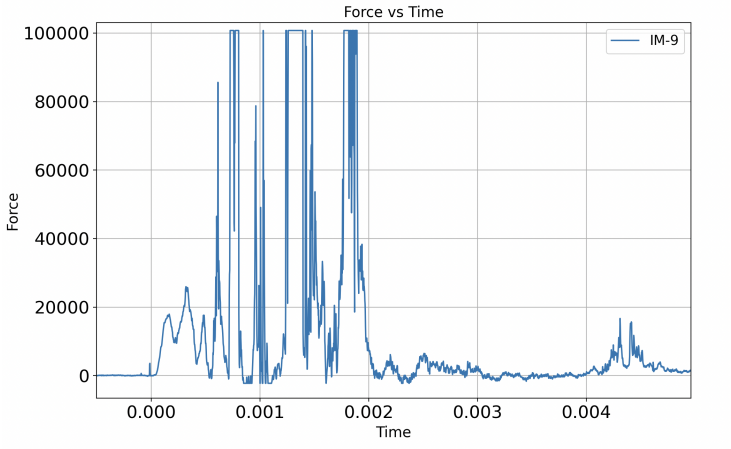
Finally, Figure 6.27 presents the Force vs. Time curve of the impact tests IM-7, IM-8 and IM-9 respectively. Similar to trends of observed in IM-4 and IM-5, the curves of IM-7 and IM-8 present a trend of force that drops after the first peak and increases back up to its maximum in its second peak. Here too, the force decays smoothly with time. Yet again, there exists one specimen, IM-9, which presents a trend similar to IM-1, IM-2 and IM-3.



(a) IM-7



(b) IM-8



(c) IM-9

Figure 6.27: Force vs. Time curve, drop height $1200mm$

One of the common behavior observed in all the curves are the oscillatory behavior. There are mutliple hypothesis to reason this oscillatory behavior of the Force vs. Time curve. Firstly, the shockwaves bouncing back up to the specimen could be causing the oscillation of the specimen. In order to test this hypothesis, some preliminary calculation is performed using Equation 6.2, where c is the speed of wave through the specimen, E is the Young's modulus of the specimen, and ρ was the density of the specimen.

$$c = \sqrt{\frac{E}{\rho}} \tag{6.2}$$

Performing the calculation, the wavespeed of roughly $4000m/s$ is obtained. Calculating the time which it travels back to the loadcell, time in microseconds is roughly about $10\mu s$. The dominant oscillation observed in the force curves has a period which is much longer. Furthermore, as the specimen consists of woven fabric layers which could scatter the waves and the medium at which the wave travels changes from CFRP to steel, the chances that the such weak waves would travel sufficiently back up to the load cell is extremely low. Therefore, it was concluded that the oscillation would not be due to the waves reflecting back up.

Second hypothesis is due to the loss of stiffness of the material. The force decreases significantly soon after the specimen and impactor come into contact. The damages which the specimen suffer, specifically the delamination can degrade the stiffness of the specimen significantly easily. However, the force goes up again and reaches another peak after the first drop, therefore, while this hypothesis could be sufficient to reason the drop of force, is not sufficient to reason the oscillatory trend.

Third hypothesis was the elastic oscillation of the specimen. In order to investigate this hypothesis, the high-speed camera footage is used. Unfortunately, it is not possible to identify if the specimen is vibrating or not during the impact event. Therefore a proper conclusion could not be drawn for this hypothesis.

Last hypothesis is the oscillation of the impactor. Imagine hitting a hard suface with a hammer. Upon hitting the surface, the hammer will be vibrating very rapidly - same happens to the impactor after hitting the specimen. Thus, it is much needed to identify the natural frequencies of the impactor itself. As the impactor has a threaded part in the middle of the impactor, in order to obtain a reasonable natural frequency, rather than calculating with a simple formula, a quick, simple and easy finite element analysis is performed using Abaqus. To simplify the model's set-up, the impactor is modeled only, rather than the entire impactor dart. The connection between the impactor and the impactor rod is treated to be an encastre, constraining all degrees of freedom.

Basic parameters, namely the density of the material, Young's modulus of the material, and the Poisson's ratio of the material were used for the modeling. They can be found below in Table 6.7.

Table 6.7: Material Properties

Material Property	**Value**
Density	$7800kg/m^3$
Young's Modulus	$205000N/mm^2$
Poisson's Ratio	0.3

Due to the impactor being bulky and a slight complication in the shape, the impactor was meshed with 3D elements.

Upon running the finite element analysis, it is identified that the first axial mode natural frequency of the impactor is $4999.3Hz$, as present in Figure 6.28.

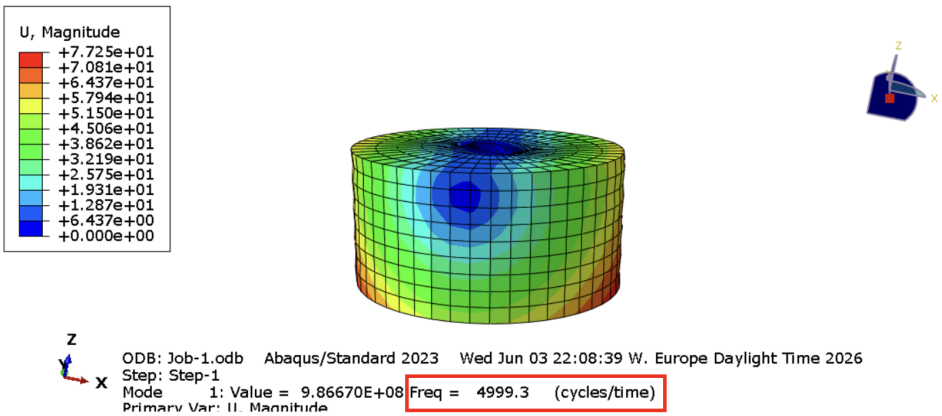


Figure 6.28: Impactor's natural frequency calculated by Abaqus

The oscillatory behavior from the Force vs. Time curve also has a frequencies between $5000Hz$ and $5500Hz$. As an example, refer to Figure 6.29, highlighting the two periods of oscillation.

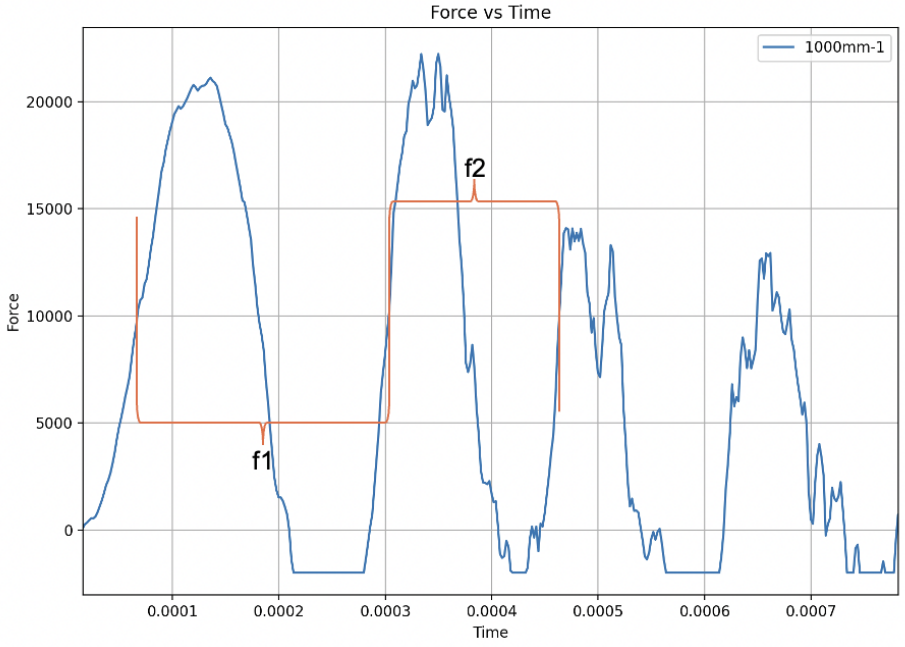


Figure 6.29: Frequency spotting for natural frequnecy analysis

Calculating the frequencies of highlighted oscillations, the following frequencies are obtained.

$$f_1 = \frac{1}{0.0002819 - 0.0000769} = 4878Hz \tag{6.3}$$

$$f_2 = \frac{1}{0.00028685 - 0.0003026} = 5571Hz \tag{6.4}$$

While not perfectly matching, these frequencies closely align with the natural frequencies of the impactor. The difference between the FEM identified frequency and the calculated frequencies are also expected, as the model only included the impactor head, rather than the entire impactor dart. The connection between the dart and the impactor are also simplified as just a cylinder with all the degrees of freedom

constrained, rather than modelling the screwed connection between the impactor and the dart. For more elaboration on the discrepancies and the possible improvement, refer to chapter 7.

Another important part of these curves are the difference in the trend per damage observed. For example, specimen from test IM-7 presented delamination and splaying upon the impact and specimen from test IM-1 presented no visible damages. Looking at the trend of the troughs of two curves after the first peak, as highlighted in Figure 6.30, the IM-7 reaches far lower than the IM-1.

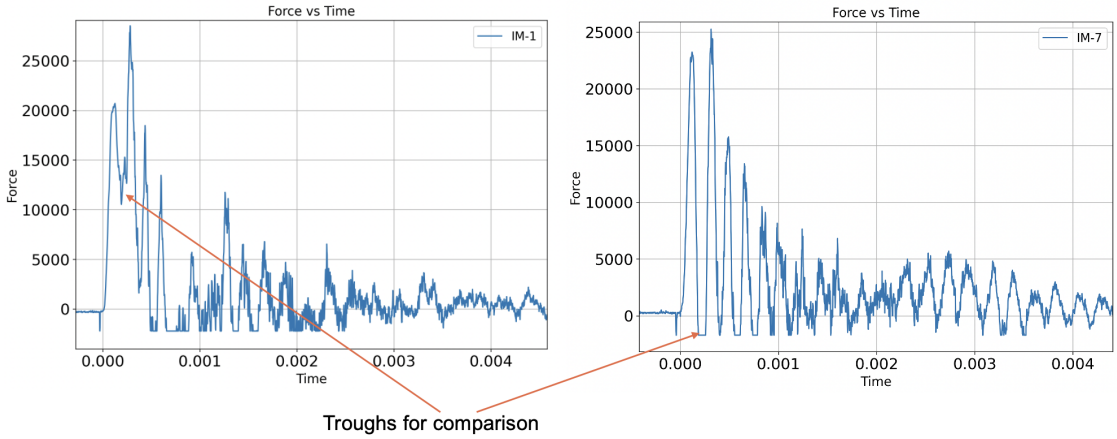


Figure 6.30: Comparison of troughs after first peak

As IM-1 showed no visible damage, it suggests that the specimen response remained predominantly elastic. However, due to the low framerate of the highspeed camera, it is not possible to investigate if the specimen is elastically vibrating, experiencing the shock. For IM-7, where the damages are significant and the specimen response is not elastic, the force drops tremendously. This could also be further investigated with a highspeed camera with a higher framerate.

6.3.2. Energy Analysis

Prior to discussing the energies absorbed by the specimen, it must be once again highlighted that $800mm$ is the lowest drop height which introduced stable repeatability for the tests. While the energy absorbed by the specimen of the impact tests are not identical of the energy absorbed by the specimen during quasi-static tests, the range of energy absorbed are similar and is sufficient to allow the comparison.

Table 6.8: Impact test results for clamped samples

Sample	Height	Clamped	Energy Before	Energy After	Energy Absorbed	Failure	Percentage
IM-1	800	Yes	10.31J	2.5J	7.81J	None	75%
IM-2	800	Yes	9.84J	2.58J	7.25J	None	74%
IM-3	800	Yes	11.54J	2.63J	8.91J	None	77%
IM-4	1000	Yes	11.71J	0.36J	11.35J	Delamination, Splaying	97%
IM-5	1000	Yes	12.10J	0.44J	11.66J	Delamination, Splaying	96%
IM-6	1000	Yes	12.22J	3.14J	9.08J	None	74%
IM-7	1200	Yes	15.01J	0.027J	14.98J	Delamination, Splaying	99%
IM-8	1200	Yes	16.91J	0.01J	16.9J	Delamination, Splaying	99%
IM-9	1200	Yes	13.12	2.93J	10.19J	None	78%

Table 6.8 presents the overview of the impact tests per heights, energy of the impactor before and after the impact, energy absorbed by the specimen, and the failure mode observed on the specimen. The kinetic energy of the impactor before and after the impact are calculated by identifying the velocity of the impactor before and after the impact with the information from the high-speed camera.

From Table 6.8, it is clear that as the kinetic energy of the impactor prior to impact increases, more energy

is absorbed by the specimen. This trend in energy is due to the combination of two main phenomena, namely the strain-rate response of the polymer and the damages observed in the specimen. The rest of this section is dedicated to dive further into these two phenomena and their effects on the energy absorption.

The energy absorption of the CFRP is heavily dependent on the behavior of the polymer. The thermoplastic polymer, specifically the PPS material used in this work, is known for its viscoelastic properties. Due to its viscoelasticity, the material changes its behavior per loading speed; it becomes brittle with increasing loading speed. Polymer's main job in a composite material is to hold the fibres together. Once the polymer starts acting brittle, the bonding betwen the fibres becomes brittle, leading the failure modes such as delamination and splaying to become more apparent. This behavior is apparent in the failure modes summarized in Table 6.8. With increasing height, which increases the kinetic energy of the impactor, more failure are observed.

The specimen with no visible damages absorbed less percentage of the impact energy, about 75%. Upon the impact loading, the specimen behaves almost elastic and retains its shape even after the loading. The elastic nature of this collision between the impactor and the specimen leads to lower absorption of energy. Specimen with damages absorbed far more energy, absorbing about $\approx$ 98% of the impact energy in average.

Commenting on the damages, delamination in CFRP is caused when the interlaminar stresses exceed the bonding strength between the adjacent plies. As the PPS becomes stiffer wiith higher strain-rate loading, the PPS transfers stresses more abruptly between composite plies, promoting delamination. Therefore, as the the drop height increases and the loading velocity increases, more delamination is observed in the specimen. Following more delamination, more energy is absorbed through the specimen as well. These behaviours of the specimen confirm the strain-rate sensitivity of the PPS material, specifically, how the carbon fibre reinforced polymer's energy absorbing behavior is strain-rate sensitive, which comes from the strain-rate sensitivity of the polymer.

6.3.3. Impulse Analysis

Impulse is one of the key element of investigating the impact events. Measuring the change of momentum during an event, impulse shows how severe the impact event is. From a Force vs. Time curve, impulse can be calculated simply through integration and identifying the area underneath the curves. In this case, the question to be answered is; which part of the curve should be used to calculate the impulse?

As mentioned previously, the Force vs. Time curves present what the impactor experiences, rather than what has gone into the specimen. Therefore the inertial effects of the impactor must be subtracted from the measured force of the impactor, to gain understanding of the force which the specimen absorbs. Besides, the curves are also hugely influenced by the natural frequnecy of the impactor. Therefore, measuring the impulse from the Force vs. Time curve obtained from this work will only be calculating the impulse which the impactor experiences.

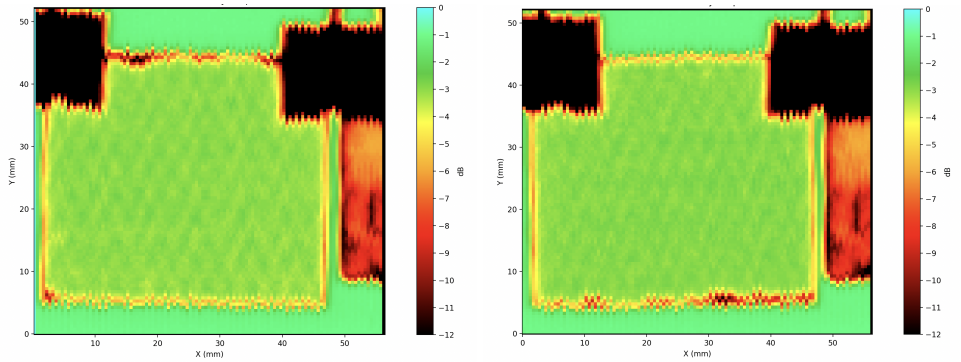
This makes it extremely challenging to obtain impulse which is exerted into specimen only. Integrating only the initial loading pulse would require selecting an arbitrary cut-off point because the transition from contact loading to structural vibration cannot be identified. Another point is the lack of information of impact event. The high-speed camera footage result is not sufficient to provide information on how long the impactor and the specimen are in contact for. The duration of contact could have provided further insights to the time interval to take into consideration for the impulse calculation, but again, it would still be the impulse which the impactor absorbs.

Therefore, impulse calculated from the measured force-time response would depend on the chosen integration limits rather than solely on the physical interaction between the impactor and the specimen. For future, in order to gain better insights of what the specimens are subjected to, a specific measurement technique which can measure what the specimen experiences would be essential. For more detailed elaboration, refer to chapter 7.

6.3.4. Ultrasonic C-Scan of Specimens

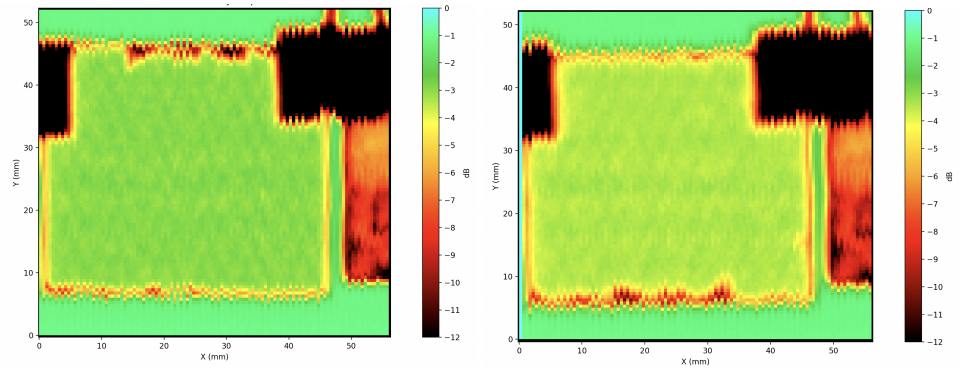
Similar to the quasi-static test, the specimens are C-Scan-ed after the impact tests. This section presents the ultrasonic scan images and elaborates on the damages observed. To understand the orientation of

the C-Scans, refer to Figure 5.29. Figure 6.31, Figure 6.32 and Figure 6.33 present the ultrasonic scan of the specimen from tests IM-1, IM-2 and IM-3 respectively. For the orientations of the specimen during the C-Scan, refer to Figure 5.29.



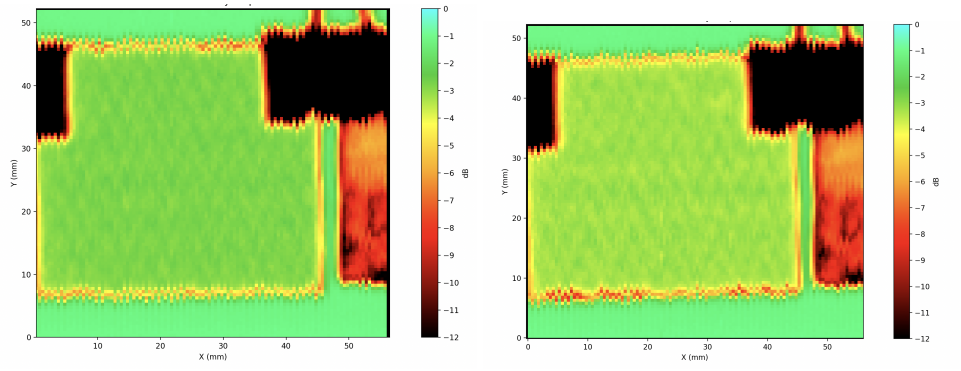
(a) Ultrasonic Scan IM-1 Scan 1 **(b)** Ultrasonic Scan IM-1 Scan 2

Figure 6.31: Ultrasonic Scan of IM-1



(a) Ultrasonic Scan of IM-2 Scan 1 **(b)** Ultrasonic Scan of IM-2 Scan 2

Figure 6.32: Ultrasonic Scan of IM-2

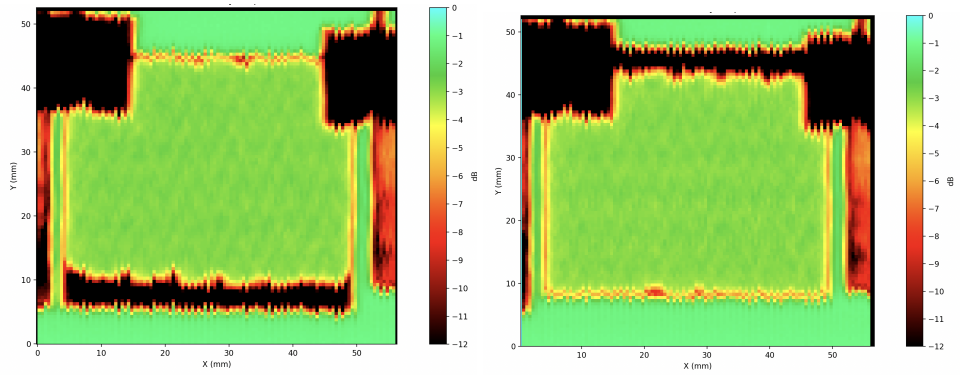


(a) Ultrasonic Scan of IM-3 Scan 1 **(b)** Ultrasonic Scan of IM-3 Scan 2

Figure 6.33: Ultrasonic Scan of IM-3

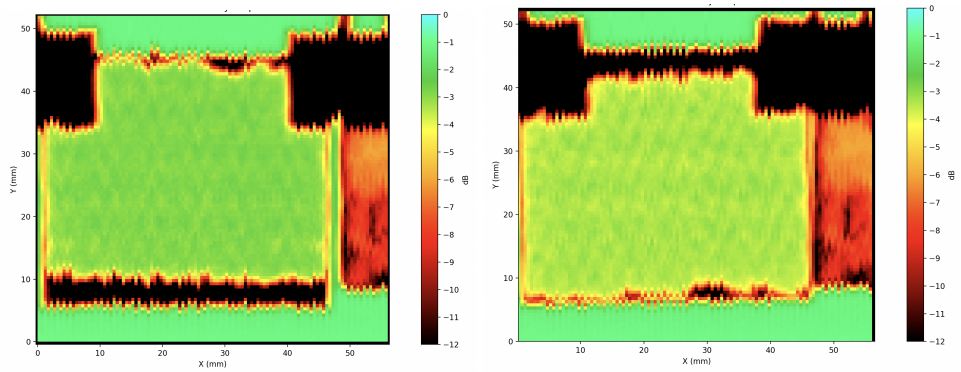
For these specimens, some local damages on the edge which the impactor hit the specimen are observed. These damages appear to be minor, with no indication of damages propagating into the interior of the specimen. Based on the minor damage observed only on the edge of the specimen, no clear visible damage on the specimen observed from the microscopy, the impact event is considered to have remained predominantly elastic, with insufficient energy transferred to initiate damages.

Figure 6.34, Figure 6.35, and Figure 6.36 present the C-Scan images of IM-4, IM-5 and IM-6 respecitvely.



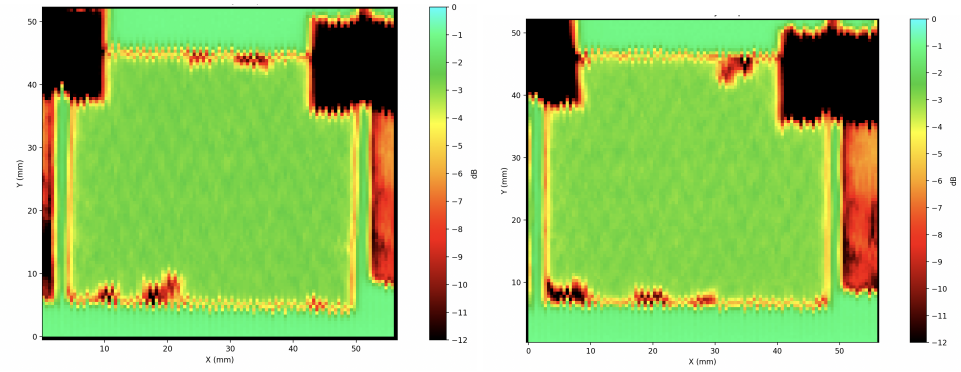
(a) Ultrasonic Scan of IM-4 Scan 1 **(b)** Ultrasonic Scan of IM-4 Scan 2

Figure 6.34: Ultrasonic Scan of IM-4



(a) Ultrasonic Scan of IM-5 Scan 1 **(b)** Ultrasonic Scan of IM-5 Scan 2

Figure 6.35: Ultrasonic Scan of IM-5



(a) Ultrasonic Scan of IM-6 Scan 1 **(b)** Ultrasonic Scan of IM-6 Scan 1

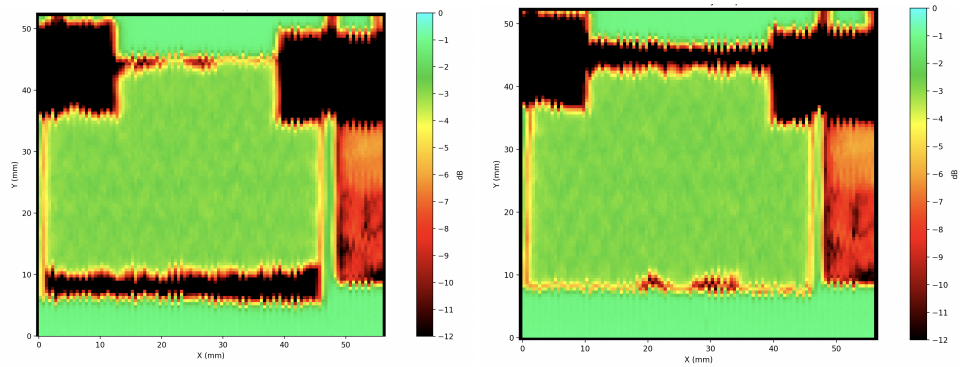
Figure 6.36: Ultrasonic Scan of IM-6

Figure 6.34 and Figure 6.35 clearly present the black colored area on the top edge of the specimen, corresponding to the area of delamination and splaying presented in the microscopy, in Figure 6.19 and Figure 6.20. Minor damages are also observed on the bottom edge, suggesting possible damages caused by the shockwaves traveling back up to the specimen from the table. However, no visible damages are apparent. Note that the damages are very localized, and they are only present on the top edges, unlike

the damages observed in the quasi-static test, which are spread out through greater area than just the loaded edge. More elaboration on this behavior and the comparison is given in section 6.4.

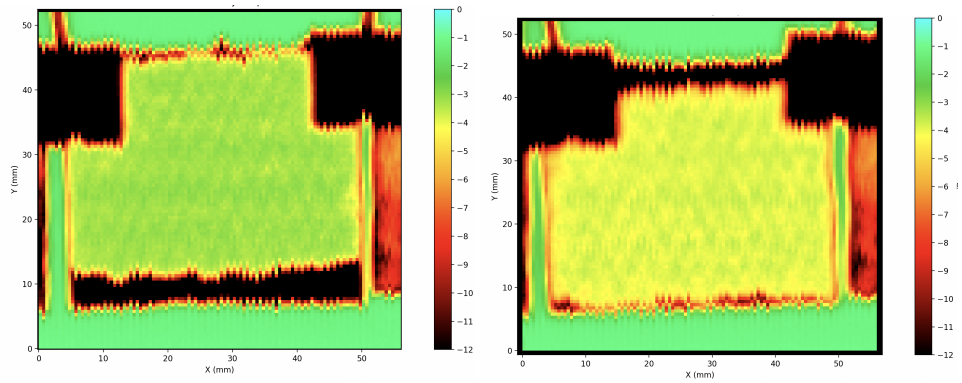
Figure 6.36, the scan of IM-6 also presents minor local damages, which is likely induced during the impact loading and the shockwaves reflected from the table. The impact loading is likely elastic as the ultrasonic scan show no visible damages in the interior of the specimen, the microscopy shows no visible damage, and the Force vs. Time curve, Figure 6.26c presents similar trends as Figure 6.25. Possible reason behind the elastic event, in contrast to other two events could be due to the misalginment of the impactor and the specimen during the impact event.

Finally, Figure 6.37, Figure 6.38 and Figure 6.39 present the C-Scan of IM-7, IM-8 and IM-9.



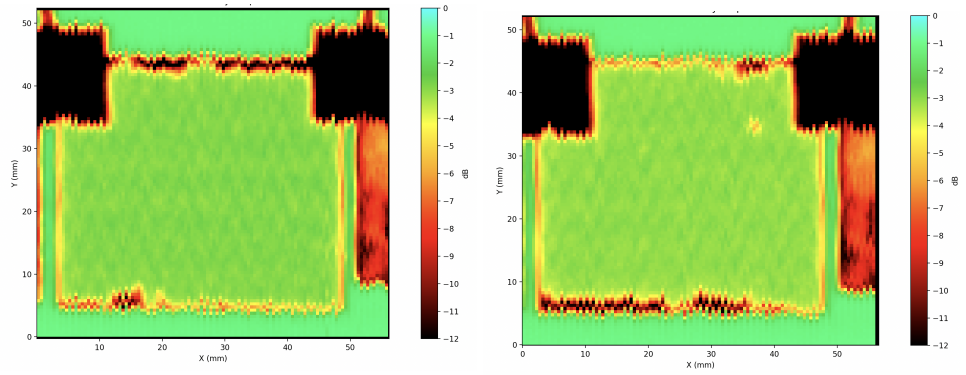
(a) Ultrasonic Scan of IM-7 Scan 1 **(b)** Ultrasonic Scan of IM-7 Scan 2

Figure 6.37: Ultrasonic Scan of IM-7



(a) Ultrasonic Scan of IM-8 Scan 1 **(b)** Ultrasonic Scan of IM-8 Scan 2

Figure 6.38: Ultrasonic Scan of IM-8



(a) Ultrasonic Scan of IM-9 Scan 1 **(b)** Ultrasonic Scan of IM-9 Scan 2

Figure 6.39: Ultrasonic Scan of IM-9

Similar to the trends observed for IM-4 and IM-5, the top edges that suffered from delamination and splaying are clearly indicated by the dark color and lower decibels. In these specimens too, the damages are extremely localized, as there is no hint of damages traveling through the interior of the specimen. Slight damages are observed in the bottom of the specimen, which are also likely caused by the shockwaves traveling back up to the specimen.

Coincidentally, there is also an elastic impact event with IM-9, as apparent in Figure 6.39. Again, this could be due to the misalignment of the impactor and the specimen during the impact. Regardless, the extent of damages are greater than of IM-6, clearly showing the increase of impact energy as intended.

6.4. Comparison Between Quasi-Static Tests and Impact Tests

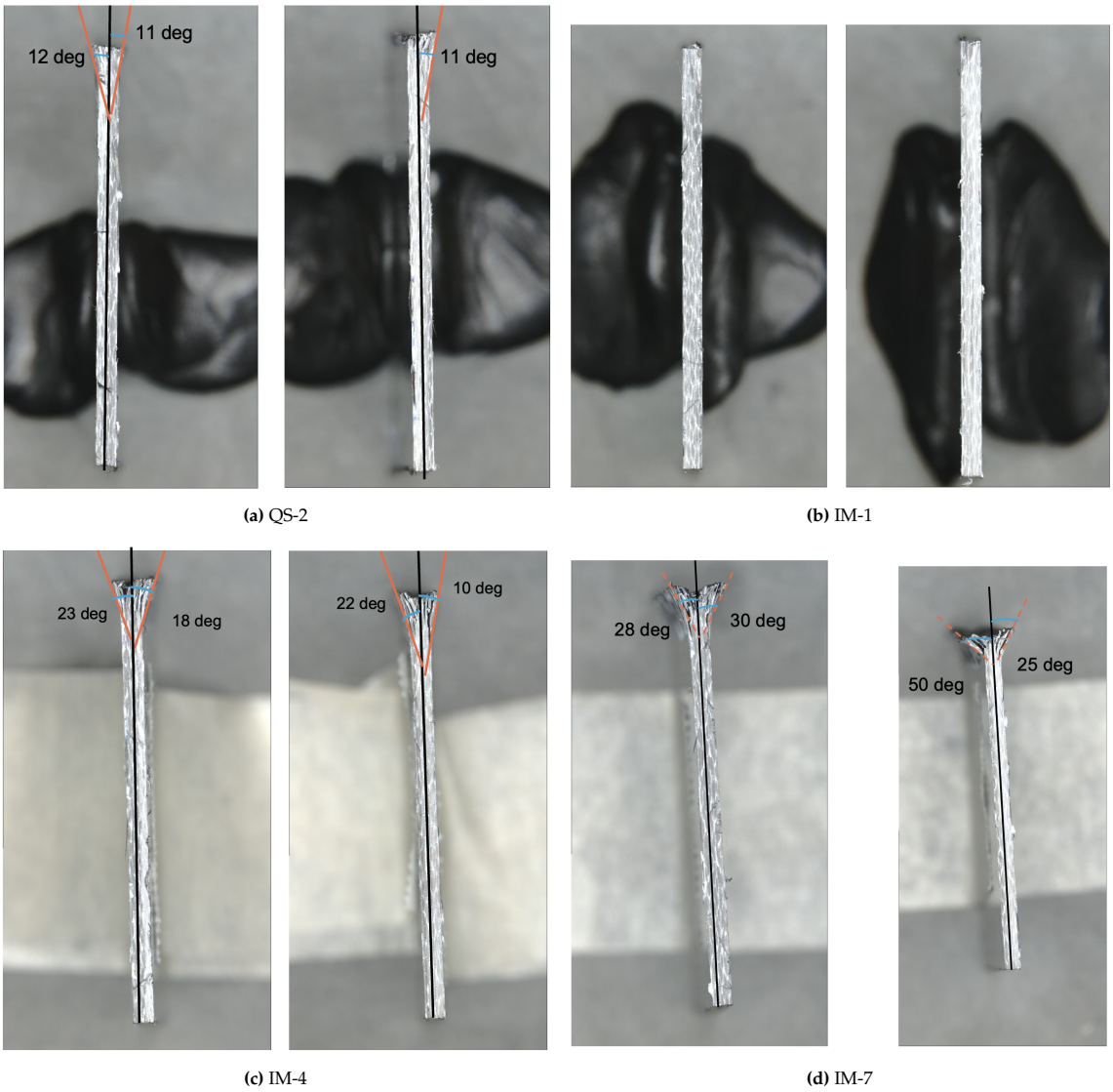
In order to gain an understanding of the strain-rate effects of the material, the impact responses of the specimens are compared against the quasi-static tests. The main point of interest is to investigate how the the specimens behave when subjected to similar amounts of energy and what energy level is required to induce the similar failure modes.

During quasi-static tests, the average maximum force observed is $23,245.14N$. During the impact tests also, the maximum force shows a similar value, in the range of $26kN$, which is as expected, as the maximum force is governed by the carbon fibre, which tends to be strain-rate insensitive. However, note that the force includes the inertial force of the impactor. Regardless, the forces are in a similar range and confirms that the maximum force is indeed not heavily influenced by the strain-rate.

The comparison of how the loads are transferred and the the types of damages is also important. Under quasi-static loading, stress waves generated by the applied load propagate through the specimen in a very slow manner, allowing the specimen to stay in near-static equilibrium mode. This gives time for the stress to redistribute and damage to be developed progressively, different damage mechanisms triggering one another. However, in the impact loading, the loading is introduced in a rapid manner, which travels through the specimen very fast and abruptly. This does not give enough time for the specimen to distribute the load throughout and leads to localized damages. This is also apparent in the damages observed, as the damages observed in the quasi-static analysis tends to extend for a longer length compared to damages caused by the impact loading.

To further assess the differences, the microscopy and the ultrasonic C-Scan captured of the specimen can be referred. The microscopy presents very distinct differences between the failure modes, specifically in terms of splaying and the delamination observed on the specimen. The specimens which are subjected to quasi-static loading present a small degree of splaying and the splaying becomes more severe for impact tests, which increses with increasing impact energies. In order to compare the specimen in a standardized manner, the angles of the splayed edges are measured. First, a vertical line which is parallel to the specimen's height is drawn through the mid-point. Then lines which are parallel to the splaying edges are drawn, which the angles are measured with. Figure 6.40 presents the angle measured for one of the sample from the quasi-static test, QS-2, from impact tests, IM-1, IM-4 and IM-7

respectively.



(a) QS-2 **(b)** IM-1

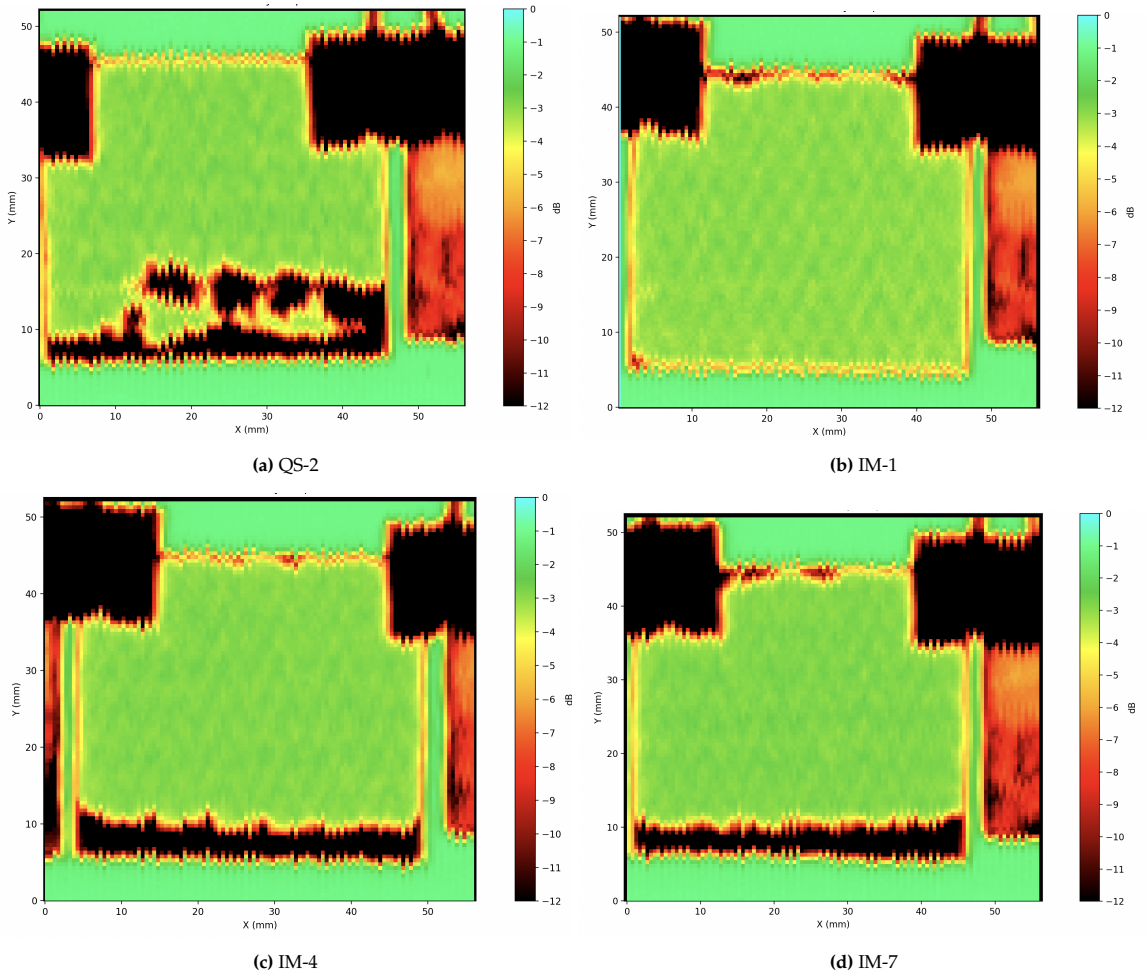
(c) IM-4 **(d)** IM-7

Figure 6.40: Splaying angles comparison

The angles measured show the severity of the splaying. QS-2 presents light splaying angles with degrees of 12° and 11° as presented in Figure 6.40a. IM-1, which experiences elastic deformation during the test, presents no splaying at all. And as the impact energies increses, the splaying increases, with splaying angles of 23°, 18°, 22°, and 10° for IM-4, and even greater with up to 50° of splaying observed in IM-7, shown in Figure 6.40c and Figure 6.40d respectively. Greater degree of splaying implies that the damages are much more localized. As mentioned, with impact loading, there is not enough time for the energy to spread out through the entire specimen and therefore damages are more local.

While the splaying angles increase with impact loading, the extent of damages observed through the ultrasonic C-Scan presents interesting insights. Figure 6.41 presents the ultrasonic scans of QS-2, IM-1, IM-4, and IM-7 respectively. First, the QS-2 presents a wide area of damage as the slow loading allows for the energy to travel through the specimen widely. Secondly, IM-1 presents almost no damage, following the assumption that the loading is elastic. For IM-4 and IM-7 where the splaying of the edge becomes more apparent, the area and the depth of the damages seem very similar, despite their splaying edge have significantly different angles. This observed behavior further validates that with higher impact energy, the damages become more localized, through the means of greater splaying, rather than

the damages spreading wider in the specimen.



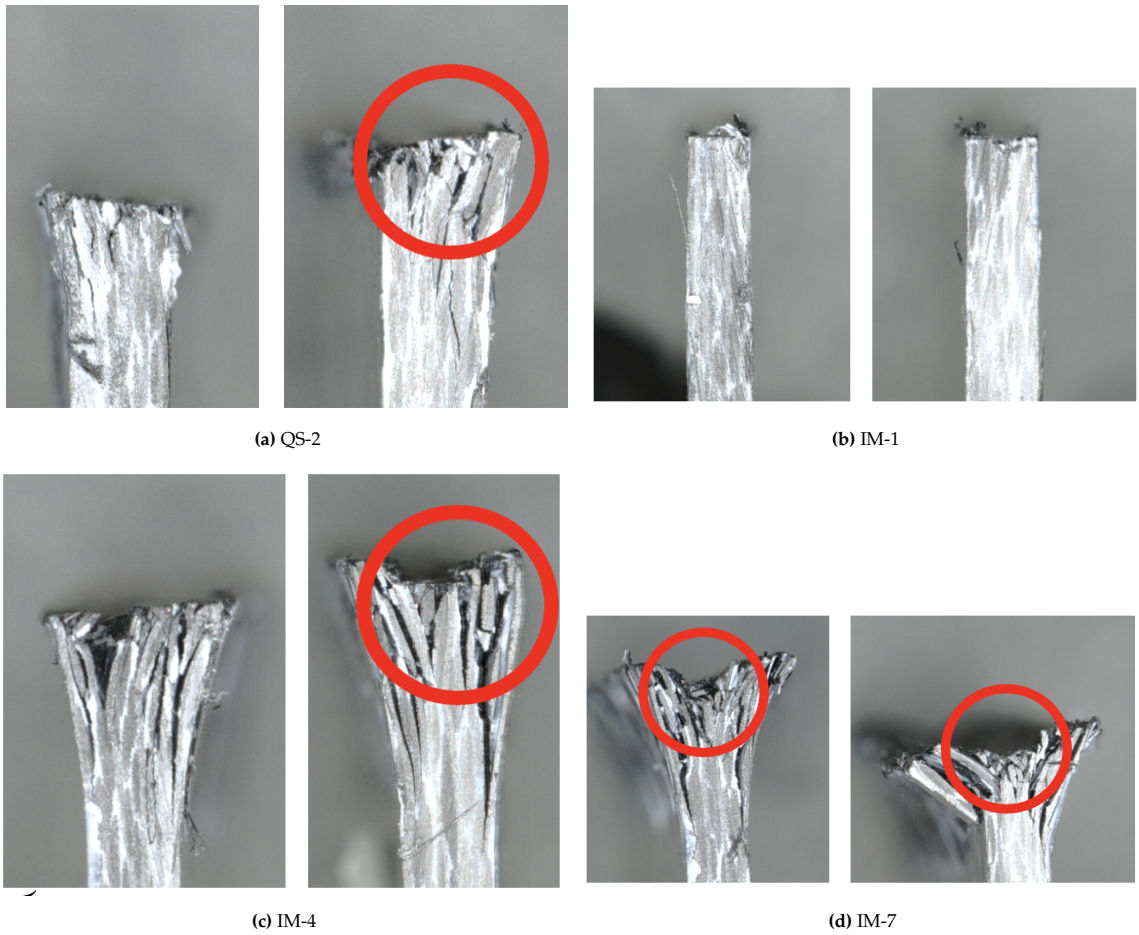
(a) QS-2 **(b)** IM-1

(c) IM-4 **(d)** IM-7

Figure 6.41: Ultrasonic scan comparison

The extent of the damages observed also relate to the energy release rate of the material and the viscoelastic nature of the polymer. The brittle nature of the thermoplastic polymer when subjected to higher loading speed makes the critical energy release rate of the specimen lower, promoting easier crack developments, hence why more localized and uniform cracks are observed together as present in Figure 6.41c and Figure 6.41d. On the other hand, during the quasi-static test, the polymer is more ductile, which makes the critical energy release rate to be higher, constraining the cracks to grow in a uniform manner, as present in Figure 6.41a.

Besides the splaying angles and the extent of the damages, the severity of the damages are also of interest. During the impact, the outer edges of the specimen present splaying behavior and the mid point experiences crushing. The crushing too presents a more localized behavior transitioning from quasi-static testings to impact tests. Figure 6.42 presents magnified view and highlights a specific part where the crushing is observed. This specific failure observed is called the debris wedge, where fragmented fibres and crushed matrix material become trapped at the crush front [29]. This failure mechanism is not observed under quasi-static loading because the slower crushing process allows the fragmented material to escape from the crush front, preventing significant accumulation of debris.



(a) QS-2 **(b)** IM-1

(c) IM-4 **(d)** IM-7

Figure 6.42: Splaying degree comparison

During the quasi-static test, despite a wide damage area observed from the C-Scan, no heavy fibre crushing is observed, as highlighted by the red circle in Figure 6.42a. On the other hand, specimen subjected to impact loading which suffer damage present a heavy fibre crushing, except for IM-1, which remains elastic during the impact due to the low impact energy. With increasing impact energy, the fibre crushing became more localized and severe. Figure 6.42c and Figure 6.42d presents how the wedges of the specimen travels down deeper, as the impact energy increaes. Figure 6.42c's IM-4 shows how the wedge is not fully crushed, however the wedge observed in IM-7, are heavily deformed and completely crushed. This behaviour solidifies the understanding of how the rapid application of load promotes more localized failure before the damage propagates over a larger area.

As mentioned, due to the viscoelastic behavior of the polymer, the polymer presents strain-rate behavior. This is apparent from the experiment results, as in order to induce similar damages, there needs much greater energy. However, due to the localized effects present on the specimen with impact loadings, it is not possible to induce identical failure modes, as observed in the quasi-static tests.

To conlude, Table 6.9 presents the summary of the damage information discussed in this section. The strain-rate behavior captured from the experiment clearly provides important insights about the specimens. By altering the loading speed, different damages are observed, and the degree of those observe damages also are influenced.

Table 6.9: Comparison of observed damage characteristics

Specimen	Damage Types	Average Splaying Degree	Delamination Extent (C-Scan)	Top Edge Debris Wedges
QS-2	Splaying, Delamination	11.3 deg	Widespread	None
IM-1	None	None	None	None
IM-4	Splaying, Delamination	18.3 deg	Top edges only	Light
IM-7	Splaying, Delamination	33.25 deg	Top edges only	Heavy

6.5. Conclusion

In conclusion, the test results showed valuable insights as well as the limitations of the current set-up. While the energy analysis and the damage observations provides great insights towards how the specimen behaves when subjected impact, force and impulse analysis could not be fully completed as it was not possible to identify the loading exerted on the specimen. While this is unfortunate, this gives a lot of room for potential improvements and understanding of the current set-up. Next section is dedicated to describe what could be possible done in the future to get better understanding of strain-rate loading of CF/PPS.

7

Challenges, Recommendations and Evaluation

7.1. Introduction

This thesis work explored the investigation of the on-edge impact response of the CF/PPS. Throughout the research work, the energy analysis and force analysis are performed in order to evaluate the response of the materials between quasi-static and impact test. Different methods are investigated and the challenges of the methods performed are analyzed. As Winston Churchill said, failure is not fatal and it is the courage to continue that counts. This chapter details the challenges encountered throughout the work and possible improvements that could be made to tackle these challenges for any future research.

7.2. Dropping Heights

As mentioned previously, it is not possible to analytically calculate the height which the impactor should be dropped from to subject the specimen to the same energy, which the specimen absorbed during the quasi-static tests. In earlier stages of the thesis, significant time and resources were spent on finding the appropriate height through trial and error. Almost 30 specimens were used for this purposes and performing the post-processing parallel with the tests was challenging.

For future reference, finite element analysis could perhaps be first utilized in order to estimate the appropriate heights. Of course, since finite element analysis is only a simulation and must be validated, further calibration should take place prior to the actual experiemnt. Gaining such understandings could reduce waste of resources, including time, material and manpower.

Another point is the fact that the minimum dropheight which introduced stable measurements are a little too high. A height of $500mm$, $600mm$ would have been optimal, but the droptower is not built for such low dropheights. It is physically not possible to change this at the droptower, therefore a droptower of a smaller scale and more precise mechanisms would be beneficial to allow for more spot-on comparison with the quasi-static tests.

7.3. Boundary Conditions

Boundary condition is one of the biggest challenge in this thesis work. In earlier stages of the thesis, the objective was to not fully clamp the specimen. The reason for this is to ensure that the specimen fully absorbs the load and prevent energy dissipation due to friction. Thus, initially, the specimen was standing with the support of the clamp blocks, but not enough clamp force to induce friction. However, with this condition, the specimen vibrated significantly and it was not possible to obtain a reasonale Force vs. Time curve. Therefore, the specimen was clamped in the end, with preliminary understanding that the friction plays a small role. As the preliminary calculations present, the possible energy loss was roughly 6.1% of the lowest energy case for impacts and 10% of the quasi-static case. While it may seem low, the friction surely plays a role in the energy absorbed. This was inevitable for this set-up and needs

further investigation as the objective is to present a method to assess the material's behavior, which can only take place when the material's behavior is solely isolated.

Similar example of clamping the specimen with a reasonably small set-up is the ASTM D6641, presented earlier in this work. This set-up uses total of 8 fasteners and has a gripper surface which prevents specimen from moving, even if it is a static test, as present in Figure 7.1.

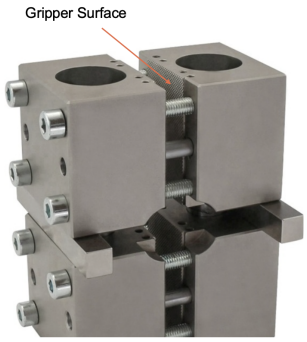


Figure 7.1: ASTM D6641 Gripper Surface [34]

For future studies, the boundary condition could include more and bigger fasteners to introduce greater friction, with a combination of gripper surface. This could reduce the possible slipping between the specimen and the boundary condition. One may say if the Force vs. Time curve was not fully utilized, it may make sense to go back to the set-up of not clamping the specimen, to neglect the effects of friction completely in a confident manner. While this is a valid point, Force vs. Time curve will provide significantly valuable insights to the specimen, such as the impulse during the impact. Thus more efforts should be devoted into clamping the specimen with greater force as well as a better measurement techinque is recommneded.

7.4. Measurements

One of the key element used in this work to draw conclusions is the Force vs. Time curve of the impactor. The objective however, is to obtain the force which the specimen experiences. As the Force vs. Time curve is obtained from the impactor, the measurement is not be able to accurately capture what the specimen goes through. For future, it would be necessary to subtract this effect or find a strategy to only measure what the specimen goes through.

In earlier stages of the thesis work it was considered to place strain gauges on to the specimen to track the displacement. However, due to the small area of the specimen which are exposed above the boundary condition and the fact that the impact loading may crush the strain gauges, it was not possible to implement this to the set-up.

This work presented that the specimens remain elastic for lower impact energy, thus in the end, it could be an option to place strain-gauages on to the exposed area for impacts with lower energy to obtain the force experienced by the specimen. For higher impact energies, as the impacts are very localized, perhaps the strain-gauges could be placed on the lower end of the exposed area to track the force. This would be an underestimate, but would provide insightful information to understand how much force the specimen experienced during the loading. Another possible method would be to apply a filter on the Force vs. Time data to remove the influence of the natural frequencies and subtract the inertial effects. This too, would not be a direct measurement and therefore may be subject to discussion for its accuracy.

7.5. High-Speed Camera

One of the unfortunate result of this thesis was the fact that the high-speed camera was not able to capture the behavior of the speciemn during the impact. As mentioned in chapter 5, the high-speed

camera is used to track the velocity of the impactor before and after the impacts. One other thing which would have been great to observe from the high-speed camera was the behavior of the specimen during the impact. It would have been valuable to investigate how the shockwave travels through the specimen and to see if the specimen behaves during the impact. It would also be great to capture the vibration of the impactor after the impact, to assess if the natural frequency of the impactor is influencing the Force vs. Time as anticipated in earlier in the work.

Specifically for the natural frequency of the impactor, as the Nyquist criterion can be referred as a starting point. The Nyquist criterion requires that the measuring frequency must be twice greater than the frequency of interest, in order to capture the frequency of interest. For the expected natural frequency of $5000Hz$, the highspeed camera's framerate should be at least $10,000Hz$ to even attempt to trace the natural frequency of the impactor. This however, is the bare minimum and therefore in order to gain a confident understanding of the natural frequency of the impactor, it would be necessary to capture the response of the impactor with a highspeed camera with a greater framerate. Ideally, based on engineering judgement, about 10 times the natural frequency would be sufficient to capture the vibration of the impactor after the impact. This means that a framerate of at least $50,000$ is necessary.

Other option during the thesis work was to increase the size of the pixel and increase the framerate. However due to the small size of the specimen, it was not reasonable to sacrifice the resolution quality for framerate enhancement as one will not be able to assess how the specimen behaves due to the low quality video.

7.6. Abaqus Analysis

As mentioned in the result section, Abaqus analysis is used to check if the natural frequencies. Just like any simulation model, there exists some parts that could use some improvements to increase the confidence in the analysis and computational efficiency. This section lists the possible improvements that could be made in the future.

The contact could have been better modeled, specifically with the M10 threaded part of the impactor. During the modeling stage, to simplify the model, the threaded parts were treated as smooth cylindrically inward extruded part. While in reality it is true that the threaded part essentially constrains the movements in all six degrees of freedom, including the threaded geometric characteristics to the impactor and giving it specific boundary conditions which serve the purpose of the threads could increase the accuracy of the simulation and provide much stronger confidence of the analysis regarding the oscillation observed in the Force vs. Time curve.

The element type could also have been different. The impactor was modeled with 3D elements to capture the full geometric details. Looking back, in order to increase the computational efficiency, the 2D axis-symmetry option could also have been used. As the shape of the impactor is symmetric around its axis, 2D Axis-symmetry option would also have been reasonable, if computational efficiency is part of a consideration.

8

Conclusion

This this work presented a set-up to investigate the on-edge impact performance of the woven CF/PPS laminates both under quasi-static and impact loading conditions. Through a combination of mechanical testing, force-response analysis, and post-test damage characterization, the influence of strain-rate on the mechanical behavior is analyzed. Through those analysis, the feasibility of the presented experiment set-up are also evaluated. Particular effort is also devoted into understanding the transition between the damage mechanisms observed under quasi-static loading and those activated during the impact event.

The experimental results demonstrated that the failure behavior of the laminate is strongly dependent on the loading condition. Damages observed in impact tests were much more localized than of quasi-static tests. The Force vs. Time curve from the impact tests were heavily governed by the post-oscillation of the impactor after the impact event, which hindered the analysis for force absorbed by the specimen and the impulse analysis. Energy analysis on the other hand, is succesfully completed, showing the difference as the loading speed increases. It demonstrated how much of an influence polymer's strain-rate dependent behavior has on the entire composite material's failure.

To conclude, the research objectives are revisited and commented assessing if they have been successfully achieved.

RO.1: Characterize failure mechanisms of composite under on-edge loading

RO.1 is succesfully achieved through investigating the damages after the quasi-static and impact tests. Through micrscopy, highspeed camera footage and ultrasonic scans as well as the measured data Force vs. Dipslacement and Force vs. Time curves, the failure mechanisms and more prominent failures are identified for the on-edge loading of composite coupons.

RO.2: Quantify the energy absorption of composite materials under quasi-static loading to define equivalent impact energy levels for dynamic testing

RO.2 is also achieved by taking a step further from **RO.1**. By post-processing the data from the quasi-static tests, the energy absorbed by the specimen during quasi-static tests are quantified and they are succesfully used as input for the impact tests.

RO.3: Compare failure modes between quasi-static and impact loading for on-edge loading case

RO.3 too is achieved by choosing suitable measures and using them for comparison. These measures are ones used to achieve **RO.1**, which provide thorough understanding of the specimens' mechanical performances as well as their failure behaviors.

RO.4: Investigate how increasing impact energy influences the strain rate-dependent behaviour of composite materials under on-edge loading

Finally, taking a step further with the impact tests by increasing the impact energies and assessing the damages formed, force and energy responses the **RO.4** is achieved. The evoluation of the failures of the specimens are also investigated with microscopy and C-scans.

RO.Main: Investigate the influence of on-edge impact loading on the strain-rate-dependent behavior of composite materials and to develop a cost-effective experimental approach for their evaluation in aerospace applications.

Summing all the previous research objectives, it can also be said that the **RO.Main** is also achieved, as a succesful investigation of the on-edge impact loading are completed in this thesis work, with a set-up that is cost-effective. However, as mentioned there still exists some room for improvement, specifically for the boundary conditions and the test set-up, to ensure that the performance of the materials are even better captured.

In conclusion, the research objectives are successfully achieved, with some improvements that could be made for future studies. This work was an exploratory work, whcih explored a possible option for on-edge impact loading, which has not been invesetigated fully in the field. This work could be a foundation for the next work in this topic. The thesis is concluded in the hopes that this provides a better map to the new on-edge impact researcher's goals.

References

[1] Mohamed Ali, Yasser Shaban, and Samy Lawaty. "Impact-Induced Damage Mechanisms in PPS-Based Laminates: Experimental Characterization and ANN Prediction of Residual Mechanical Properties". In: *Journal of Engineering and Applied Science* 72 (2025), p. 213. DOI: 10.1186/s44147-025-00792-9.

[2] A. Arteiro, P. J. Gray, and P. P. Camanho. "Simulation of edge impact and compression after edge impact in CFRP laminates". In: *Composite Structures* 240 (2020), p. 112018. DOI: 10.1016/j.compstruct.2020.112018.

[3] Richard G. Budynas and J. Keith Nisbett. *Shigley's Mechanical Engineering Design*. 10th ed. New York, NY: McGraw-Hill Education, 2015. ISBN: 978-0-07-339820-4.

[4] Carbon (Xiamen) New Material Co., Ltd. *PPS CF Reinforced Composites*. Product overview and material properties for carbon fiber reinforced polyphenylene sulfide (PPS-CF) composites. CARBONELE. 2024. URL: https://www.carbonele.com/products/cf-series/pps-cf-series/ (visited on 06/30/2026).

[5] N. A. Fleck. "Compressive Failure of Fiber Composites". In: *Advances in Applied Mechanics*. Vol. 33. Academic Press, 1997, pp. 43–117.

[6] N. A. Fleck, P. M. Jelf, and P. T. Curtis. "Compressive Failure of Laminated and Woven Composites". In: *Journal of Composites Technology and Research* 17.3 (1995), pp. 212–220.

[7] Hottinger Brüel & Kjaer (HBK). *Strain Gauge Selection and Installation Workshop*. 2026. URL: https://www.hbm.com/index.php?L=0&id=2996 (visited on 06/08/2026).

[8] Instron. *ASTM D6641 – Compressive Properties of Polymer Matrix Composite Materials Using a Combined Loading Compression (CLC) Test Fixture*. Instron. 2024. URL: https://www.instron.com/en/testing-solutions/astm-standards/astm-d6641/ (visited on 06/29/2026).

[9] George C. Jacob et al. "Energy Absorption in Polymer Composite Materials for Automotive Crashworthiness". In: *Journal of Composite Materials* 36.7 (2002), pp. 813–850. DOI: 10.1177/0021998302036007279.

[10] Vassilios Kostopoulos. *Composites Testing as Part of a Building Block Approach, Part 2: Upper Building Block Levels*. CompositesWorld. Nov. 19, 2021. URL: https://www.compositesworld.com/articles/composites-testing-as-part-of-a-building-block-approach-part-2-upper-building-block-levels (visited on 06/11/2026).

[11] Dragan Kreculj and Boško Rašuo. "Impact damage modeling in laminated composite aircraft structures". In: *Sustainable Composites for Aerospace Applications*. Ed. by P. W. R. Beaumont, C. Soutis, and A. Hodzic. Elsevier, 2018. Chap. 7, pp. 125–153. DOI: 10.1016/B978-0-08-102131-6.00007-4.

[12] N. Li and P. H. Chen. "Experimental investigation on edge impact damage and compression-after-impact behavior of stiffened composite panels". In: *Composite Structures* 138 (2016), pp. 134–150. DOI: 10.1016/j.compstruct.2015.11.060.

[13] Haibao Liu, Brian G. Falzon, and Wei Tan. "Experimental and numerical studies on the impact response of damage-tolerant hybrid unidirectional/woven carbon-fibre reinforced composite laminates". In: *Composites Part B: Engineering* 136 (2018), pp. 101–118. DOI: 10.1016/j.compositesb.2017.10.016.

[14] Lulu Ma et al. "Review of Strain Rate Effects of Fiber-Reinforced Polymer Composites". In: *Polymers* 13.17 (2021), p. 2839. DOI: 10.3390/polym13172839.

[15] A. Malhotra and F. J. Guild. "Impact damage to composite laminates: Effect of impact location". In: *Applied Composite Materials* 21 (2014), pp. 165–177. DOI: 10.1007/s10443-013-9382-z.

[16] A. Malhotra, F. J. Guild, and M. J. Pavier. "Edge impact to composite laminates: Experiments and simulations". In: *Journal of Materials Science* 43 (2008), pp. 6661–6667. DOI: 10.1007/s10853-008-2863-z.

[17] P. K. Mallick. "Failure of Polymer Matrix Composites (PMCs) in Automotive and Transportation Applications". In: *Failure Mechanisms in Polymer Matrix Composites*. Woodhead Publishing, 2012. Chap. 12, pp. 368–392. ISBN: 9781845697501.

[18] T. H. G. Megson. *Aircraft Structures for Engineering Students*. 7th ed. Oxford, UK: Butterworth-Heinemann, 2021. ISBN: 9780128228685.

[19] Nagaraj Murugesan and Vasudevan Rajamohan. "Prediction of Progressive Ply Failure of Laminated Composite Structures: A Review". In: *Archives of Computational Methods in Engineering* (2016). ISSN: 1134–3060. DOI: 10.1007/s11831-016-9191-2.

[20] Masato Nishi, Kei Saito, and Bo Ren. "Discrete FE Modeling to Simulate Micro-Fracture Modes in Progressive Crushing of Fiber Reinforced Composite Tubes". In: *18th European Conference on Composite Materials* (Athens, Greece). 2018, pp. 1–8.

[21] Benjamin Ostré et al. "Edge impact damage scenario on stiffened composite structure". In: *Journal of Composite Materials* (2014). DOI: 10.1177/0021998314537325.

[22] Benjamin Ostré et al. "Edge impact modeling on stiffened composite structures". In: *Composite Structures* 126 (2015), pp. 314–328. DOI: 10.1016/j.compstruct.2015.02.020.

[23] Benjamin Ostré et al. "Experimental analysis of CFRP laminates subjected to compression after edge impact". In: *Composite Structures* 152 (2016), pp. 767–778. DOI: 10.1016/j.compstruct.2016.05.068.

[24] Benjamin Ostré et al. "Finite element analysis of CFRP laminates subjected to compression after edge impact". In: *Composite Structures* 153 (2016), pp. 478–489. DOI: 10.1016/j.compstruct.2016.06.041.

[25] Phu Thai Tech. *Torque Wrench 1 Nm–6 Nm 1/4 Inch GARANT 656050 6*. Product page for the GARANT 656050 6 adjustable torque wrench (1–6 N·m). Phu Thai Tech. 2019. URL: https://phuthaitech.com.vn/products/can-siet-luc-1-nm-6-nm-14-inch-garant-656050-6 (visited on 06/30/2026).

[26] Carolina Ramirez et al. "High Strain Rate Characterization of Thermoplastic Fiber-Reinforced Composites under Compressive Loading". In: *Aerospace Engineering*. IntechOpen, 2019. DOI: 10.5772/intechopen.82215.

[27] Andrew T. Rhead, David Marchant, and Richard Butler. "Compressive strength of composite laminates following free edge impact". In: *Composites Part A: Applied Science and Manufacturing* 41.8 (2010), pp. 1056–1065. DOI: 10.1016/j.compositesa.2009.10.024.

[28] Svetlana Risteska et al. "The In-Plane Compression Response of Thermoplastic Composites: Effects of High Strain Rate and Type of Thermoplastic Matrix". In: *Journal of Composites Science* 9.6 (2025), p. 293. DOI: 10.3390/jcs9060293.

[29] J. Michael Starbuck, Daniel O. Adams, and Marc Courteau. "Energy Absorbing Damage Mechanisms in Progressive Crushing of Composite Tubes". In: *Proceedings of the American Society for Composites Technical Conference* (2011), pp. 1–15.

[30] Riming Tan et al. "Relationship Between Matrix Cracking and Delamination in CFRP Cross-Ply Laminates Subjected to Low Velocity Impact". In: *Materials* 12.23 (2019), p. 3990. DOI: 10.3390/ma12233990.

[31] Wei Tan and Brian G. Falzon. "Modelling the Crush Behaviour of Thermoplastic Composites". In: *Composites Science and Technology* 134 (2016), pp. 57–71. ISSN: 0266-3538. DOI: 10.1016/j.compscitech.2016.07.015.

[32] Wei Tan et al. "The Role of Material Characterisation in the Crush Modelling of Thermoplastic Composite Structures". In: *Composite Structures* 153 (2016), pp. 914–927. DOI: 10.1016/j.compstruct.2016.07.011.

[33] R. Telford et al. “Experimental and numerical study of bending-induced buckling of stiffened composite plate assemblies”. In: *Composites Part B: Engineering* 233 (2022), p. 109642. DOI: 10.1016/j.compositesb.2022.109642.

[34] TestResources. *ASTM D6641 Compression Testing for Polymer Matrix Composite Laminates*. Overview of ASTM D6641 compression testing using the Combined Loading Compression (CLC) fixture. TestResources. 2024. URL: https://www.testresources.net/applications/standards/astm/astm-d6641-compression-testing-for-polymer-matrix-composite-laminates (visited on 06/30/2026).

[35] Solver I. Thorsson, Anthony M. Waas, and Mostafa Rassai. “Numerical investigation of composite laminates subject to low-velocity edge-on impact and compression after impact”. In: *Composite Structures* 203 (2018), pp. 648–658. DOI: 10.1016/j.compstruct.2018.06.094.

[36] Solver I. Thorsson et al. “Experimental investigation of composite laminates subject to low-velocity edge-on impact and compression after impact”. In: *Composite Structures* 186 (2018), pp. 335–346. DOI: 10.1016/j.compstruct.2017.11.084.

[37] S. Viswanath. “Predicting Bearing Failure of Composites with FEM”. Master’s Thesis. Delft, The Netherlands: Delft University of Technology, Faculty of Aerospace Engineering, 2025. URL: https://resolver.tudelft.nl/uuid:2dd45290-9ce6-4797-bc7a-6ccc23db06e6 (visited on 06/20/2026).

[38] Fang Wang, Jun Ding, and Zhiqian Chen. “Statistical Analysis of the Progressive Failure Behavior for Fiber-Reinforced Polymer Composites under Tensile Loading”. In: *Polymers* 6.1 (2014), pp. 145–159. DOI: 10.3390/polym6010145.

[39] H. Wang. “Rate-dependent stress–strain properties of solders”. In: *Robust Design of Microelectronics Assemblies Against Mechanical Shock, Temperature and Moisture*. Elsevier, 2015. Chap. 12, pp. 411–446. DOI: 10.1016/B978-1-84569-528-6.00012-5.

[40] Shiyu Wang et al. “Influence of Strain Rate and Temperature on Mechanical Properties of Carbon Woven-Ply PPS Thermoplastic Laminates under Dynamic Compression”. In: *Polymer Testing* 89 (2020), p. 106725. DOI: 10.1016/j.polymertesting.2020.106725.

[41] Shiyu Wang et al. “Influence of strain rate and temperature on mechanical properties of carbon woven-ply PPS thermoplastic laminates under dynamic compression”. In: *Polymer Testing* 89 (2020), p. 106725. DOI: 10.1016/j.polymertesting.2020.106725.

[42] Wenjun Xu, Longquan Liu, and Wu Xu. “Experiments and Finite Element Simulations of Composite Laminates Following Low Velocity On-Edge Impact Damage”. In: *Polymers* 14.9 (2022), p. 1744. DOI: 10.3390/polym14091744.

[43] Ahmet Yapici and Mehmet Metin. “Effect of Low Velocity Impact Damage on Buckling Properties”. In: *Engineering* 1 (2009), pp. 161–166. DOI: 10.4236/eng.2009.13019.

[44] Shizhuo Zou et al. “Development of the Split-Hopkinson Pressure Bar and Its Application in Testing the Dynamic Mechanical Properties of Quasi-Brittle Materials: A Review”. In: *Journal of Materials Research and Technology* 33 (2024), pp. 9463–9483. DOI: 10.1016/j.jmrt.2024.11.244.

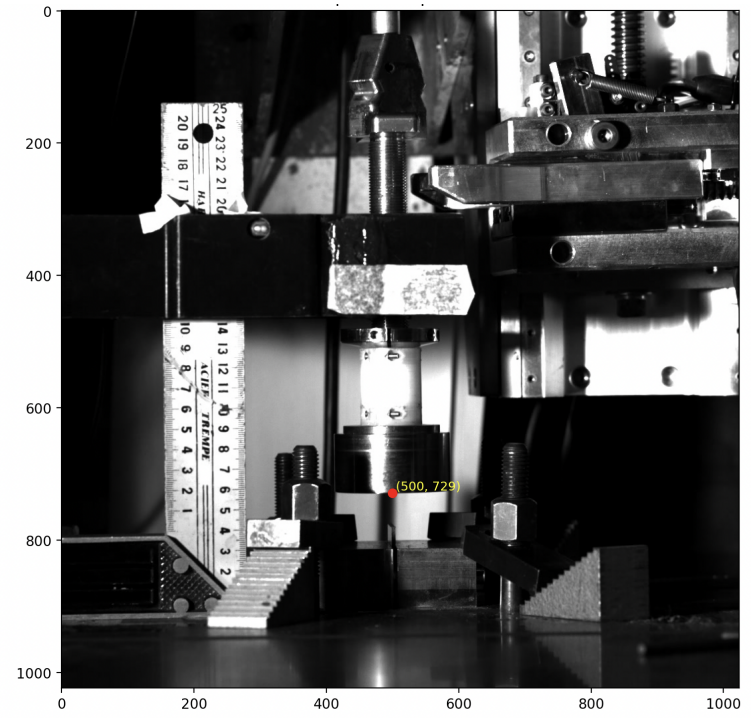
A

High-Speed Camera Footage

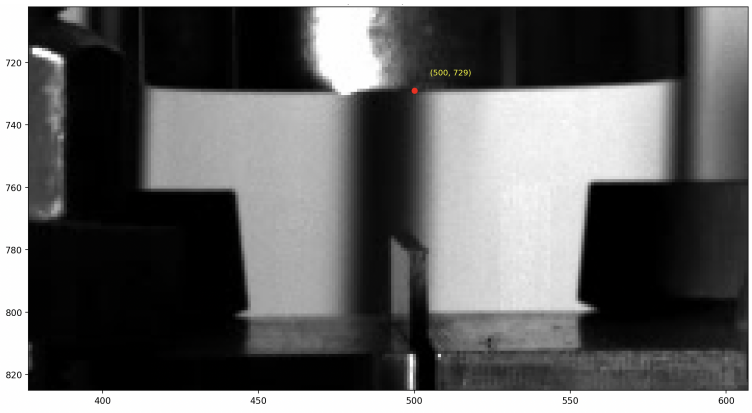
This appendix presents the high-speed camera footage, along with the frames used for the velocity measurements.

A.1. IM-1

A.1.1. IM-1 Before Impact Energy Calculation

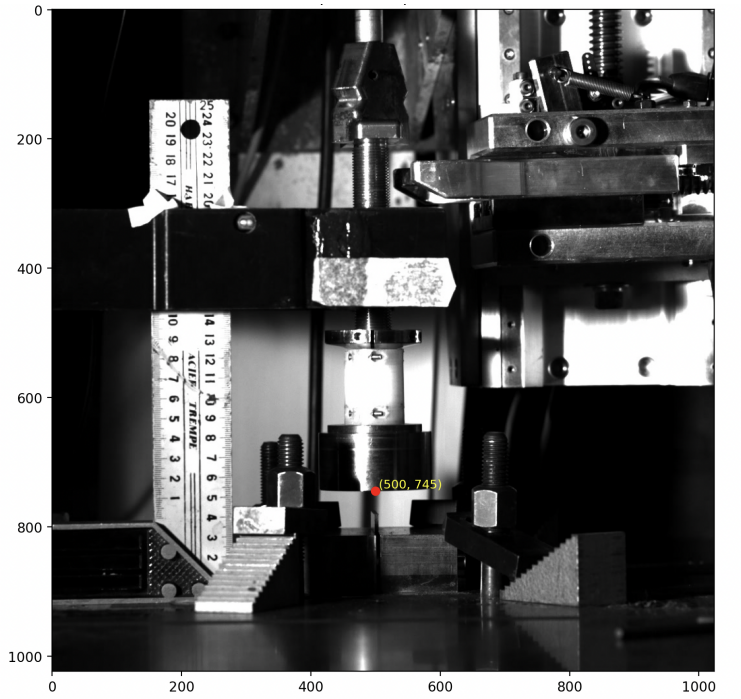


(a)

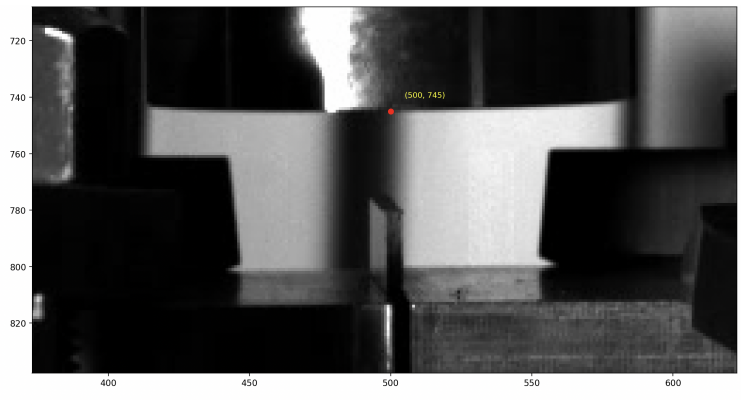


(b)

Figure A.1: IM-1 Frame 729



(a)



(b)

Figure A.2: IM-1 Frame 745

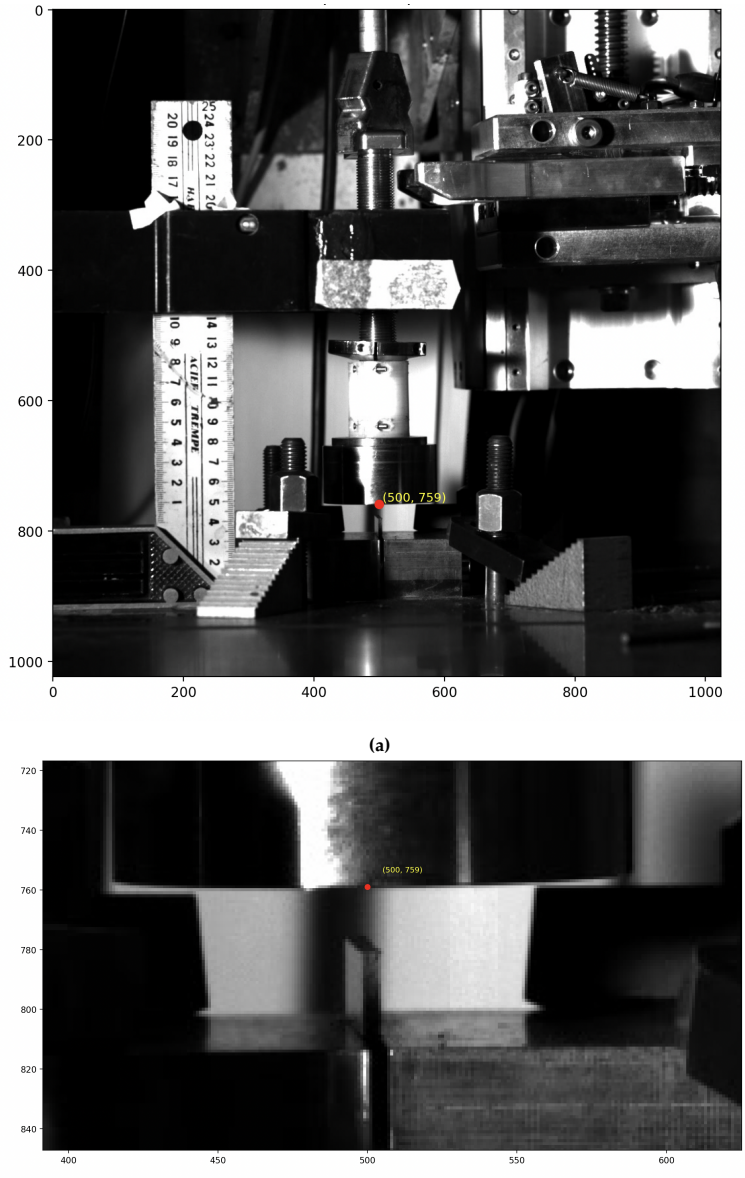
$$\Delta y = 745 - 729 = 16$$

$$\Delta t = \frac{10}{6400} = 0.001563 \text{ s}$$

$$v = 2.99 \text{ m/s}$$

$$E_k = 10.31 \text{ J}$$

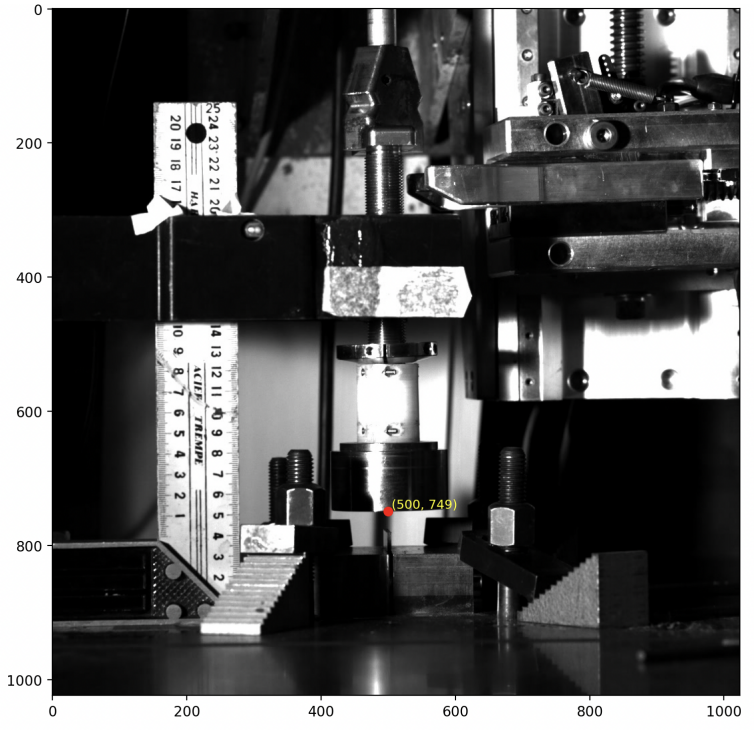
A.1.2. IM-1 After Impact Energy Calculation



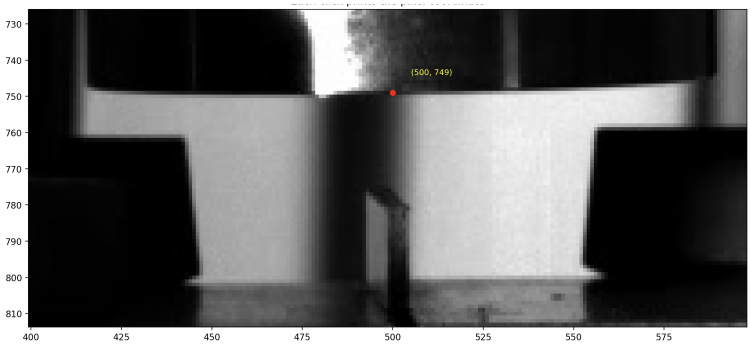
(a)

(b)

Figure A.3: IM-1 Frame 749



(a)



(b)

Figure A.4: IM-1 Frame 759

$$\Delta y = 759 - 749 = 10$$

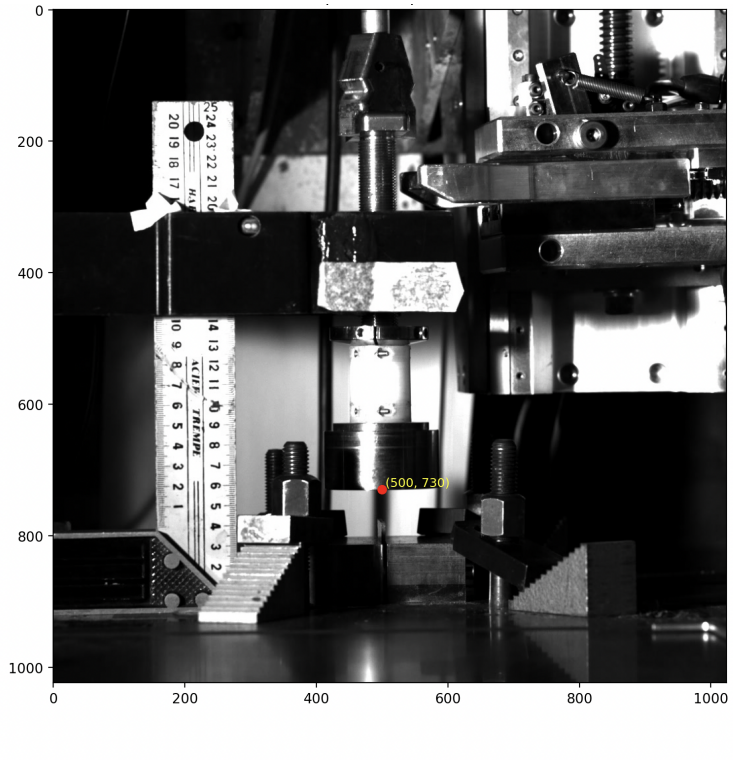
$$\Delta t = \frac{14}{6400} = 0.002188 \text{ s}$$

$$v = 1.47 \text{ m/s}$$

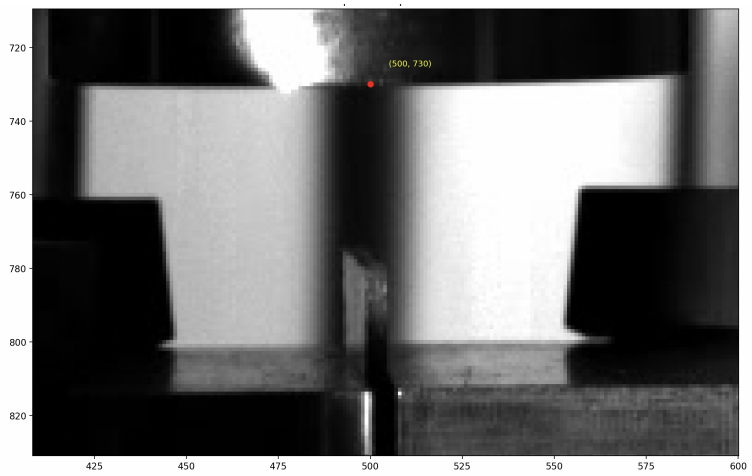
$$E_k = 2.50 \text{ J}$$

A.2. IM-2

A.2.1. IM-2 Before Impact Energy Calculation

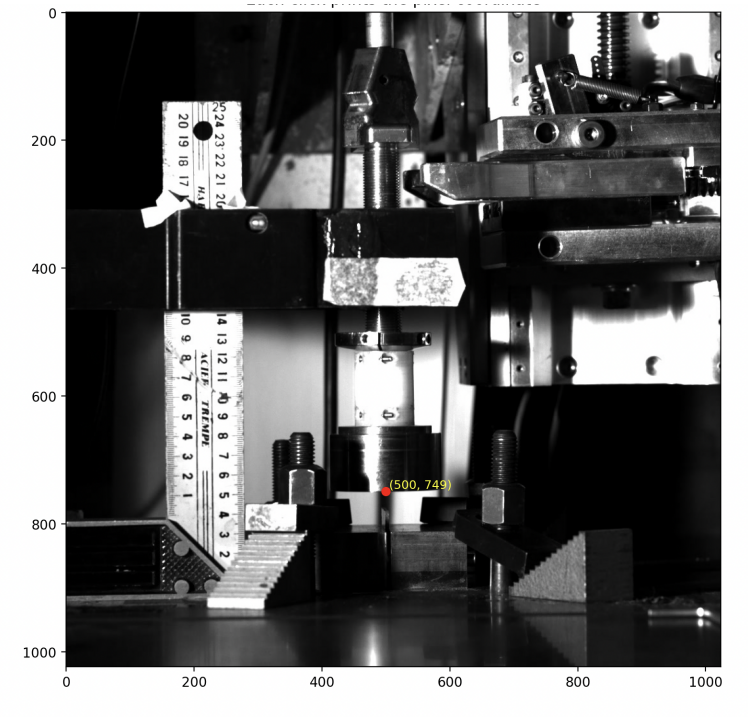


(a)

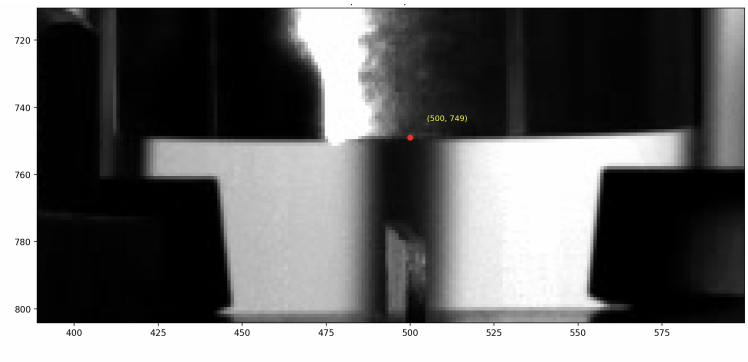


(b)

Figure A.5: IM-2 Frame 730



(a)



(b)

Figure A.6: IM-2 Frame 749

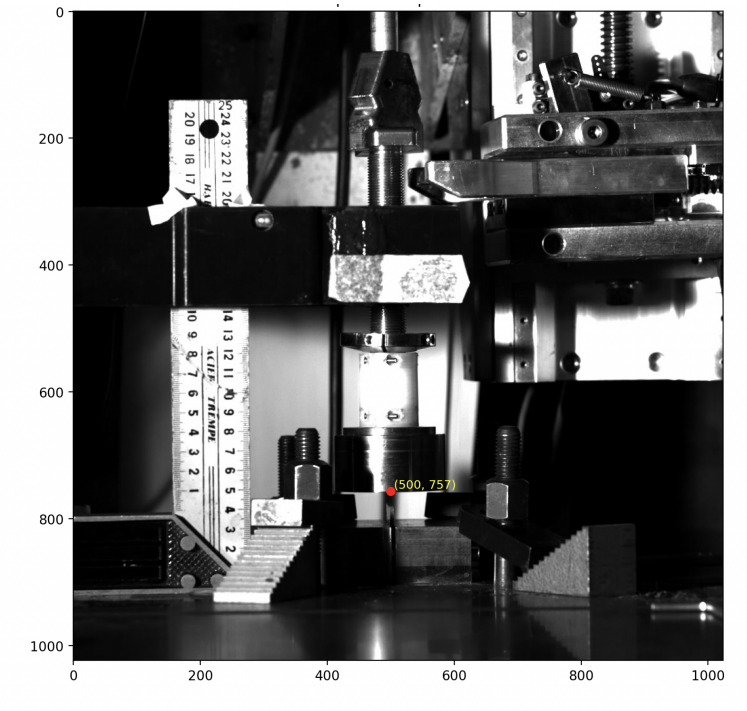
$$\Delta y = 749 - 730 = 19$$

$$\Delta t = \frac{12}{6400} = 0.001875 \text{ s}$$

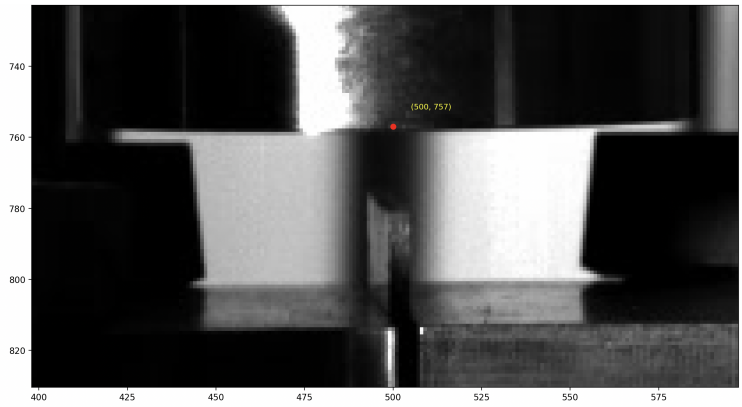
$$v = 2.92 \text{ m/s}$$

$$E_k = 9.84 \text{ J}$$

A.2.2. IM-2 After Impact Energy Calculation

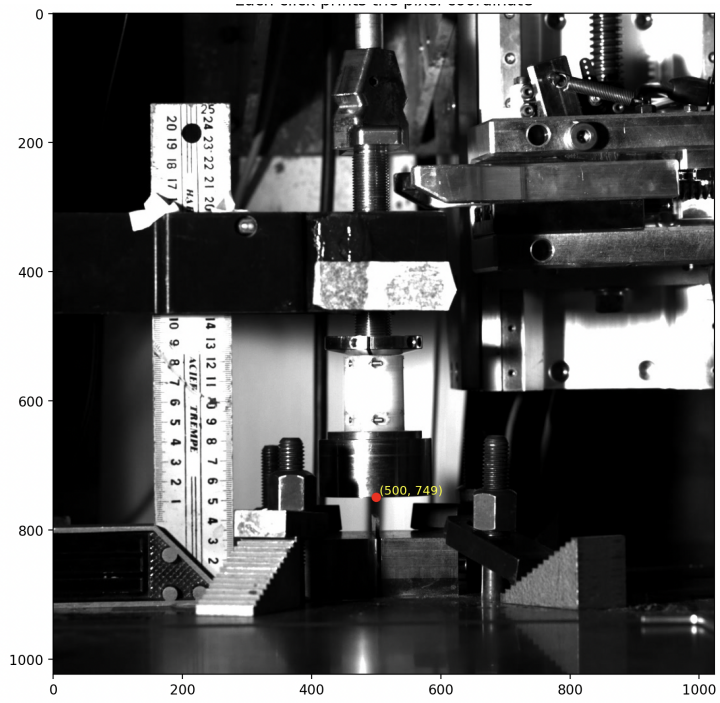


(a)

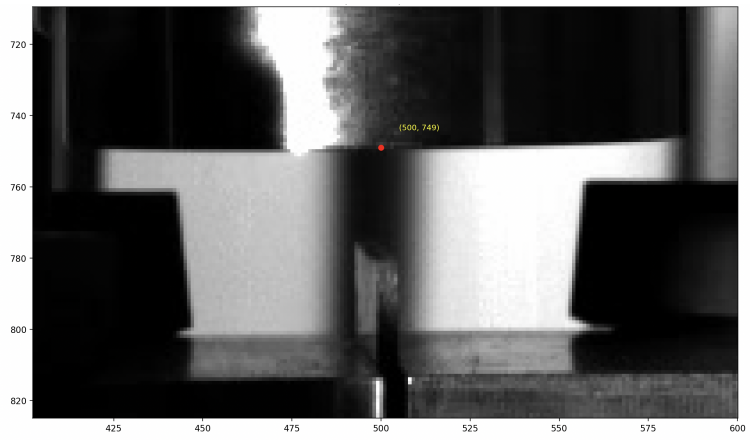


(b)

Figure A.7: IM-2 Frame 749



(a)



(b)

Figure A.8: IM-2 Frame 757

$$\Delta y = 757 - 749 = 8$$

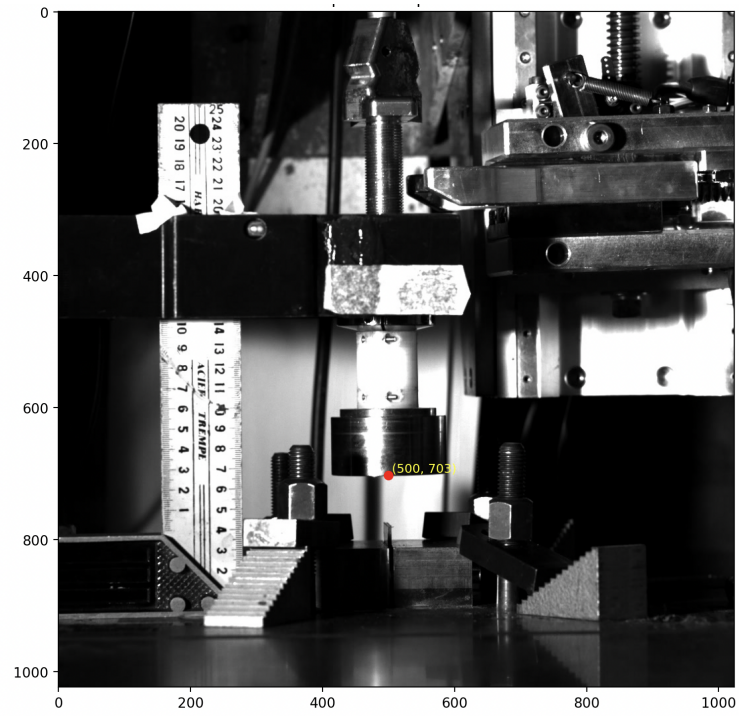
$$\Delta t = \frac{11}{6400} = 0.001719 \text{ s}$$

$$v = 1.50 \text{ m/s}$$

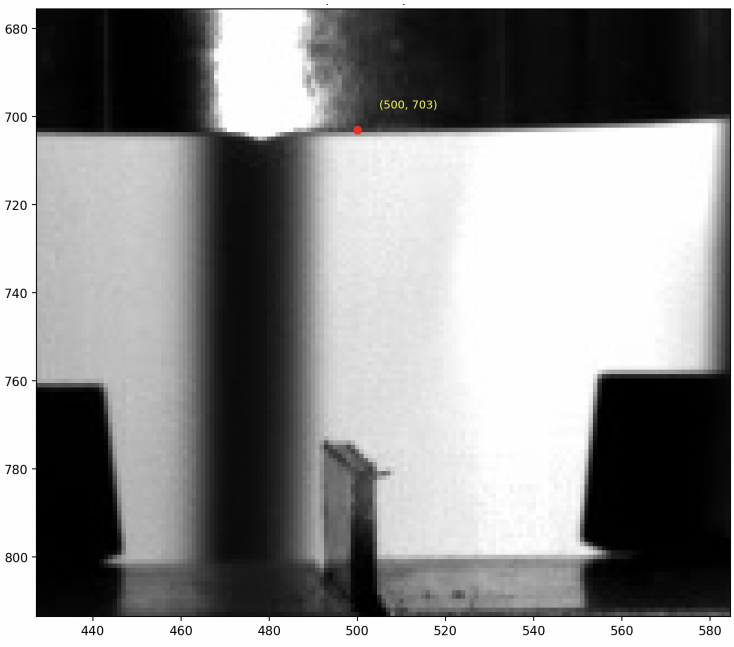
$$E_k = 2.59 \text{ J}$$

A.3. IM-3

A.3.1. IM-3 Before Impact Energy Calculation

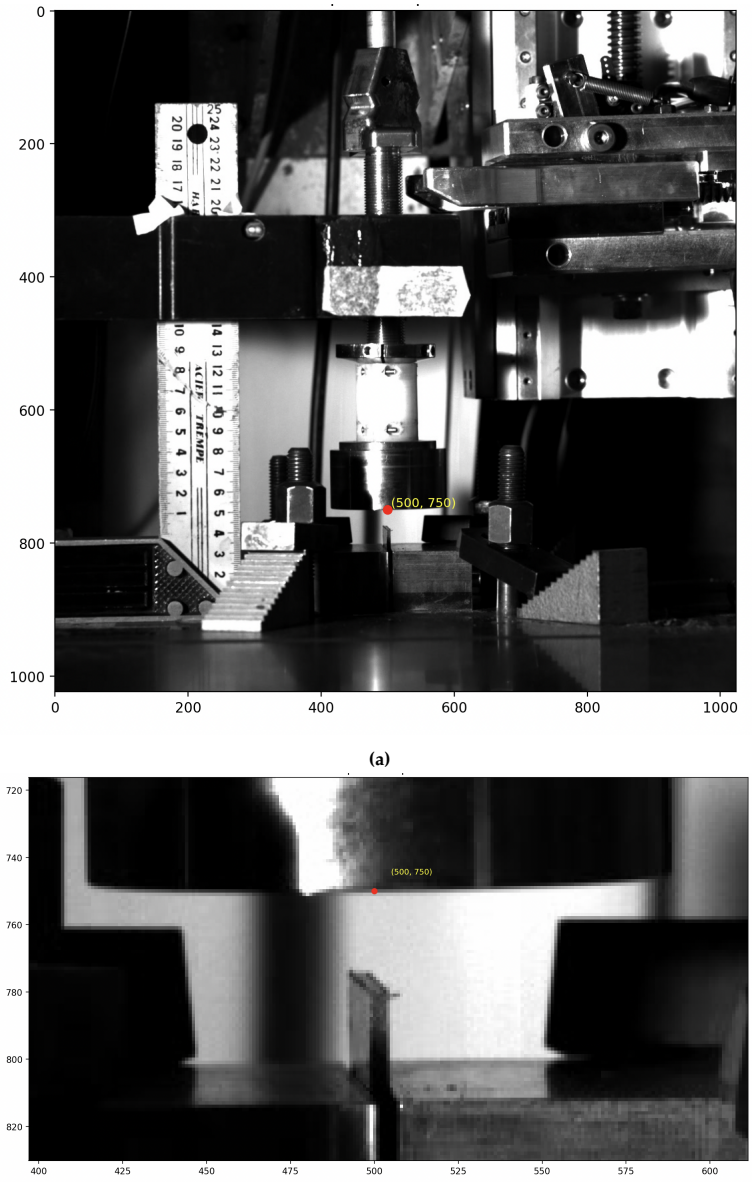


(a)



(b)

Figure A.9: IM-3 Frame 703



(a)

(b)

Figure A.10: IM-3 Frame 750

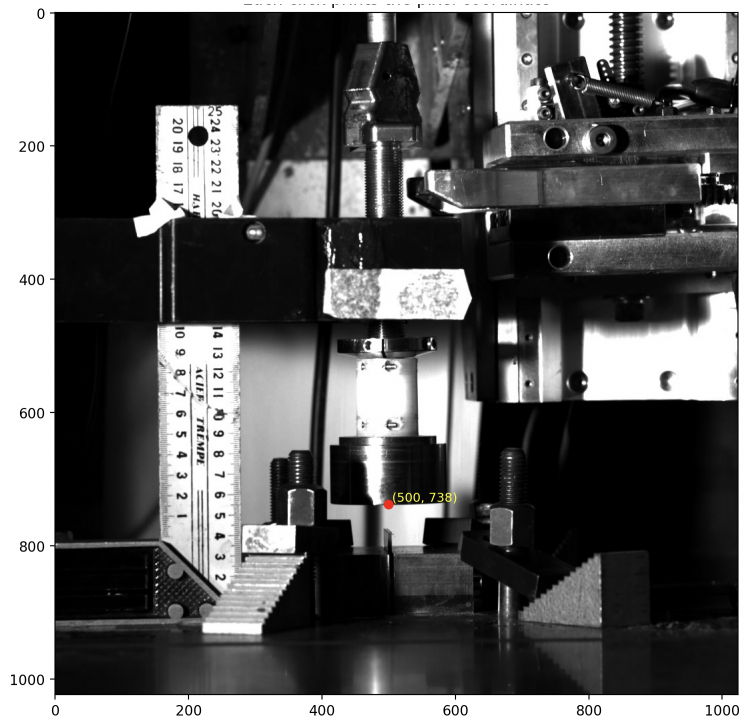
$$\Delta y = 749 - 703 = 46$$

$$\Delta t = \frac{30}{6400} = 0.0046875 \text{ s}$$

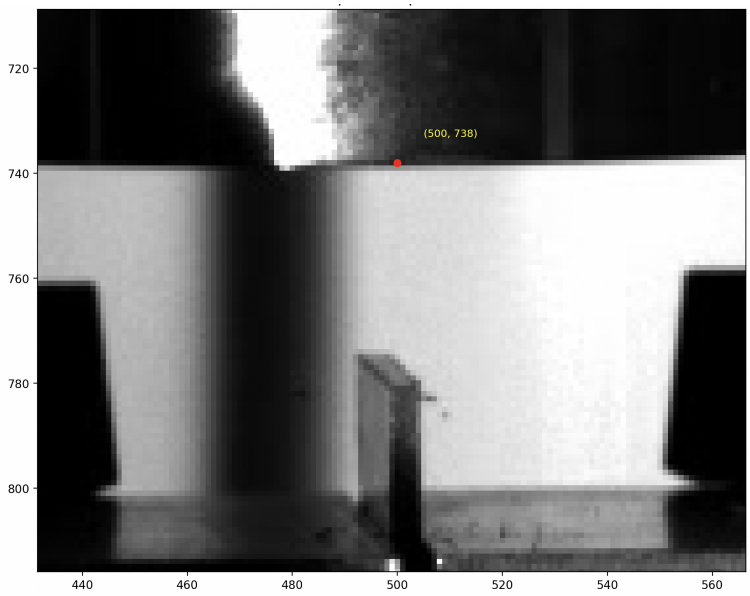
$$v = 3.17 \text{ m/s}$$

$$E_k = 11.54 \text{ J}$$

A.3.2. IM-3 After Impact Energy Calculation

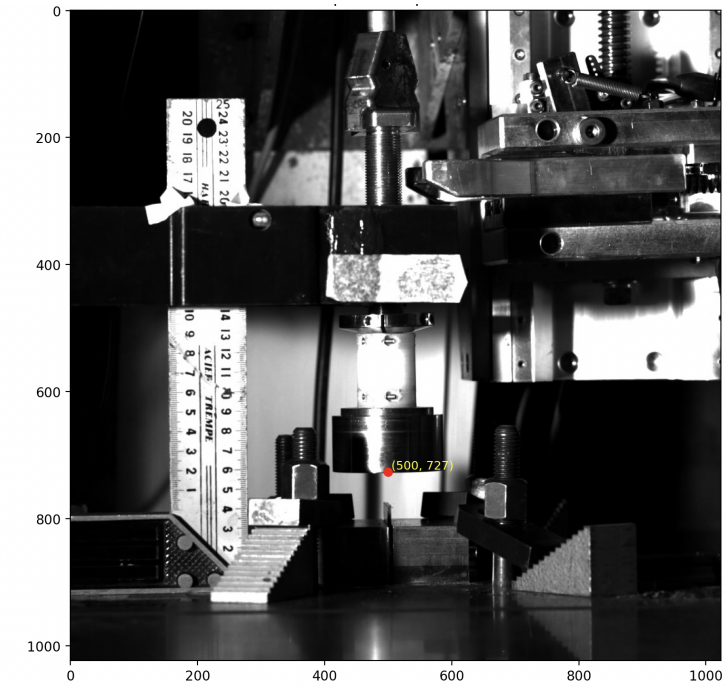


(a)

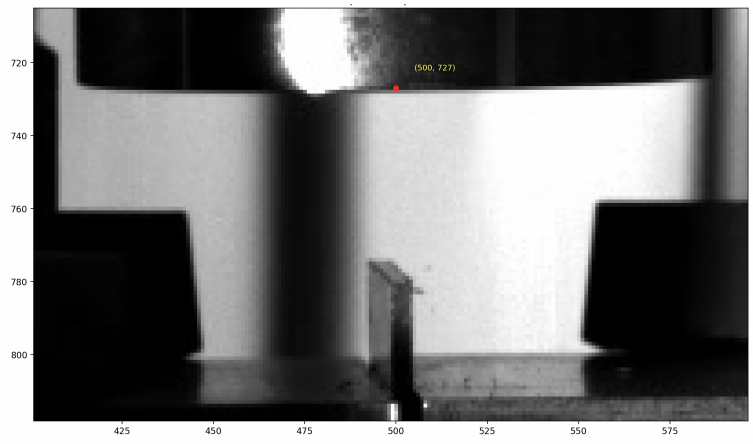


(b)

Figure A.11: IM-3 Frame 727



(a)



(b)

Figure A.12: IM-3 Frame 738

$$\Delta y = 738 - 727 = 11$$

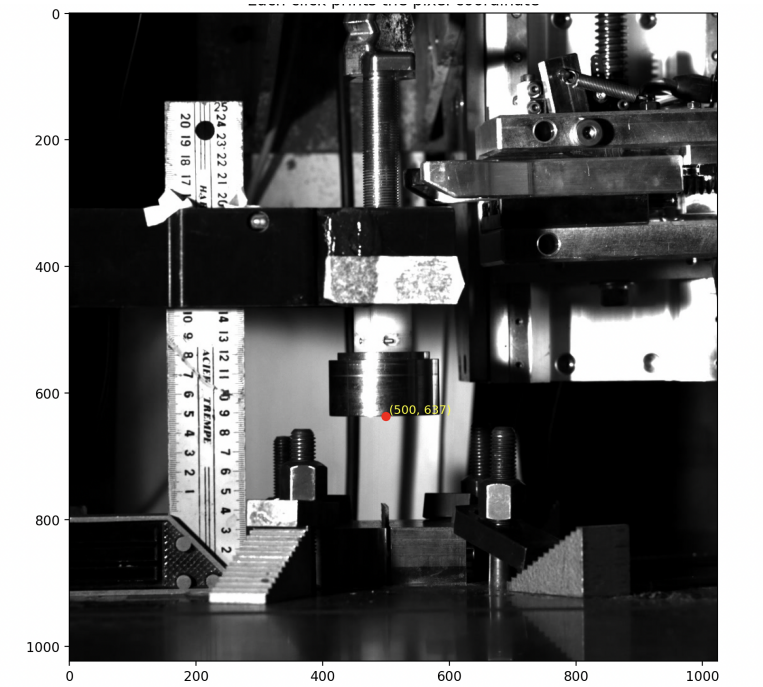
$$\Delta t = \frac{15}{6400} = 0.002344 \text{ s}$$

$$v = 1.51 \text{ m/s}$$

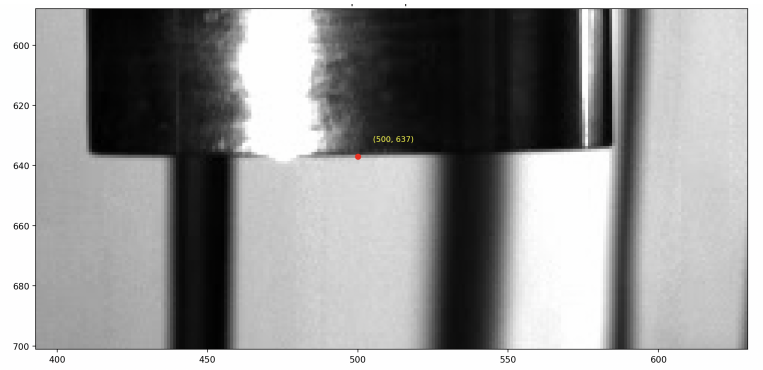
$$E_k = 2.63 \text{ J}$$

A.4. IM-4

A.4.1. IM-4 Before Impact Energy Calculation

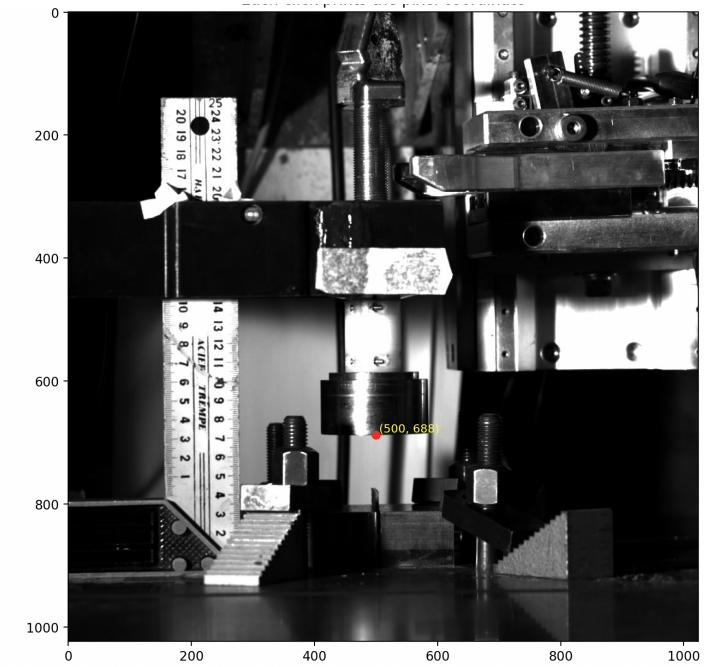


(a)

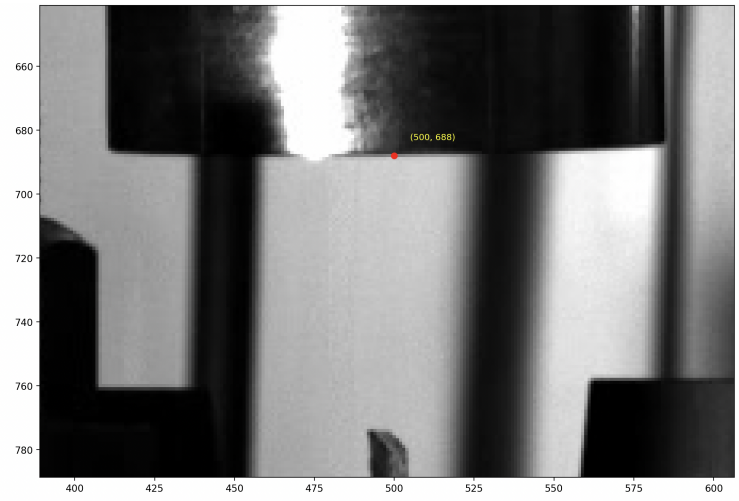


(b)

Figure A.13: IM-4 Frame 637



(a)



(b)

Figure A.14: IM-4 Frame 688

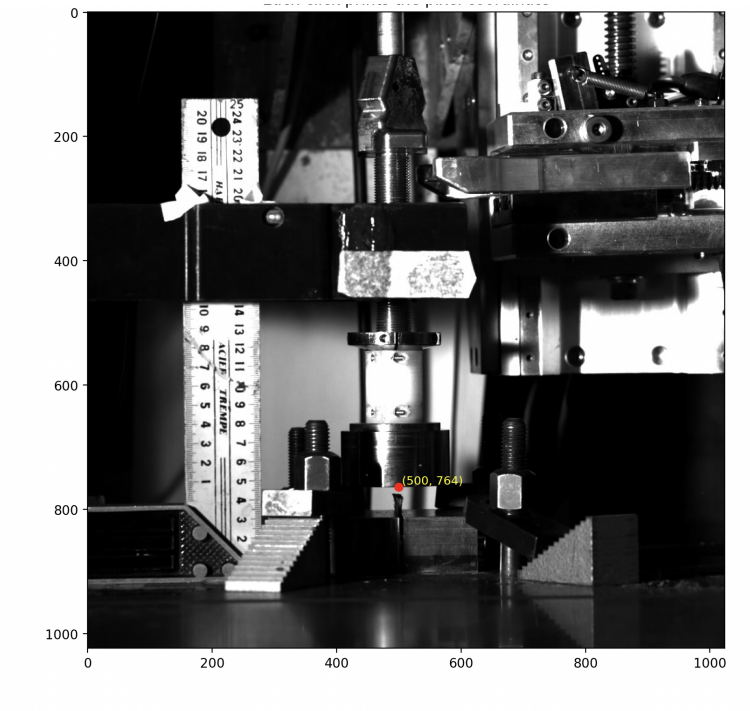
$$\Delta y = 688 - 637 = 51$$

$$\Delta t = \frac{33}{6400} = 0.005156 \text{ s}$$

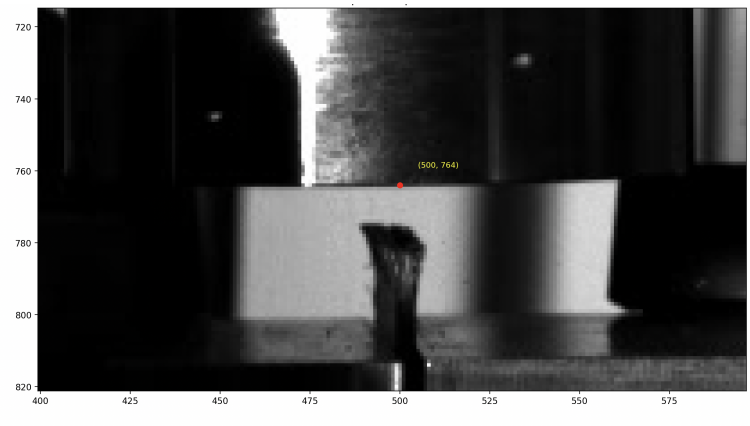
$$v = 3.19 \text{ m/s}$$

$$E_k = 11.71 \text{ J}$$

A.4.2. IM-4 After Impact Energy Calculation

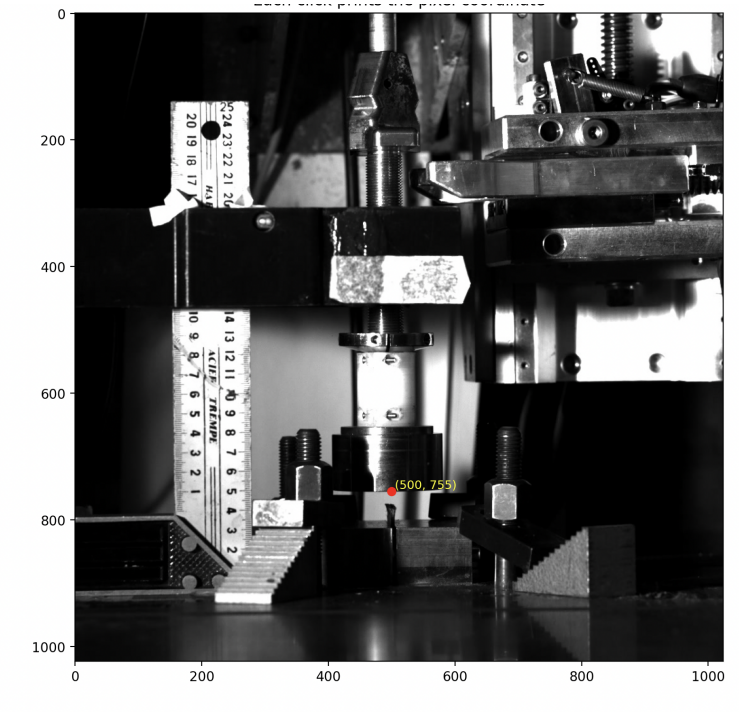


(a)

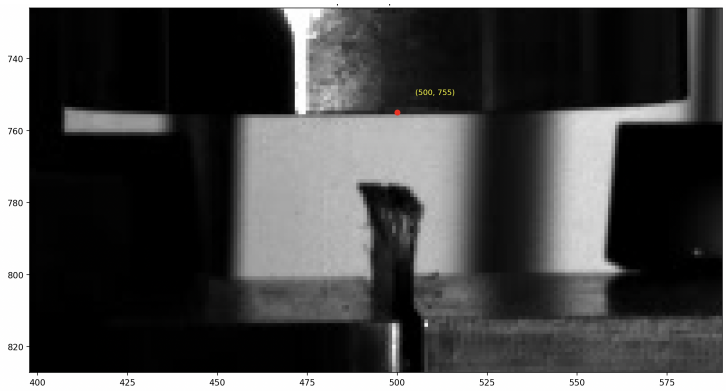


(b)

Figure A.15: IM-4 Frame 755



(a)



(b)

Figure A.16: IM-4 Frame 764

$$\Delta y = 764 - 755 = 9$$

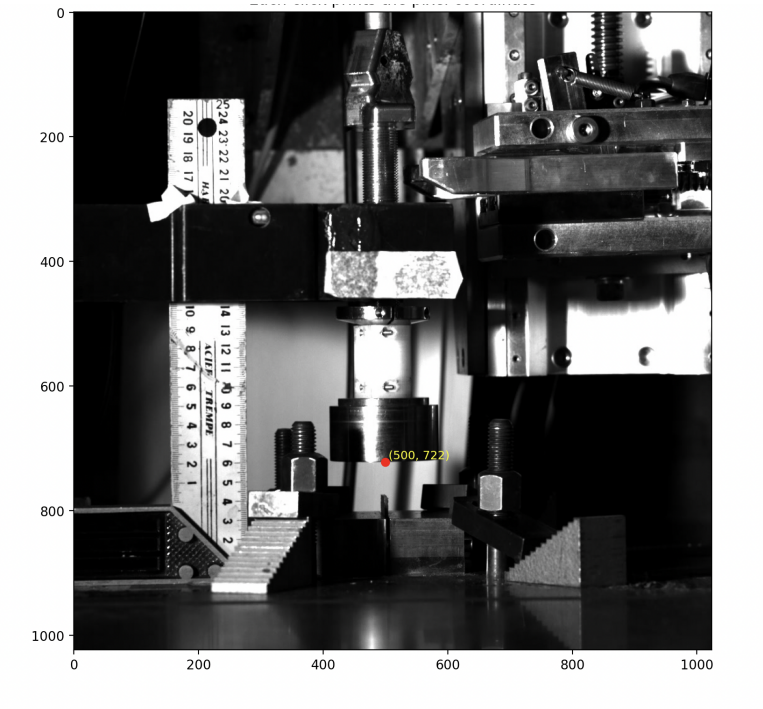
$$\Delta t = \frac{33}{6400} = 0.005156 \text{ s}$$

$$v = 0.56 \text{ m/s}$$

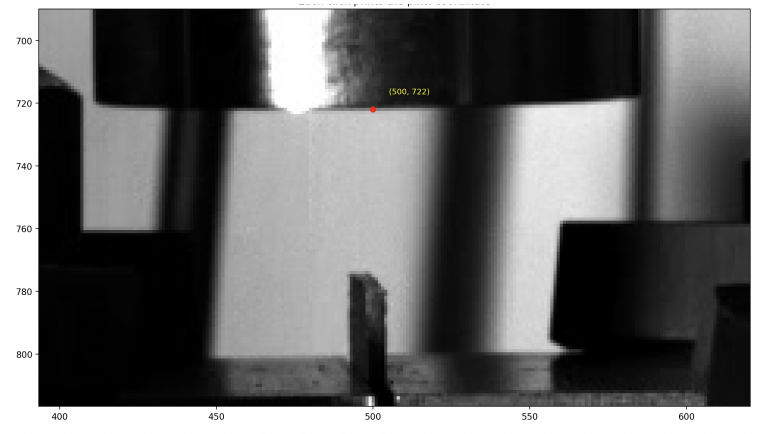
$$E_k = 0.36 \text{ J}$$

A.5. IM-5

A.5.1. IM-5 Before Impact Energy Calculation

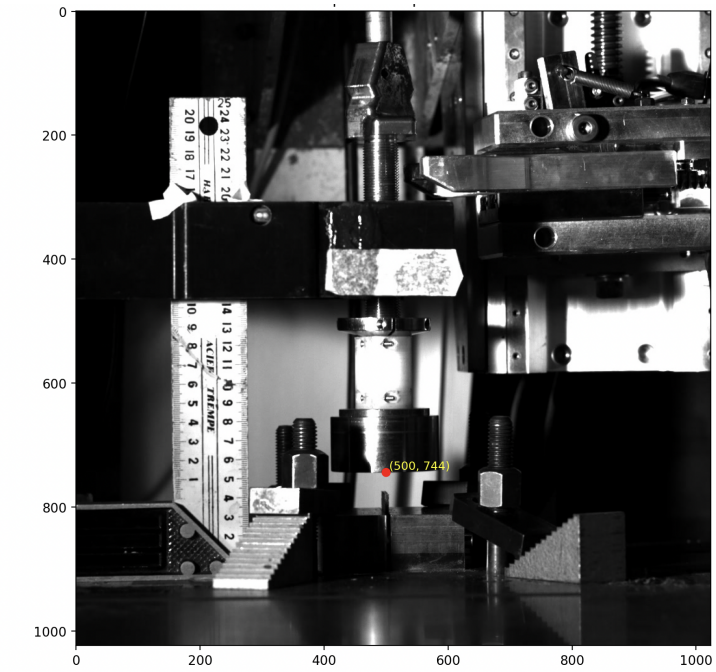


(a)

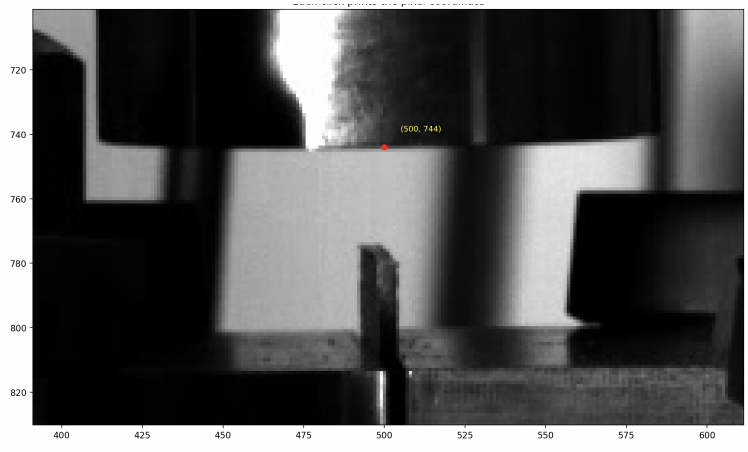


(b)

Figure A.17: IM-5 Frame 722



(a)



(b)

Figure A.18: IM-5 Frame 744

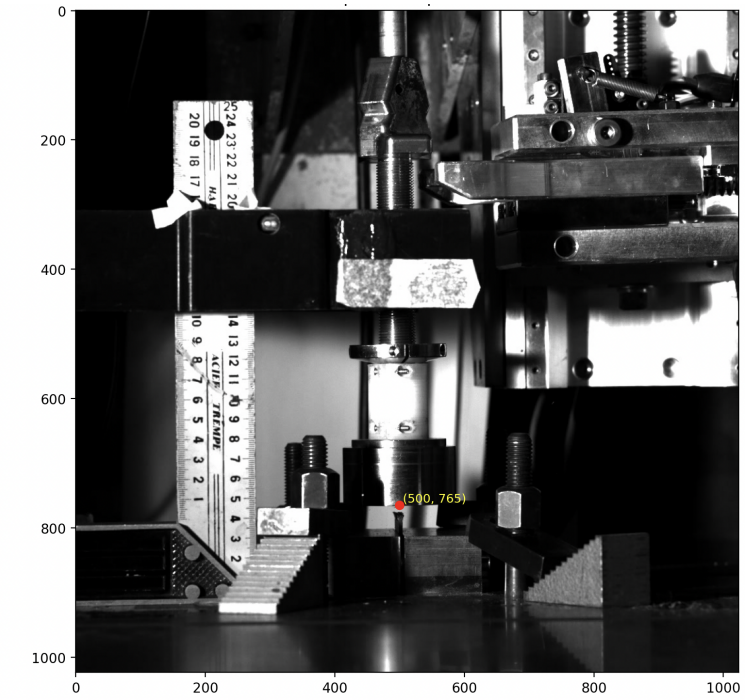
$$\Delta y = 744 - 722 = 22$$

$$\Delta t = \frac{14}{6400} = 0.002188 \text{ s}$$

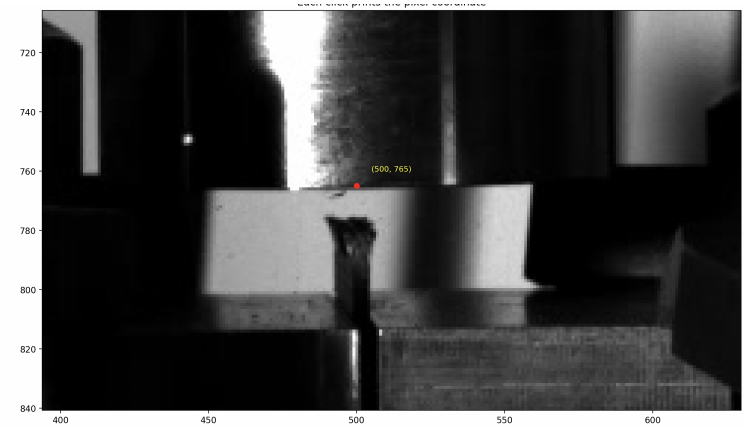
$$v = 3.24 \text{ m/s}$$

$$E_k = 12.10 \text{ J}$$

A.5.2. IM-5 After Impact Energy Calculation

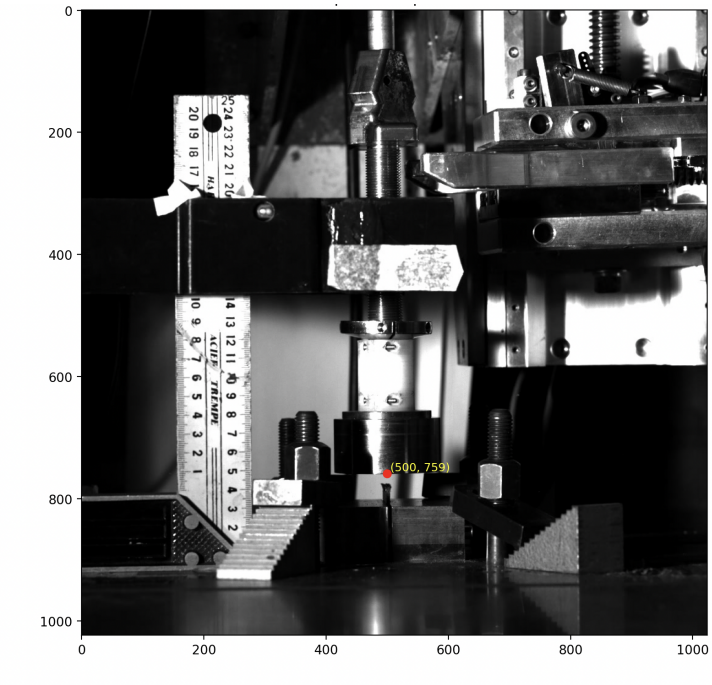


(a)

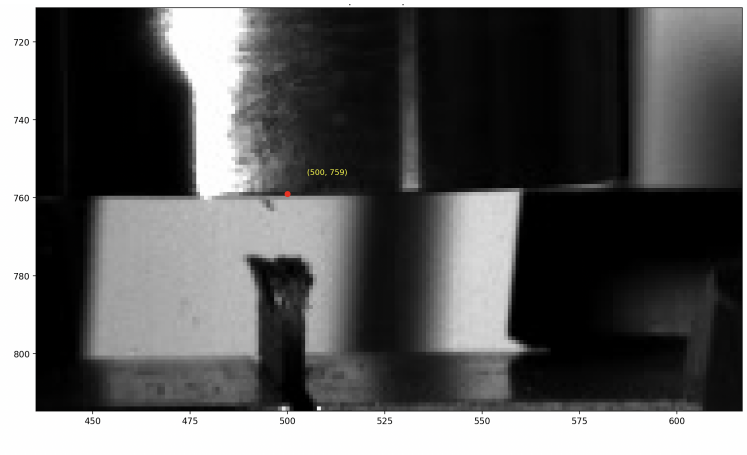


(b)

Figure A.19: IM-5 Frame 759



(a)



(b)

Figure A.20: IM-5 Frame 765

$$\Delta y = 765 - 759 = 6$$

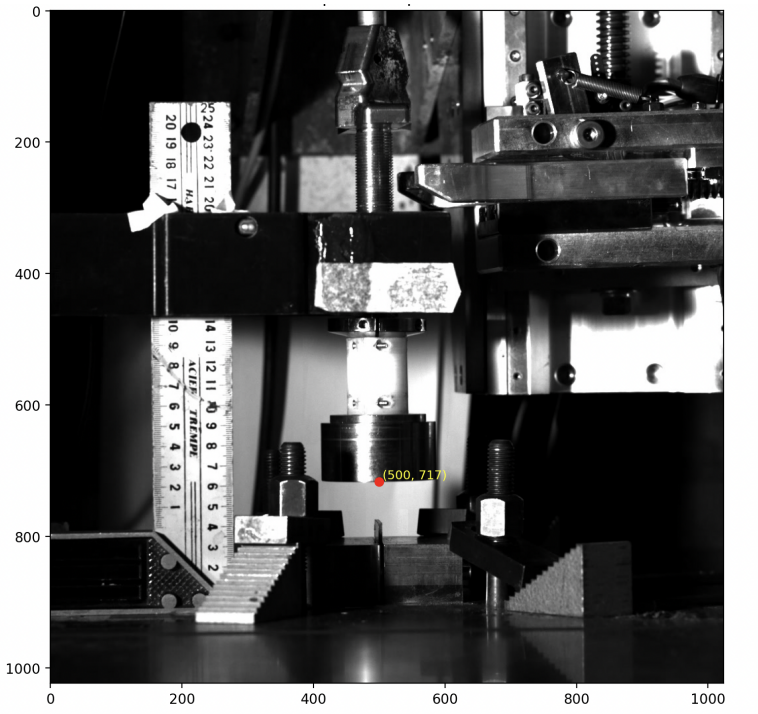
$$\Delta t = \frac{20}{6400} = 0.003125 \text{ s}$$

$$v = 0.62 \text{ m/s}$$

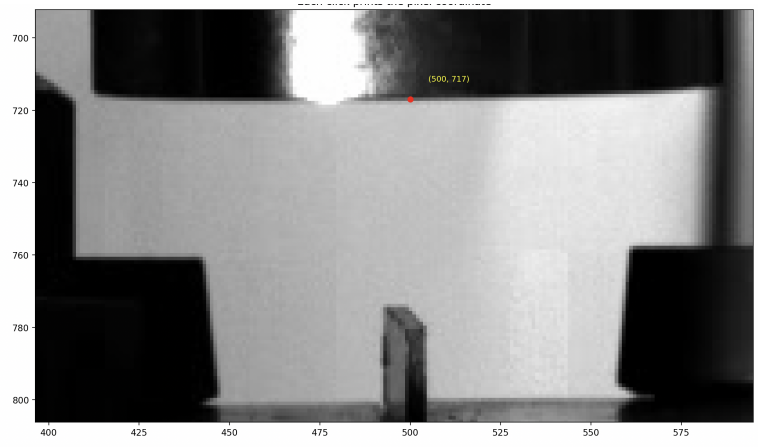
$$E_k = 0.44 \text{ J}$$

A.6. IM-6

A.6.1. IM-6 Before Impact Energy Calculation

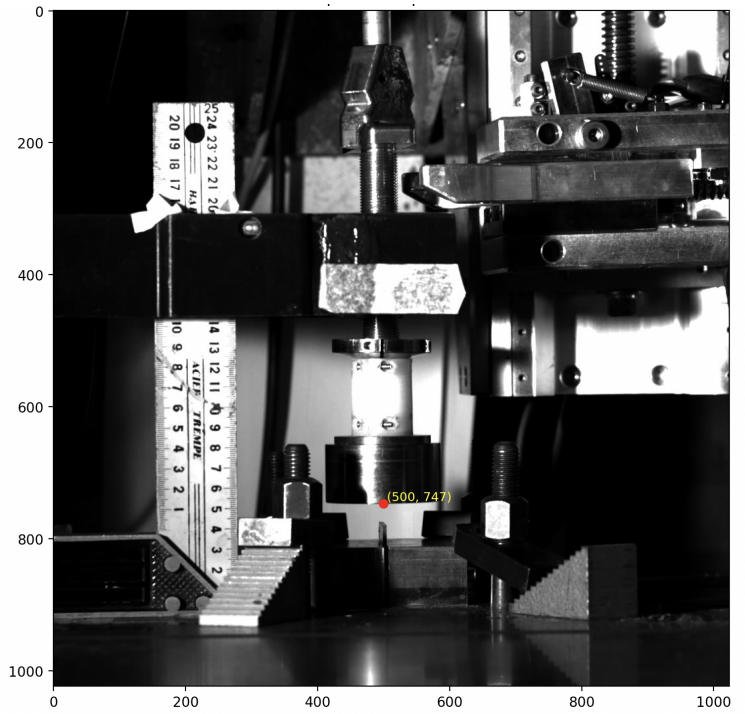


(a)

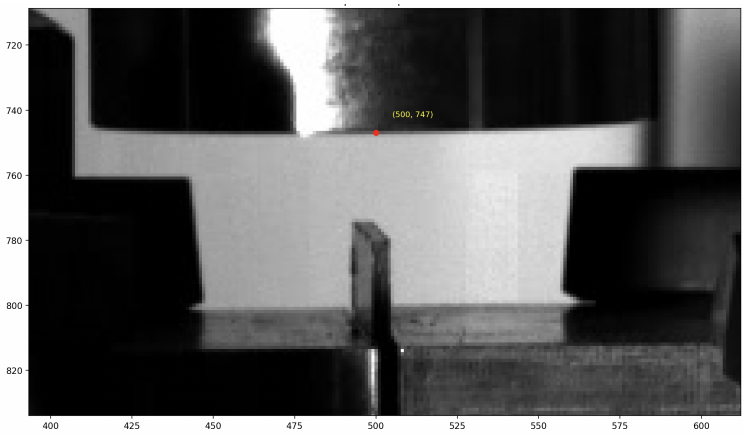


(b)

Figure A.21: IM-6 Frame 717



(a)



(b)

Figure A.22: IM-6 Frame 747

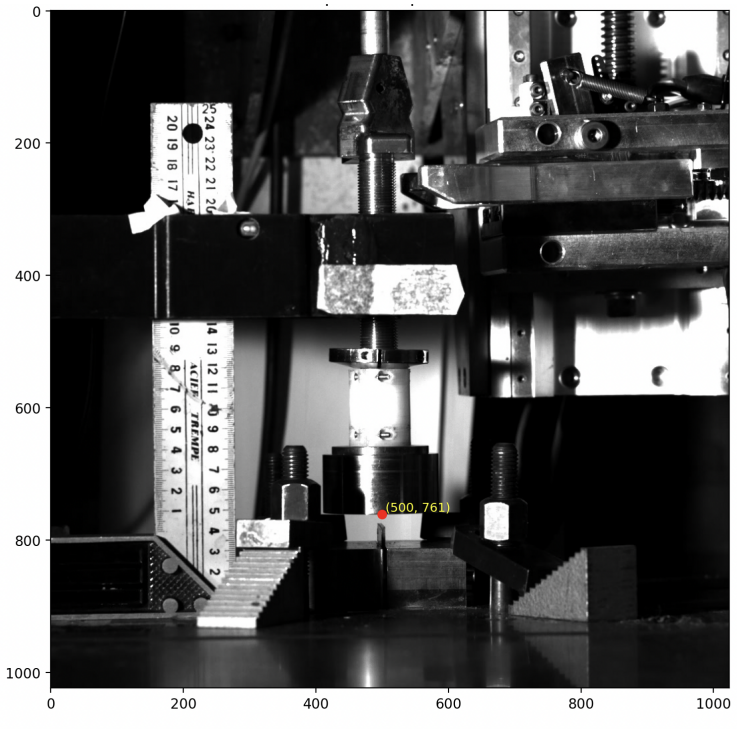
$$\Delta y = 747 - 717 = 30$$

$$\Delta t = \frac{19}{6400} = 0.002969 \text{ s}$$

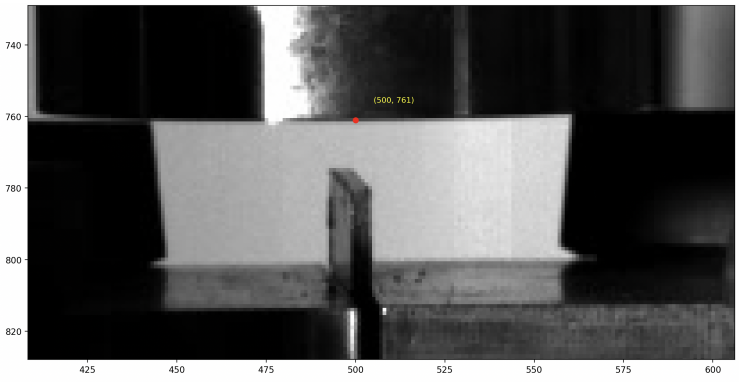
$$v = 3.26 \text{ m/s}$$

$$E_k = 12.22 \text{ J}$$

A.6.2. IM-6 After Impact Energy Calculation

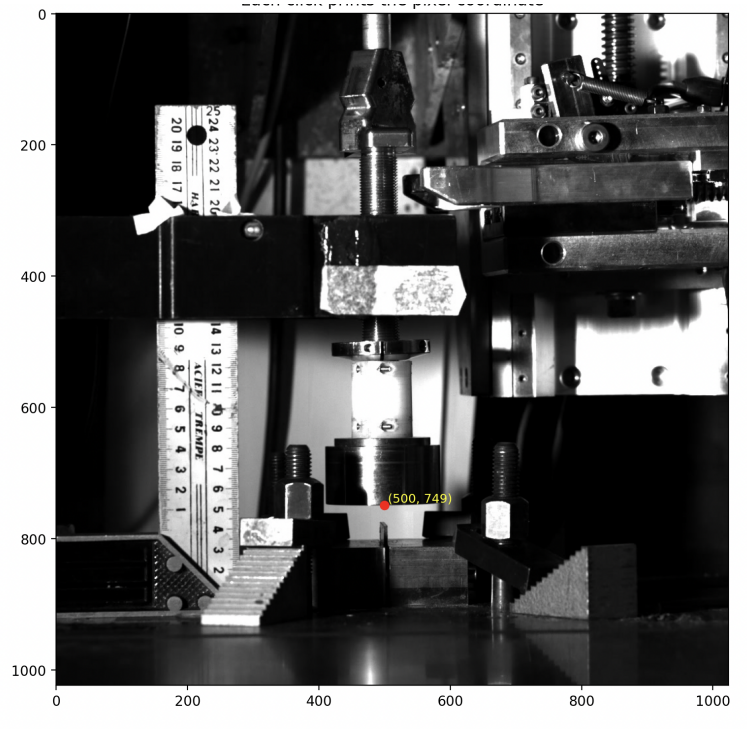


(a)

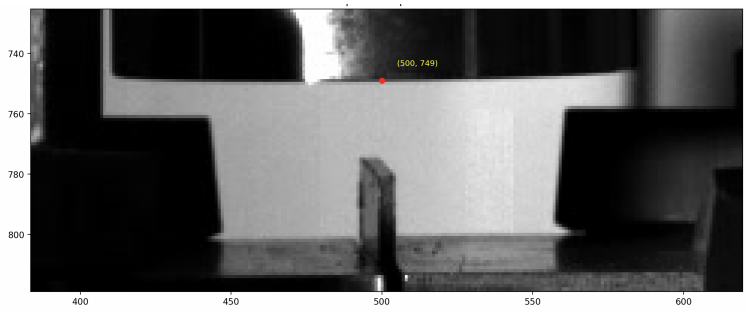


(b)

Figure A.23: IM-6 Frame 749



(a)



(b)

Figure A.24: IM-6 Frame 761

$$\Delta y = 761 - 749 = 12$$

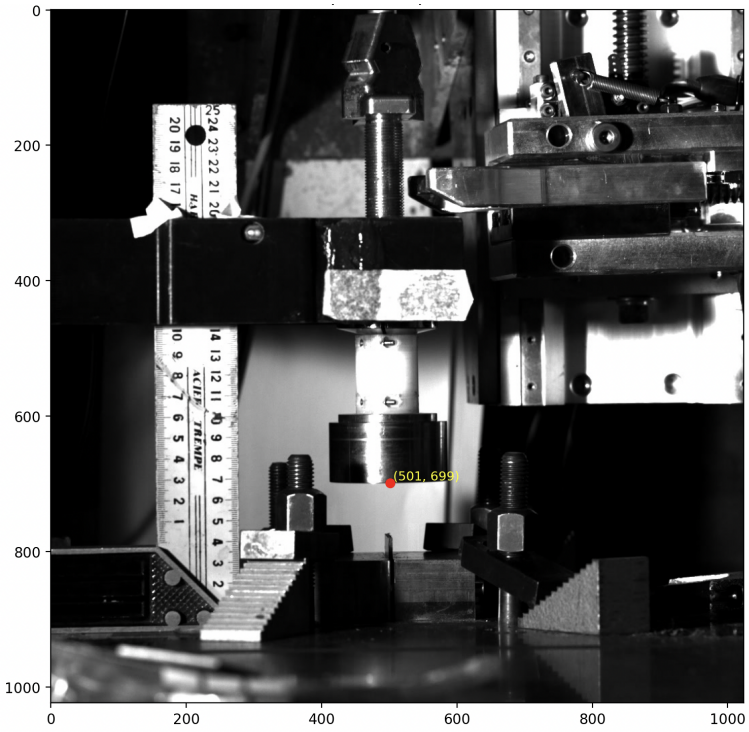
$$\Delta t = \frac{15}{6400} = 0.002344 \text{ s}$$

$$v = 1.65 \text{ m/s}$$

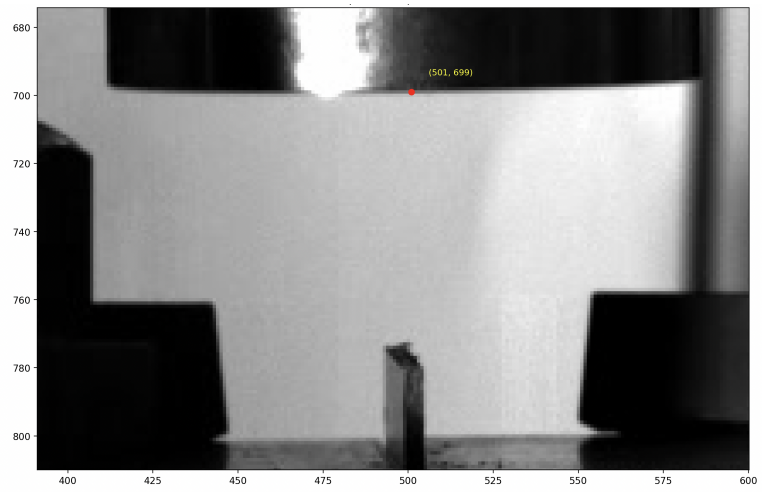
$$E_k = 3.14 \text{ J}$$

A.7. IM-7

A.7.1. IM-7 Before Impact Energy Calculation

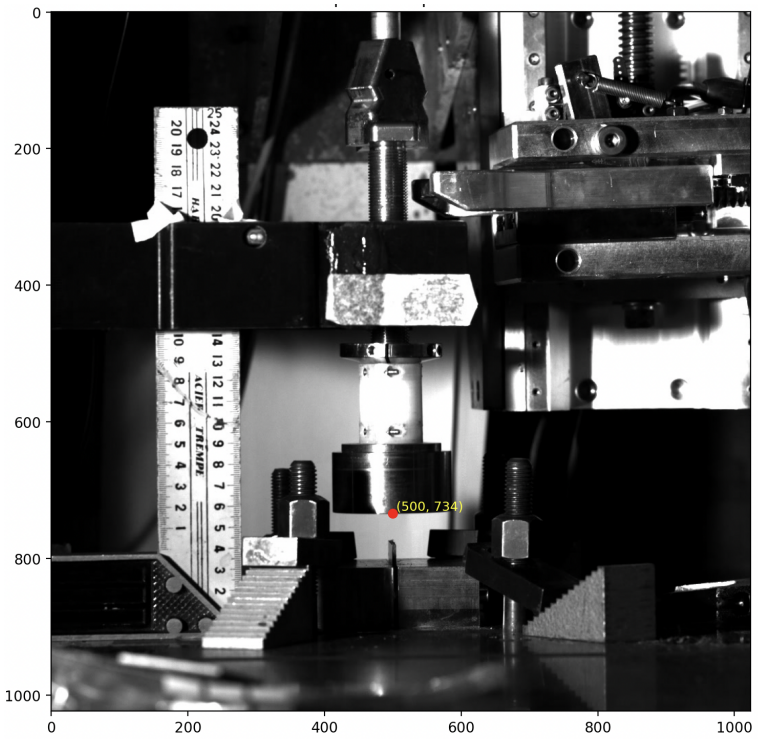


(a)

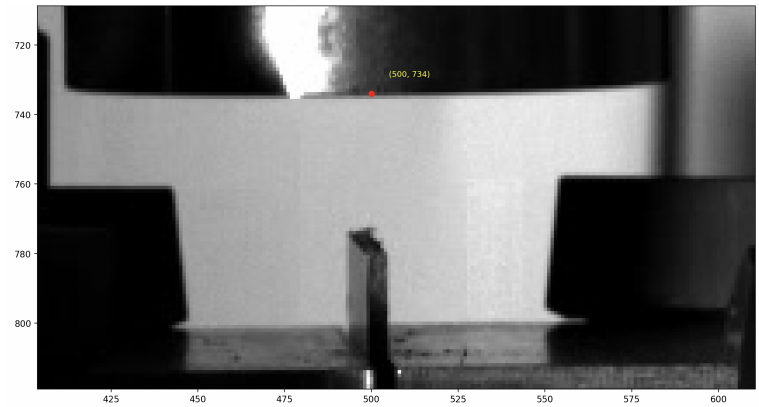


(b)

Figure A.25: IM-7 Frame 699



(a)



(b)

Figure A.26: IM-7 Frame 734

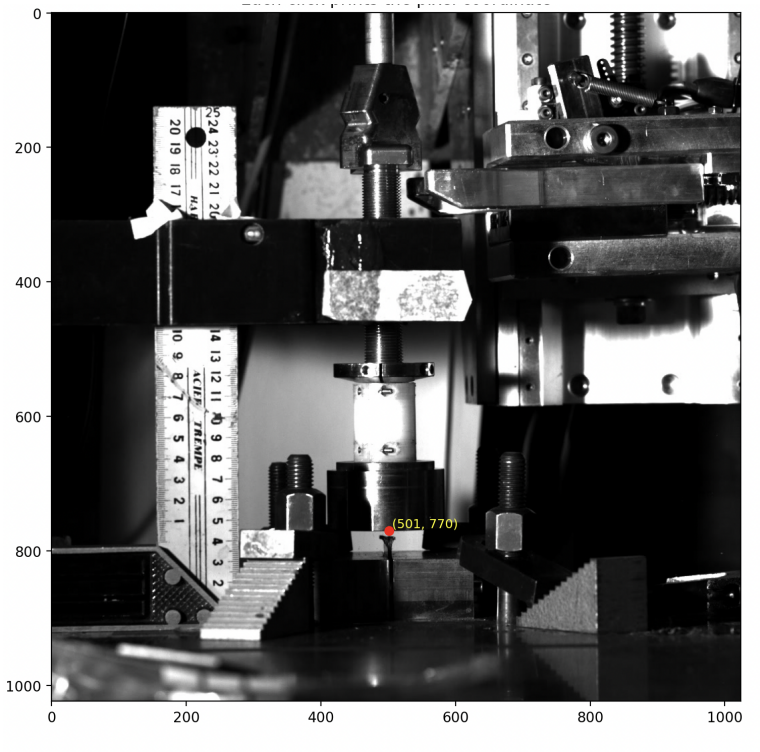
$$\Delta y = 734 - 699 = 35$$

$$\Delta t = \frac{20}{6400} = 0.003125 \text{ s}$$

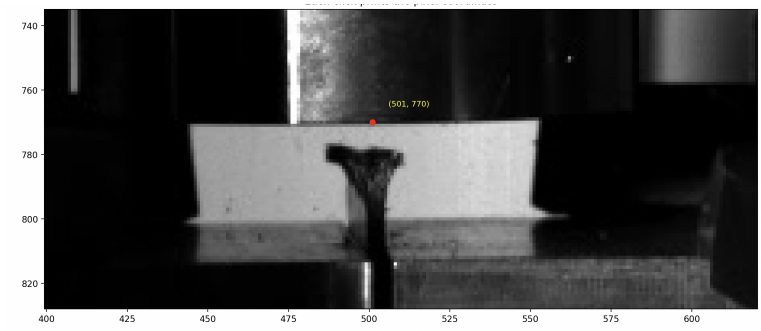
$$v = 3.61 \text{ m/s}$$

$$E_k = 15.01 \text{ J}$$

A.7.2. IM-7 After Impact Energy Calculation

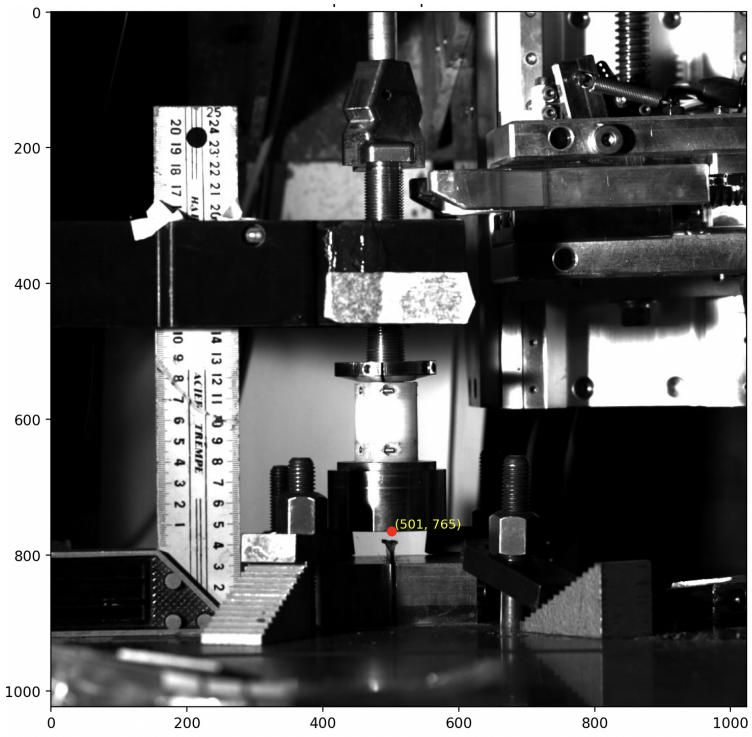


(a)

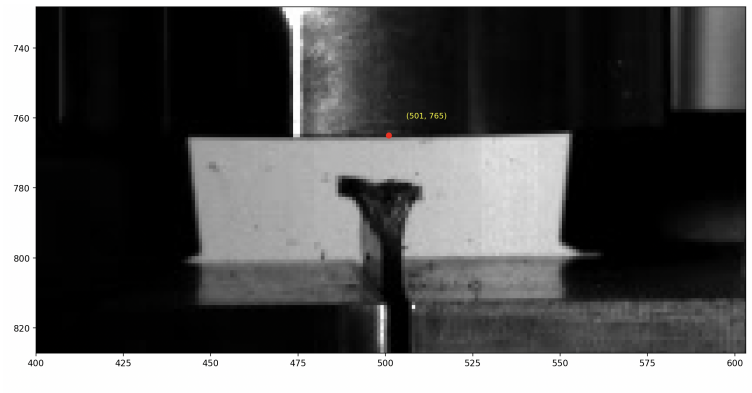


(b)

Figure A.27: IM-7 Frame 765



(a)



(b)

Figure A.28: IM-7 Frame 770

$$\Delta y = 770 - 765 = 5$$

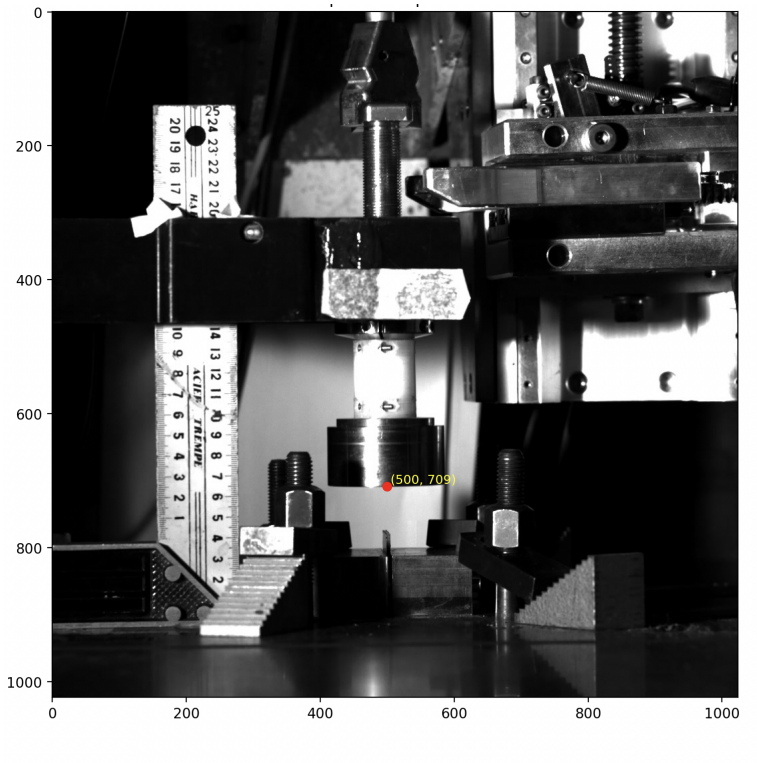
$$\Delta t = \frac{68}{6400} = 0.010625 \text{ s}$$

$$v = 0.15 \text{ m/s}$$

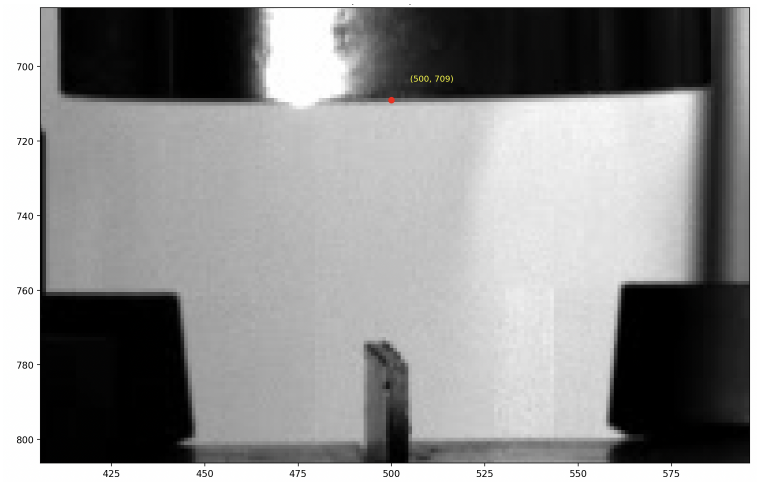
$$E_k = 0.027 \text{ J}$$

A.8. IM-8

A.8.1. IM-8 Before Impact Energy Calculation

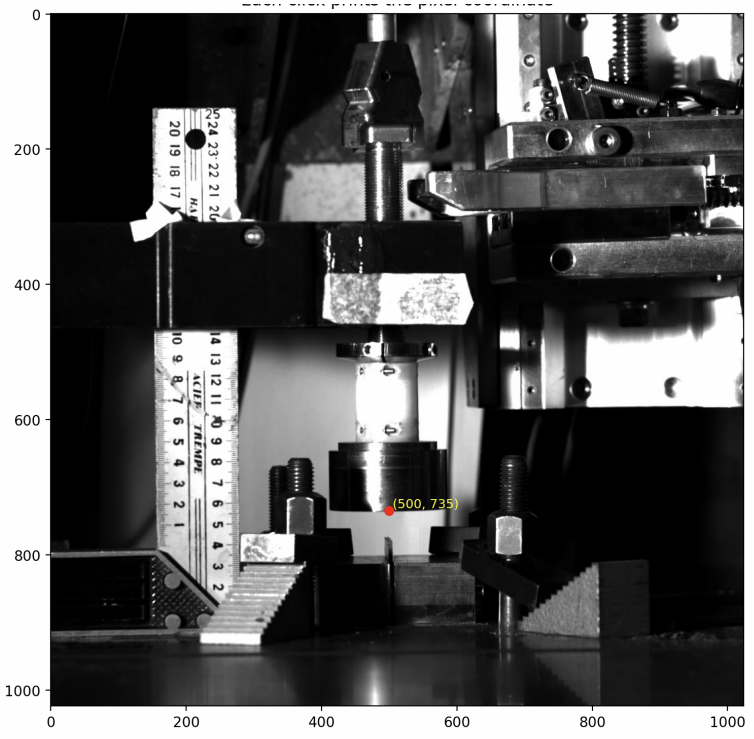


(a)

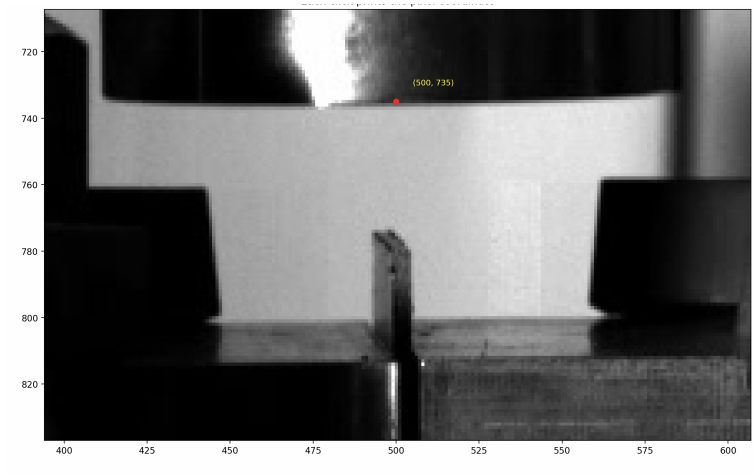


(b)

Figure A.29: IM-8 Frame 709



(a)



(b)

Figure A.30: IM-8 Frame 735

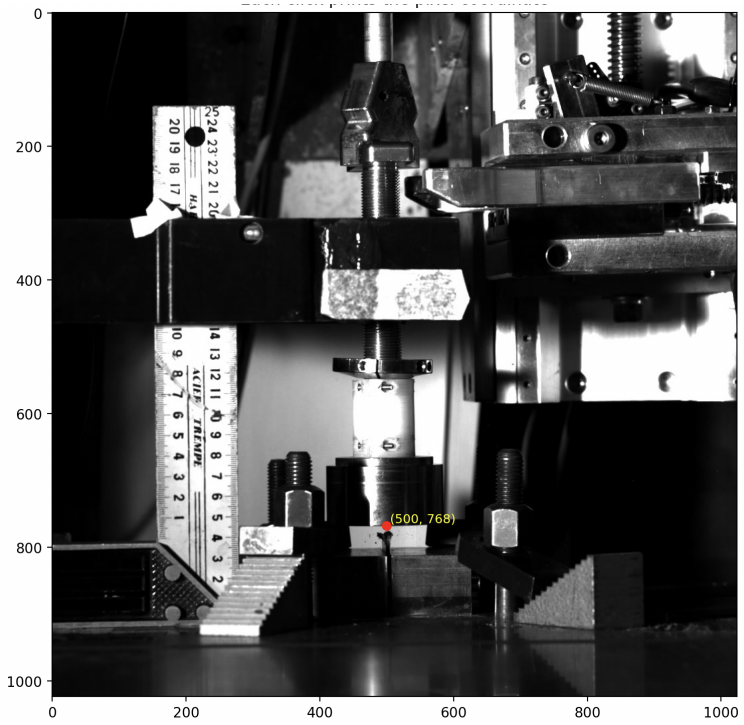
$$\Delta y = 735 - 709 = 26$$

$$\Delta t = \frac{14}{6400} = 0.002188 \text{ s}$$

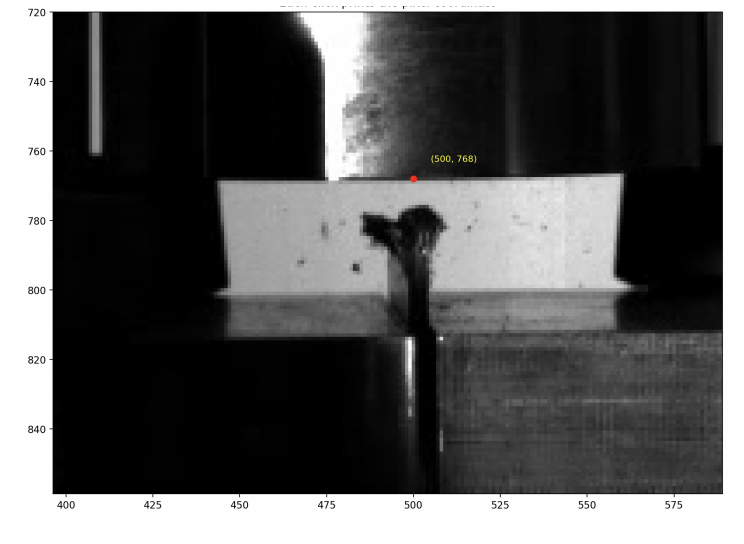
$$v = 3.83 \text{ m/s}$$

$$E_k = 16.91 \text{ J}$$

A.8.2. IM-8 After Impact Energy Calculation

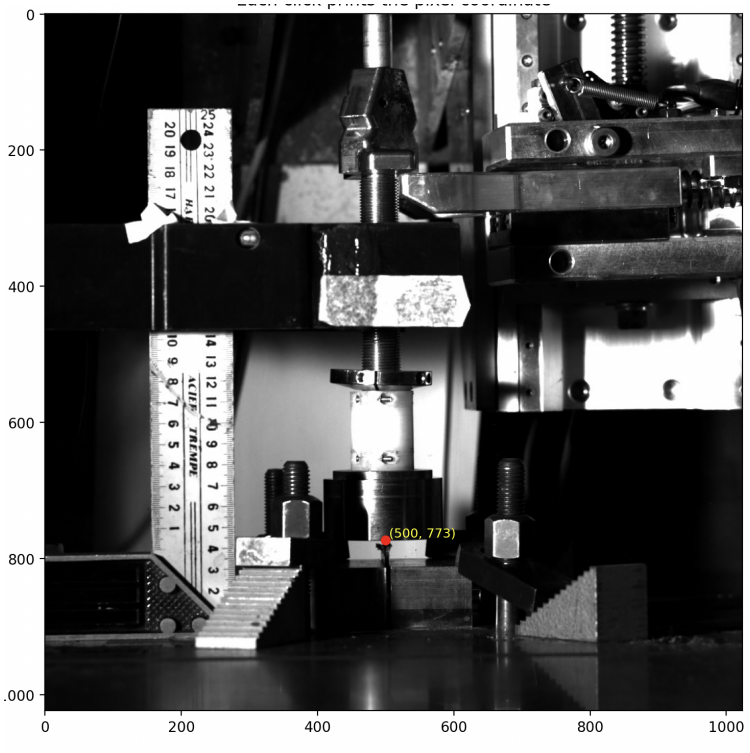


(a)

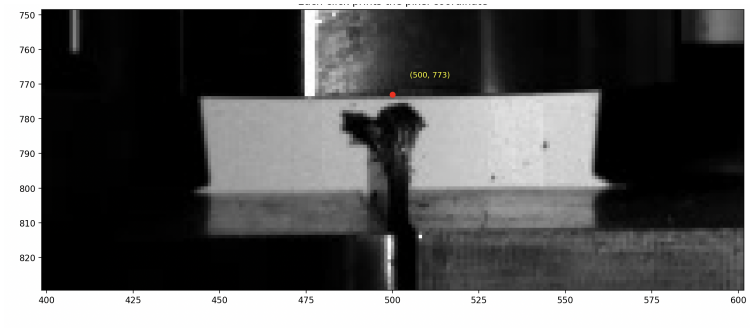


(b)

Figure A.31: IM-8 Frame 768



(a)



(b)

Figure A.32: IM-8 Frame 773

$$\Delta y = 773 - 768 = 5$$

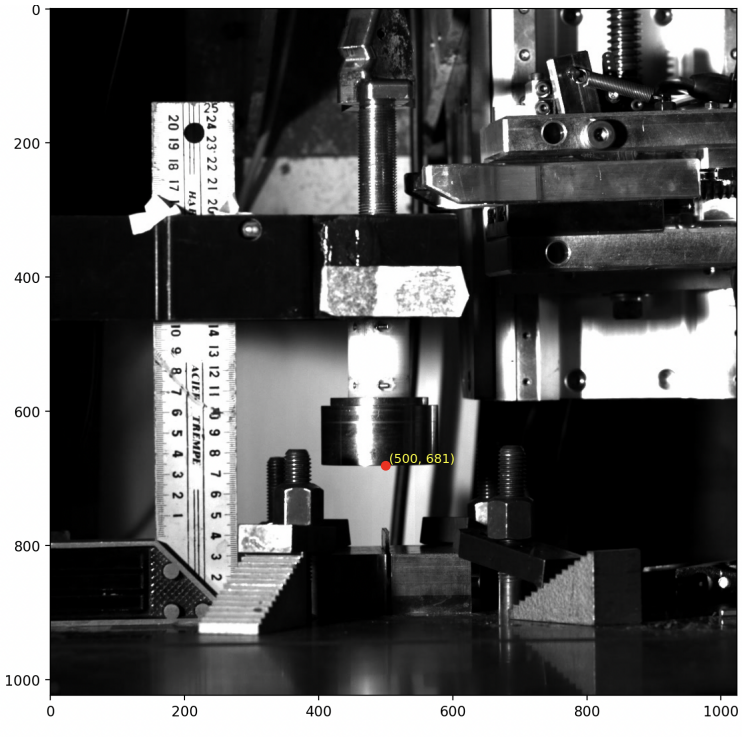
$$\Delta t = \frac{125}{6400} = 0.019531 \text{ s}$$

$$v = 0.08 \text{ m/s}$$

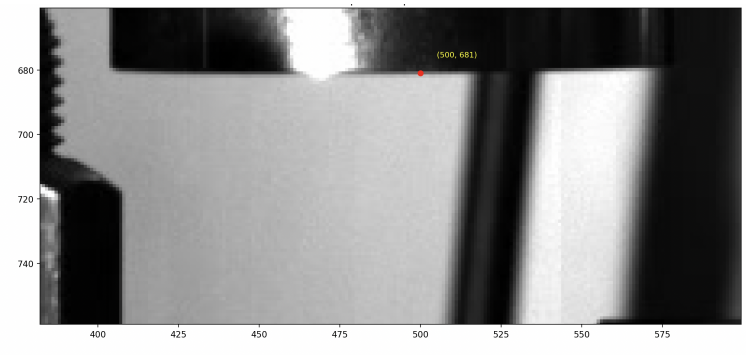
$$E_k = 0.008 \text{ J}$$

A.9. IM-9

A.9.1. IM-9 Before Impact Energy Calculation

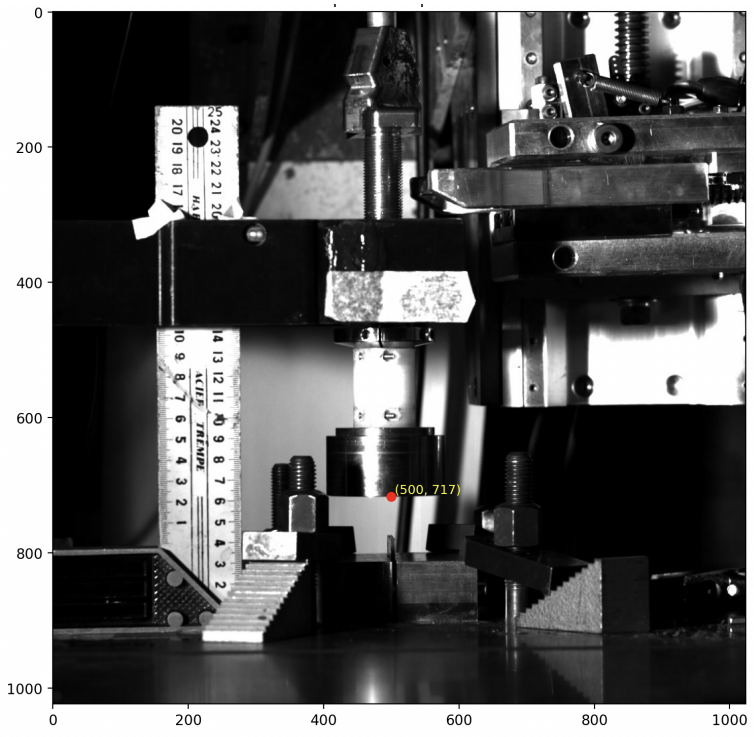


(a)

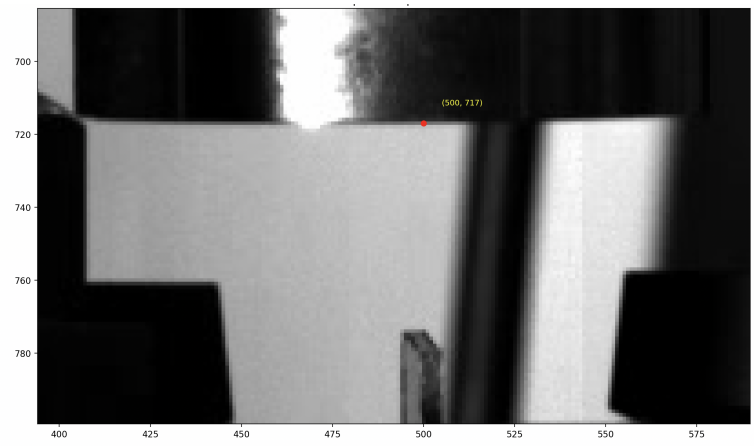


(b)

Figure A.33: IM-9 Frame 681



(a)



(b)

Figure A.34: IM-9 Frame 717

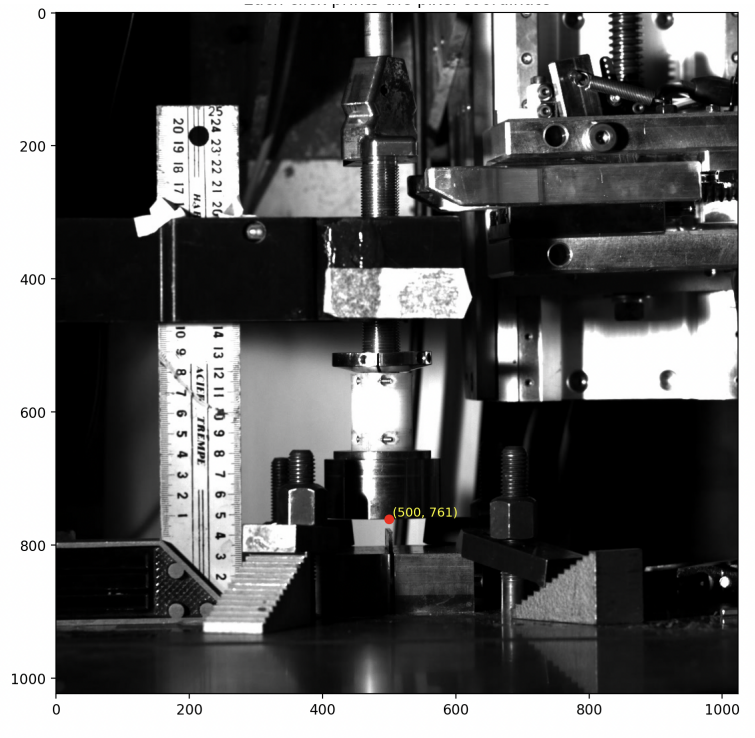
$$\Delta y = 717 - 681 = 36$$

$$\Delta t = \frac{22}{6400} = 0.003438 \text{ s}$$

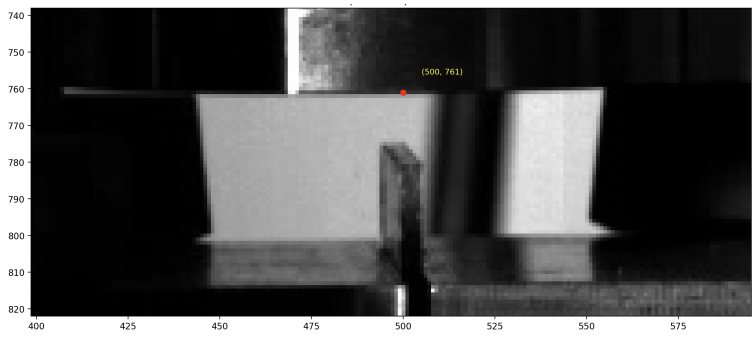
$$v = 3.38 \text{ m/s}$$

$$E_k = 13.12 \text{ J}$$

A.9.2. IM-9 After Impact Energy Calculation

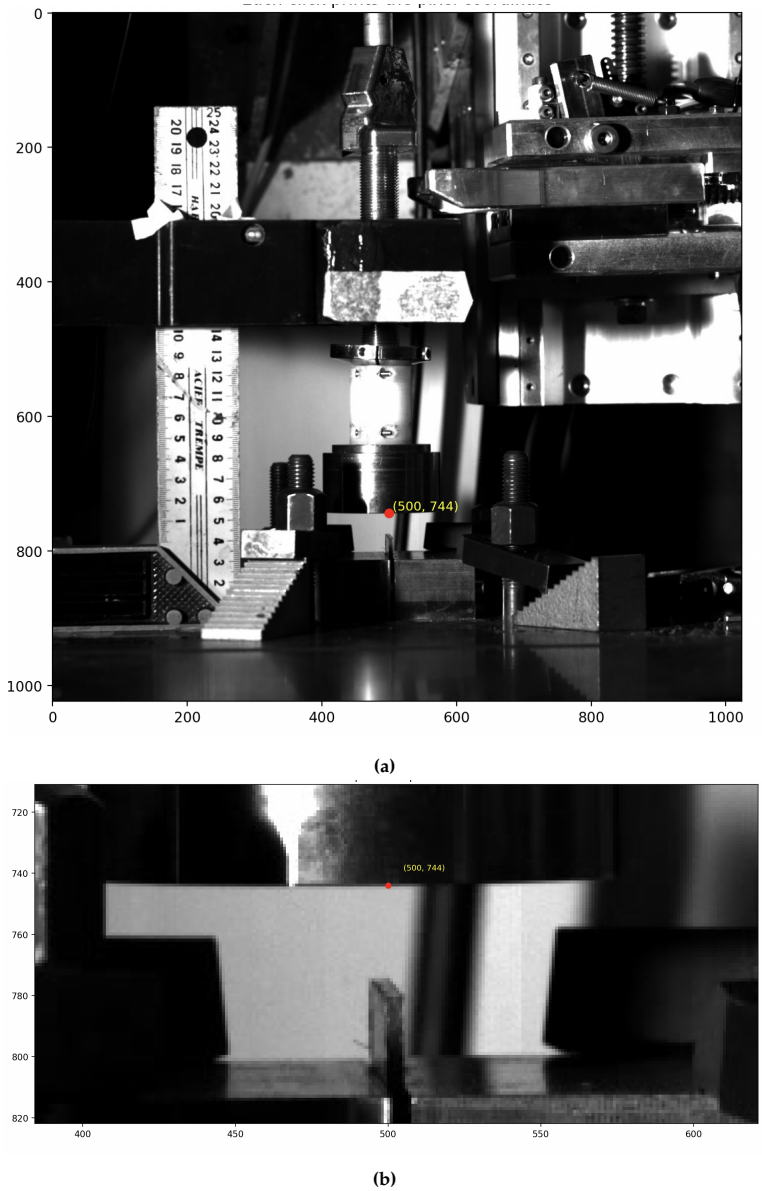


(a)



(b)

Figure A.35: IM-9 Frame 744



(a)

(b)

Figure A.36: IM-9 Frame 761

$$\Delta y = 761 - 744 = 17$$

$$\Delta t = \frac{22}{6400} = 0.003438 \text{ s}$$

$$v = 1.60 \text{ m/s}$$

$$E_k = 2.93 \text{ J}$$